



MASTER'S THESIS:

CONTINUOUS MEASUREMENTS OF  
NITROUS OXIDE ISOTOPOMERS  
PRODUCED BY NITRIFYING AND  
DENITRIFYING BACTERIA

BY:

MALTE NORDMANN WINTHER

DUE TUESDAY OCTOBER 15 2013

ACADEMIC SUPERVISOR:

PROF. THOMAS BLUNIER

CENTER FOR ICE AND CLIMATE

NIELS BOHR INSTITUTE

UNIVERSITY OF COPENHAGEN, DENMARK



## Resumé

Lattergas ( $N_2O$ ) er en vigtig drivhus gas, som primært bliver dannet ved nitrifikations og denitrifikations processer. Tidligere studier har præsenteret resultater, der indikerer at kilden til  $N_2O$  kan identificeres ved brug af "site preference" (SP) af den intramolekylære isotop sammensætning. De tidligere målinger er alle blevet udført ved brug af diskontinuierlige metoder.

I denne afhandling præsenteres nogle af de første kontinuerte målinger af isotop forholdene og af gas koncentrationen af  $N_2O$ . Der er præsenteret eksperimenter udført med både monokulturer samt prøver fra naturlige økosystemer. Til at udføre målingerne er der brugt et recirkulations system hvor af prototypen på Picarros G5101-i instrument er en del. Dette instrument bruger "cavity ring-down" spektroskopi til at måle  $N_2O$  gasserne. For at demonstrere potentialet af SP til identifikation af kilderne til  $N_2O$ , præsenteres der i denne afhandling kontinuerte målinger af både nitrifikations og denitrifikations forsøg. Der er blevet udført forsøg med både komplette denitrifikations bakterier (*Pseudomonas Fluorescens*) og med ukomplette denitrifikations bakterier (*Pseudomonas Chlororaphis*). Disse forsøg gav SP værdier på mellem -20 ‰ og +10 ‰. Nitrifikations forsøgene indikerede SP værdier på over 30 ‰. Derudover viste forsøgene med denitrifikations bakterier den kontinuerte overgang mellem produktion og destruktion af  $N_2O$ .

Målinger af gas-prøver opsamlet fra arktiske egne på Disko-øen viser, at en differentiering mellem  $N_2O$ , dannet i lavtliggende vådområder og højt-liggende tørre områder, er mulig. Fra vådområderne blev SP af  $N_2O$  gasserne målt til at være ca. 0 ‰, hvor de i de våde områder blev målt til at være højere end 20 ‰. Denne tendens er også observeret i målinger fra en skråning i Buresø, Danmark. Det bliver yderligere præsenteret i denne afhandling, at målinger tyder på, at den primære produktion af lattergas i arktiske egne finder sted i den øverste del af det aktive jordlag. Målinger viser også vigtigheden af gas transporterende planter.

## Abstract

Nitrous oxide ( $\text{N}_2\text{O}$ ) is an important greenhouse gas which is primarily produced through nitrification and denitrification processes. Previous studies have presented experiments which indicate that the site preference (SP) of the intramolecular isotopic composition, of  $\text{N}_2\text{O}$ , can be used to distinguish the source. These former measurements were conducted using non-continuous measurement techniques.

This thesis presents some of the first continuous measurements of both concentration and isotopic composition of  $\text{N}_2\text{O}$  from mono-culture experiments and natural ecosystems. The measurements were conducted using a recirculation setup with the prototype of the Picarro G5101-i analyzer. The analyzer uses the cavity ring-down spectroscopy technique for measuring the  $\text{N}_2\text{O}$  gas. Continuous measurements of nitrifying and denitrifying mono-cultures are presented to demonstrate the potential for differentiating the source of  $\text{N}_2\text{O}$  from the SP. Continuous measurements of complete denitrifying bacteria (*Pseudomonas Fluorescens*) and of incomplete denitrifying bacteria (*Pseudomonas Chlororaphis*) provide SP values between  $-20\text{ ‰}$  and  $+10\text{ ‰}$ . The nitrification experiments indicate SP values above  $30\text{ ‰}$ . The continuous measurements show the denitrifying transition between production and consumption of  $\text{N}_2\text{O}$ .

Measurements from gas samples collected at Arctic sites on Disko Island show a differentiation between  $\text{N}_2\text{O}$  produced from low swampy areas and from drier higher elevated areas. The emitted  $\text{N}_2\text{O}$  at the wet sites was measured with a SP of approximately  $0\text{ ‰}$ , where the  $\text{N}_2\text{O}$  from the dry sites was measured to have a SP above  $+20\text{ ‰}$ . The same tendency was found from measurements of gas samples from a slope in Buresoe, Denmark. Furthermore, additional measurements are presented. These measurements indicate that  $\text{N}_2\text{O}$  primarily is produced in the upper part of the active layer. Measurements presenting the importance of plants as gas transporters has been conducted as well.

## Acknowledgements

First of all I would like to thank my supervisor Professor Thomas Blunier, for giving me the opportunity of making my Master's thesis in his group. I like to thank Thomas for introducing me to the scientific work environment at the Center for Ice and Climate, for supporting me through the past year, and providing guidance to make this Master's thesis successful and fun.

Secondly I like to give my thanks to my unofficial co-supervisor, David Balslev-Clausen. Without his support, guidance, and many informative conversations this study would not have been as successful, and for that I am thankful.

I want to thank Professor Bo Elberling for his support and guidance during the past year. Further, a thanks needs to be given to Bo for giving me the opportunity of a stay at the Arctic station on Disko Island. A special thanks is also needed to the CENPERM group for making my stay at the Arctic station so much fun in spite of the long working days and nights. I like to thank Professor Søren Christensen for his guidance and for helping me with the questions concerning the biology part of my thesis. Christian Emil Kjærsgaard, my partner in the field, needs a thank for all the fun we had during the field work both at Disko Island and in Buresoe.

Furthermore, I like to thank Christopher Stowasser for his technical guidance and advices in the beginning of my work. I like to thank Corentin Reutenauer and Gabriela Ciobanu for helping me proof reading and for their general support. Alexander Hansen and Pia Englyst need special thanks for proof reading my thesis. I want to thank Bo Frederiksen for the many fun times at the office and for helping me with MatLab problems.

I will conclude by giving a special thank to my girlfriend Jannie, and the rest of my family for supporting me all the way through my studies. Without their love and support my studies would not have been as successful.

Malte N. Winther  
Copenhagen, October 2013



# Contents

<b>1</b>	<b>Introduction</b>	<b>1</b>
1.1	Motivation . . . . .	1
1.2	Climate history . . . . .	2
<b>2</b>	<b>Background theory</b>	<b>4</b>
2.1	Stable isotopes . . . . .	4
2.1.1	Fractionation . . . . .	5
2.2	Nitrous Oxide . . . . .	7
2.2.1	Terminologie of the isotopomers . . . . .	8
2.2.2	Intramolecular distribution of the nitrogen-15 . . . . .	9
2.2.3	Sources of nitrous oxide . . . . .	11
2.2.4	Sink of nitrous oxide . . . . .	12
2.3	Production of nitrous oxide . . . . .	13
2.3.1	Nitrification . . . . .	13
2.3.2	Denitrification . . . . .	15
2.3.3	Nitrifier denitrification . . . . .	16
2.4	Isotopic difference in nitrous oxide isotopomer . . . . .	17
<b>3</b>	<b>Instrumental theory</b>	<b>19</b>
3.1	Absorption spectroscopy . . . . .	19
3.2	Mid-infrared spectroscopy . . . . .	23
3.3	Cavity Ring Down Spectroscopy . . . . .	25
<b>4</b>	<b>Experimental setup</b>	<b>30</b>
4.1	Picarro G5101-i analyzer . . . . .	31

4.1.1	The cavity . . . . .	31
4.2	The flushing system . . . . .	32
4.3	The sample bag measuring setup . . . . .	35
4.4	Gas collection setup . . . . .	35
<b>5</b>	<b>Setup components</b>	<b>37</b>
5.1	Gas drying components . . . . .	37
5.1.1	Nafion unit . . . . .	37
5.1.2	Ascarite Trap . . . . .	40
5.2	Leak-reduced pump . . . . .	41
5.3	External gases used . . . . .	42
5.3.1	Standard gasses and calibration . . . . .	44
<b>6</b>	<b>Mono-Culture experiment</b>	<b>48</b>
6.1	Nitrification bacteria experiment . . . . .	48
6.2	Denitrification bacteria experiment . . . . .	50
6.3	Validation of mono-culture experiments . . . . .	54
<b>7</b>	<b>Incubation experiment</b>	<b>56</b>
7.1	Experimental description . . . . .	56
<b>8</b>	<b>Field experiment at Buresoe</b>	<b>59</b>
8.1	Site description and location . . . . .	59
8.2	Experimental description and results . . . . .	60
<b>9</b>	<b>Field experiments at Disko Island</b>	<b>62</b>
9.1	Site description and location . . . . .	62
9.2	Experimental description and results . . . . .	63
9.2.1	Dry snow-fence site . . . . .	64
9.2.2	Wet snow-fence site . . . . .	66
9.2.3	Transportation of Nitrous Oxide . . . . .	67
9.2.4	Arctic active layer production . . . . .	69
<b>10</b>	<b>Discussion</b>	<b>71</b>
<b>11</b>	<b>Conclusions</b>	<b>77</b>
<b>12</b>	<b>Outlook</b>	<b>79</b>

<b>Bibliography</b>	<b>80</b>
<b>Appendices</b>	<b>86</b>
<b>A Abbreviation</b>	<b>87</b>
<b>B Derivation of Beer-Lambert's law</b>	<b>89</b>
<b>C Atmospheric air measurements at Disko</b>	<b>90</b>
<b>D Dry snow-fence site experiment plots</b>	<b>91</b>
<b>E Active layer experiment plots</b>	<b>95</b>



## Introduction

### 1.1 Motivation

Nitrous oxide ( $\text{N}_2\text{O}$ ) is an important greenhouse gas. Today (2005) the atmospheric concentration is approximately  $319 \pm 0.12$  ppb. The concentration has increased by 49 ppb (from 270 ppb) since 1750. This is an approximate linear increase of  $0.26 \text{ \% yr}^{-1}$ . This increased concentration has resulted in an increased radiative forcing (RF) of  $0.16 \pm 0.02 \frac{\text{W}}{\text{m}^2}$ . Today only  $\text{CH}_4$  and  $\text{CO}_2$  have a larger RF than  $\text{N}_2\text{O}$ . [14]

The sources of  $\text{N}_2\text{O}$  is well known to be primarily through nitrification and denitrification in terrestrial ecosystems and in the oceans. High resolution measurements of the isotopic composition have been proven to create opportunities for identifying the sources of  $\text{N}_2\text{O}$ . The first entire atmospheric  $\text{N}_2\text{O}$  concentration profile was presented by Schilt et al., 2010 [43]. Schilt et al., 2010 show increasing  $\text{N}_2\text{O}$  concentrations long before the offset of dramatic changes in the climate. It has been suggested that  $\text{N}_2\text{O}$  emissions are dominated at low latitudes. The NEEM drilling project has resulted in another  $\text{N}_2\text{O}$  concentration profile. So far no continuous measurements of the isotopic composition of  $\text{N}_2\text{O}$  have been measured.

The purpose of this project is to conduct continuous  $\text{N}_2\text{O}$  measurements with the prototype of the Picarro G5101-i analyzer. Through high-finesse Cavity Ring-Down Spectroscopy measurements this instrument measures both the concentration and the isotopic composition of  $\text{N}_2\text{O}$  gasses.

In this thesis different mono-cultures will be measured continuously through the production and destruction of  $\text{N}_2\text{O}$ . These measurements will be a verification of the previous measurements presented by Park et al., 2011 [37].

Continuous measurements will also be conducted of natural soil and permafrost. Two experiments will possibly be presented with ecosystems at locations in Denmark. One location

will be on Disko Island (Greenland) where multiple experiments take place.

All of the experiments presented in this thesis are the first steps to the ultimate objective. This ultimate objective is to conduct continuous measurements of the deep ice cores. Thereby, investigation of the signatures of the past and present atmosphere will hopefully lead to a better understanding of the changes in  $N_2O$ .

## 1.2 Climate history

It is a known fact, that the climate on Earth has always oscillated between glacial periods and warm periods. The Earth-Sun relation is the primary source for the temperature oscillations on Earth. The fluctuating factors are the variations of the Earth's orbital motion and rotation. The three phenomena of interest are the periods of precession, obliquity and eccentricity. These phenomena are the cause of periodic changes in solar insolation on Earth, at rates of 23.000 yr, 41.000 yr and 100.000 yr respectively [21]. These periodic variations are known and can be measured. However, they cannot explain every climatic event. Inside the atmosphere the climate system is considered a complex system. Interactions between different components can generate non-linear dynamics and events. Two examples of such events are the El Niño and the Dansgaard-Oeschger (DO) events [6] [10]. In the northern hemisphere the DO events show a rapid warming followed by a slower cooling. The DO events have been found in both the northern and the southern hemisphere, through measurements of atmospheric concentrations of methane [4].

The polar ice cores have proven to be very important climate archives. Recent measurements have shown information from the past approx. 130.000 yrs in Greenland (NEEM ice core [9]) and approx. 800.000 yrs in Antarctica (Dome C ice core [23]). These long archives are acquired through ice core drilling projects. One example of these drilling projects is the NEEM project. At NEEM a 2540 m long core was acquired from 2008-2012. [9]

It is possible to gain knowledge and reconstruct the past atmospheric concentrations of greenhouse gases by analyzing ice cores. A reconstruction of the well established North-GRIP core is presented in figure 1.1.

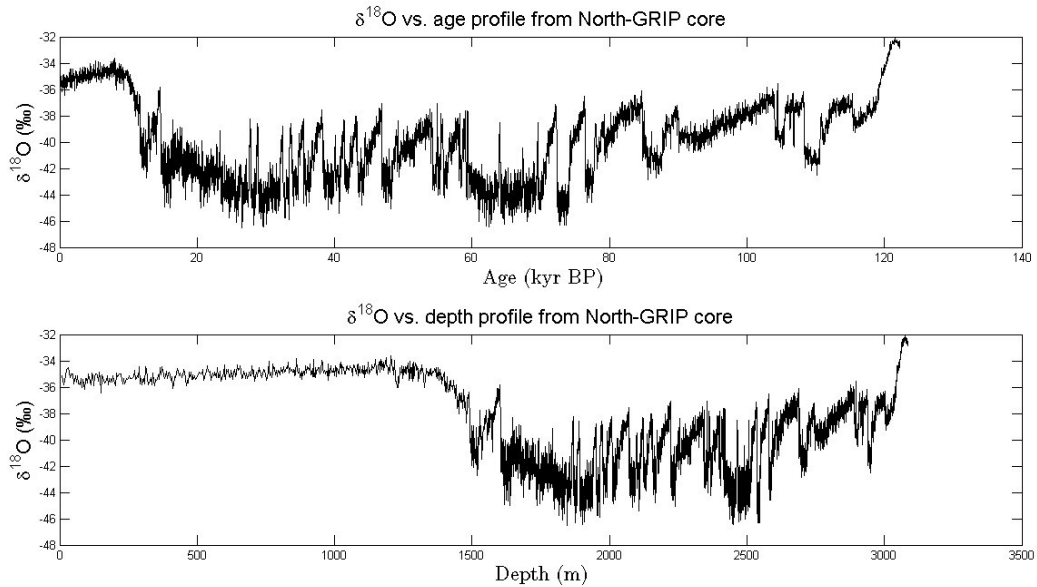


Figure 1.1: *Reconstruction of the  $\delta^{18}O$  concentrations acquired from the North-GRIP ice core drilling project. The top figure shows the change in  $\delta^{18}O$  concentrations over time. The lower figure shows the change in  $\delta^{18}O$  concentrations as a function of depth.[1]*

In this figure, the  $\delta^{18}O$  concentrations are plotted versus the GICC05modelext (extended merging Greenland Ice Core Chronology 2005) time scale and the depth-profile respectively. The data used is 20 year means of  $\delta^{18}O$  data from North-GRIP. The corresponding time scale is going back to 123 kyr BP, and a depth of 3085 m. [1]. The plotted time scale represents the last glacial period, and the first part of the last interglacial (Eemian time period). From both of the plotted profiles the climatic variations are clearly seen over this glacial period.

## Background theory

The main focus in this work is the isotopic composition of nitrous oxide. Nitrous oxide is a greenhouse gas consisting of stable isotopes. Nitrous oxide is primarily produced by nitrification and denitrification processes. In the following chapter the background theory for this is presented.

### 2.1 Stable isotopes

In climate research one of the most important elements are the stable isotopes. Isotopes are the name of a group of the same element having different numbers of neutrons and thus different masses. These are therefore called the isotopes of the atom (for example Nitrogen). In nature most of the elements are unstable, which means that the isotopes over time will go through a radioactive decay into other isotopes. The special - and for climate researchers very important - difference between the appearance of stable and unstable isotopes is that stable isotopes do not decay and they are therefore possible to trace over time. The stable isotopes provide an opportunity for researchers to track the specific isotopes back in time not only to their origin, but also to their sources and their chemical cycle path. This is done by using measurements of the molar concentration ratios and the fractionation processes of the "life" stories of the different isotopes.

The isotopes of different elements do not appear equally in nature. In table 2.1 the most abundant stable isotopes of relevance to climate researchers are given. [27]

The difference in abundance depends on the location in which the ratio is measured. The isotopic ratios are usually small numbers. In equation 2.1 the quantification of the isotopic ratio is calculated by the molar concentration ratio.

$$R_A = \frac{A}{B} \quad (2.1)$$

In this equation,  $A$  is the molar concentration of the less abundant isotope (e.g.,  $^{15}\text{N}$ ).  $B$  is

Element	Isotopic abundance in percent			
<b>Hydrogen</b>	$^1\text{H} : 99.985$	$^2\text{H} : 0.015$	$^3\text{H} : 10^{-3} - 10^{-17}$	
<b>Carbon</b>	$^{12}\text{C} : 98.89$	$^{13}\text{C} : 1.11$	$^{14}\text{C} : 1.2 \cdot 10^{-10}$	
<b>Nitrogen</b>	$^{14}\text{N} : 99.63$	$^{15}\text{N} : 0.37$		
<b>Oxygen</b>	$^{16}\text{O} : 99.759$	$^{17}\text{O} : 0.204$	$^{18}\text{O} : 0.037$	
<b>Sulfur</b>	$^{32}\text{S} : 94.93$	$^{33}\text{S} : 0.76$	$^{34}\text{S} : 4.29$	$^{36}\text{S} : 0.02$

Table 2.1: Important stable isotopes and their mean global abundance percentage

the molar concentration of the abundant isotope (e.g.,  $^{14}\text{N}$ ). The isotopic ratios are typically very small and difficult to calculate in absolute. Therefore it is convenient to express the absolute ratio with respect to a reference. This value is written as a  $\delta$ -value and it is given in parts per thousand (‰). [27]

$$\delta R_{\text{sample}} = \left( \frac{R_{\text{sample}}}{R_{\text{reference}}} - 1 \right) \cdot 1000 [\text{‰}] \quad (2.2)$$

The reference standards used to calculate these ratios are calculated and provided by international agencies, for example the International Atomic Energy Agency (IAEA). The standards for the five isotopes listed in table (2.1) are:

	Accepted ratio	International scale
<b>Hydrogen</b> $\left( \frac{[^2\text{H}]}{[^1\text{H}]} \right)$	$155.75 \cdot 10^{-6}$	VSMOW
<b>Carbon</b> $\left( \frac{[^{13}\text{C}]}{[^{12}\text{C}]} \right)$	$11180.2 \cdot 10^{-6}$	VPDB
<b>Nitrogen</b> $\left( \frac{[^{15}\text{N}]}{[^{14}\text{N}]} \right)$	$3678.2 \cdot 10^{-6}$	AIR-N <sub>2</sub>
<b>Oxygen</b> $\left( \frac{[^{18}\text{O}]}{[^{16}\text{O}]} \right)$	$2005.2 \cdot 10^{-6}$	VSMOW
	$2067.2 \cdot 10^{-6}$	VDPB
<b>Sulfur</b> $\left( \frac{[^{32}\text{S}]}{[^{34}\text{S}]} \right)$	$44150.9 \cdot 10^{-6}$	VCDT

Table 2.2: Absolute isotope ratios from the international Vienna Standards [56]

### 2.1.1 Fractionation

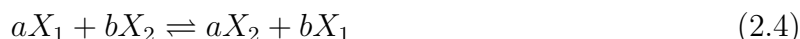
The isotopic composition of a given molecule can in principle be altered by any biogeochemical process, compared to its original composition. The processes needed to alter the isotopes are called fractionation. The general fractionation factor is given in equation 2.3.

This fractionation factor is defined as a convenient way to calculate the ratio between two isotope ratios of chemical components ( $A$  and  $B$ ) of a molecule. [28]

$$\alpha_{A/B} = \frac{R_A}{R_B} \quad (2.3)$$

Fractionation processes can be divided into different categories. The three most important ones are: equilibrium isotope fractionation, kinetic isotope fractionation and the mass-independent isotope fractionation. The two first types of fractionation are both mass-dependent, and differ by their process mechanisms.

**Equilibrium isotope fractionation** occurs when a chemical reaction is in an equilibrium state, in which two molecules are reacting with each other and thereby exchanging both the heavy and the light isotopes. In principle such a reaction looks like:



In this equation, the two molecules are expressed as  $aX$  and  $bX$ .  $X$  represents the fractionating isotopes, and the subscripts  $_1$  and  $_2$  represent the light isotope and the heavy isotope respectively. This reaction makes it possible to calculate the equilibrium isotope fractionation factor, which is equal to the equilibrium constant ( $K_{eq}$ ). This factor is defined as the ratio of the isotope ratios for the two substances  $aX$  and  $bX$  where  $X$  represents the number of isotopes indicated. [61]

$$K_{eq} = \alpha^{a-b} = \frac{\left(\frac{X_2}{X_1}\right)_a}{\left(\frac{X_2}{X_1}\right)_b} \quad (2.5)$$

**Kinetic isotope fractionation** is defined as the process in which a single step divides the isotopes by their masses, through a unidirectional reaction. This reaction is irreversible and it happens in an infinitely short amount of time. Such a reaction could in theory be as simple as the reaction from a substrate to a product:



Without looking further into the reaction order or the specific mechanisms going on during this reaction, the kinetic fractionation factor can be solved. The kinetic fractionation factor is denoted by  $\alpha_{p/s}$  and is given by:

$$\alpha_{p/s} = \frac{R_p}{R_s} \quad (2.6)$$

where  $R_p$  is the isotope ratio of the growth of the product, and  $R_s$  is the isotope ratio of the substrate. The kinetic fractionation factor for nitrogen fractionation is for example:

$$\alpha_{p/s} = \frac{d^{15}N_p/d^{14}N_p}{^{15}N_s/^{14}N_s}$$

A more convenient way to express the fractionation factor is the "per mil enrichment factor" given as: [30]

$$\epsilon_{p/s} = (\alpha_{p/s} - 1) \cdot 1000[\text{‰}] = \left( \frac{R_p}{R_s} - 1 \right) \cdot 1000[\text{‰}] \quad (2.7)$$

An example of a kinetic fractionation could be the evaporation of seawater to clouds. During this process the oxygen-isotopes are fractionated. The oxygen isotopes in the water are a mixture of the three isotopes  $^{16}\text{O}$ ,  $^{17}\text{O}$  and  $^{18}\text{O}$ . The lighter  $^{16}\text{O}$  molecules evaporate easier than the  $^{18}\text{O}$  molecules. This means that a fractionation occurs, and the clouds become enriched with  $^{16}\text{O}$  molecules, and the seawater becomes enriched with  $^{18}\text{O}$  molecules.

The mechanism resulting in **the mass-independent isotope fractionation** has so far not been clearly defined, and the exact processes involved therefore remain questionable. So far only parts of the full set of mechanisms have been proven. Some examples of processes accounting for parts of the mass-independent isotope fractionation are, the effect of UV photolysis, stratospheric photolysis and the symmetry of the isotopomers.

The results of the mass-independent isotope fractionation have, among others, been observed in  $\text{O}_3$  and  $\text{N}_2\text{O}$ . [49] [36]

## 2.2 Nitrous Oxide

Nitrous oxide is an important greenhouse gas in the atmosphere of the Earth. At room temperature nitrous oxide is a colorless non-flammable gas with a slightly sweet smell and taste. Nitrous oxide is commonly known as one of the gasses used by doctors and dentists to give to their patients before performing a surgery. The euphoric effects a person gets when inhaling nitrous oxide (on gas form) are obtained because of its anesthetic and analgesic effects. This is also the reason for the non-professional name "Laughing gas".

Nitrous oxide is an asymmetric chemical linear three-atom molecule consisting of one oxygen-atom and two nitrogen-atoms. The chemical formula of nitrous oxide is  $\text{N}_2\text{O}$ . This molecule has one nitrogen atom (N) at the center position and one at the terminal (end) position and an oxygen atom at the other end.

Since nitrous oxide is an asymmetric linear molecule it can exist in 12 different isotopic configurations, due to the two different nitrogen atoms and the three different oxygen atoms. However, this does not mean that all of the isotopic configurations

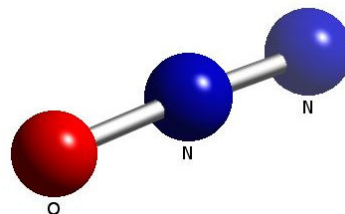


Figure 2.1: *The molecular composition of  $\text{N}_2\text{O}$*

are equally appearing in nature. The most common configurations of nitrous oxide are  $^{14}\text{N}^{14}\text{N}^{16}\text{O}$ ,  $^{14}\text{N}^{15}\text{N}^{16}\text{O}$ ,  $^{15}\text{N}^{14}\text{N}^{16}\text{O}$ ,  $^{14}\text{N}^{14}\text{N}^{17}\text{O}$  and  $^{14}\text{N}^{14}\text{N}^{18}\text{O}$  [60]. These five configurations can further be divided into a group of isotopologues and a group of isotopomers.

- **Isotopologues** are defined as a group of chemical species which are distinguished by their isotopic composition. An example of this is water which in the state of light water is  $\text{H}_2\text{O}$ , in the state of semi-light water has substituted one hydrogen atom with a deuterium atom and becomes  $\text{HDO}$  and in the state of heavy water consists of two deuterium isotopes  $\text{D}_2\text{O}$ . [17]
- **Isotopomers** are defined as a group of chemical species with an identical number of each isotope. The chemical species are then distinguished by the allocation of the atoms. An example of this could be  $\text{CH}_3\text{NHD}$  and  $\text{CH}_2\text{DNH}_2$ . [17]

The area of interest in the work presented in this thesis, is the group of the isotopomers, or more precisely  $^{14}\text{N}^{15}\text{N}^{16}\text{O}$  and  $^{15}\text{N}^{14}\text{N}^{16}\text{O}$ . These two molecules can be distinguished by the position of the  $^{15}\text{N}$  atom. The  $^{15}\text{N}$  atom can either be at the center or at the end of the molecule. This differentiation gives rise to one very interesting thing about these two isotopomers. A scientific hypothesis states that the isotopic composition depends on which of two microbial processes that produced the molecule (see section 2.2.2).

### 2.2.1 Terminologie of the isotopomers

Different terminologies are used in order to distinguish the  $\text{N}_2\text{O}$  isotopomers from each other. The most common terminologies used when the  $^{15}\text{N}$  atom is at the center of the  $\text{N}_2\text{O}$ -molecule are:

Molecule formula	Kaiser et al. 2002 [24]	Yoshida et al. 2000 [60]	$^{15}\text{N}$ position
$^{14}\text{N}^{15}\text{N}^{16}\text{O}$	$^1\delta^{15}\text{N}$	$\delta^{15}\text{N}^\alpha$	Central

The terminology used when the  $^{15}\text{N}$  atom is placed in the end of the  $\text{N}_2\text{O}$ -molecule is:

Molecule formula	Kaiser et al. 2002 [24]	Yoshida et al. 2000 [60]	$^{15}\text{N}$ position
$^{15}\text{N}^{14}\text{N}^{16}\text{O}$	$^2\delta^{15}\text{N}$	$\delta^{15}\text{N}^\beta$	Terminal

From this point, the terminology used in this thesis will be that used by Yoshida et al., 2000 ( $\alpha$  and  $\beta$ ).

From the definition of the absolute isotopic ratio, as shown in section 2.1, the ratio of  $^{15}\text{N}^\alpha$  is given in equation 2.8 and the ratio of  $^{15}\text{N}^\beta$  in equation 2.9.

$$^{15}\text{R}^\alpha = \frac{[^{14}\text{N}^{15}\text{N}^{16}\text{O}]}{[^{14}\text{N}^{14}\text{N}^{16}\text{O}]} \quad (2.8)$$

$$^{15}\text{R}^\beta = \frac{[^{15}\text{N}^{14}\text{N}^{16}\text{O}]}{[^{14}\text{N}^{14}\text{N}^{16}\text{O}]} \quad (2.9)$$

The  $\delta$ -values of  $\alpha$  and  $\beta$  are given in equations 2.10 and 2.11 in parts per thousand [‰].

$$\delta^{15}\text{N}^\alpha = \left( \frac{^{15}\text{R}_{sample}^\alpha}{^{15}\text{R}_{std}^\alpha} - 1 \right) \times 1000 \quad (2.10)$$

$$\delta^{15}\text{N}^\beta = \left( \frac{^{15}\text{R}_{sample}^\beta}{^{15}\text{R}_{std}^\beta} - 1 \right) \times 1000 \quad (2.11)$$

### 2.2.2 Intramolecular distribution of the nitrogen-15

There are two known ways of representing the determined intermolecular distribution of the nitrogen-15 ( $^{15}\text{N}$ ) atom. There are therefore also at least two ways to trace the geochemical cycle of  $\text{N}_2\text{O}$ .

The first representation of the isotope distribution is  $\alpha$  and  $\beta$  (the terminologies of the two isotopomers are introduced in section 2.2.1). The second representation is the site preference (SP) and bulk. The SP is a notation for the result of a measurement of the isotopic ratio, and it is given as the difference between the relative abundance of  $^{15}\text{N}$  at either the  $\alpha$ - or the  $\beta$ -position [53].

$$\delta^{15}\text{N}^{SP} = \delta^{15}\text{N}^\alpha - \delta^{15}\text{N}^\beta \quad (2.12)$$

According to the study by Yoshida and Toyoda [60] there is a tendency for a higher site preference in the stratosphere. This is due to a loss of  $\text{N}_2\text{O}$  because of fractionation during the ultraviolet photolysis. The lower site preference in the troposphere is (on the other hand) due to the local emission of  $\text{N}_2\text{O}$  from fossil fuel combusting and soils.

The study by Park et al., 2011 [37] indicates that there is a direct relation between SP and the source of the  $\text{N}_2\text{O}$  production. Park et al., 2011, shows that there is a potential for identifying soil microbial processes of  $\text{N}_2\text{O}$  by the SP. The measurements on which this conclusion is made upon, are shown in figure 2.2. The figure shows the primary indications of the intermolecular distribution of  $^{15}\text{N}$  is being decided by the microbial process.

The indication from the figure is that when the SP is between -10 and 0, the preferred process is **the denitrification process** (as described in section 2.3.2). This means that

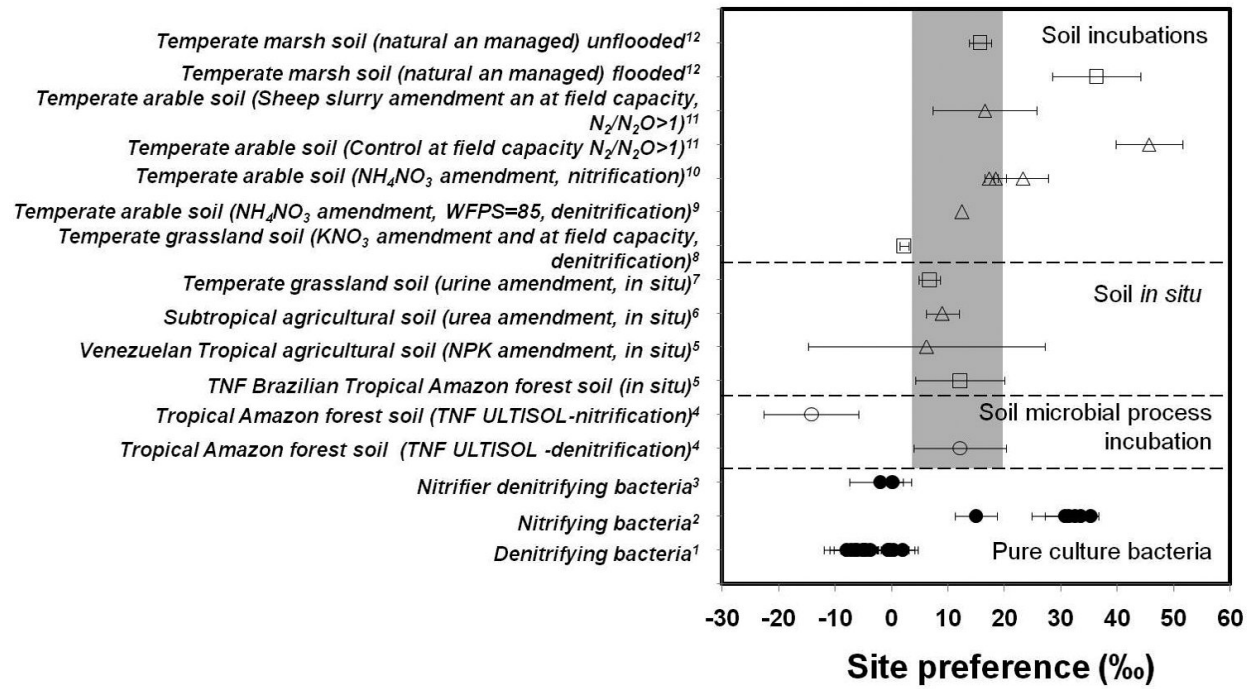


Figure 2.2: Site preference measurement from multiple different experiments with, mono bacterial streams, soil incubation, and in situ emissions. For this studie the most important results are the two in the bottom. These results represents the measurements of mono bacteria cultures (nitrification and denitrification). References can be found in the original paper by Park et al., 2011 [37]

the preferred intermolecular displacement of the heavy isotope is at the  $\beta$ -position. On the other hand is the indication that when SP is above 25, then the preferred process is **the nitrification process** (as described in section 2.3.1). These SP values mean that the preferred intermolecular displacement of the heavy isotope is at the  $\alpha$ -position.

The bulk nitrogen isotope ratio [51][52] is given as

$${}^{15}\text{R}^{bulk} = \frac{({}^{15}\text{R}^{\alpha} + {}^{15}\text{R}^{\beta})}{2}.$$

Using the equation above for  ${}^{15}\text{R}^{bulk}$  to substitute into the  $\delta$ -equation (equation 2.2), gives the bulk nitrogen isotope ratio.

$$\delta^{15}\text{R}^{bulk} = \left( \frac{{}^{15}\text{R}^{bulk}}{{}^{15}\text{R}_{(Standard)}^{bulk}} - 1 \right) \times 1000 \quad (2.13)$$

This equation can be approximated as

$$\delta^{15}\text{R}^{bulk} = \frac{\delta^{15}\text{N}^{\alpha} + \delta^{15}\text{N}^{\beta}}{2}. \quad (2.14)$$

The bulk value is the average ratio of the two isopomer ratios. The bulk value is a convenient

quantity i.e., since it is equal to the conventional nitrogen isotope ratio of  $N_2O$ , which itself does not distinguish isotopomers that contain  $^{15}N$ . [51]

### 2.2.3 Sources of nitrous oxide

There are multiple different sources of  $N_2O$  of both natural and anthropogenic nature. An overview of the sources of  $N_2O$  is shown in table 2.3.

Natural sources	Emission [TgN/yr]	Uncertainty [TgN/yr]
Soil microbial production	5.2	2.6 - 7.8
Grasslands	1.4	0.7 - 2.1
Background emissions arable land	0.9	0.4 - 1.4
Oceans	3.6	2.8 - 5.7
Atmospheric chemistry	0.6	0.3 - 1.2
Total natural sources	11.7	6.8 - 18.2
Anthropogenic sources	Emission [TgN/yr]	Uncertainty [TgN/yr]
Fossil fuel incl. aircraft	0.2	0.1 - 0.5
Industrial processes	0.3	0.1 - 0.5
Animal excreta	1.0	0 - 2
Synthetic fertilizer on arable land	1.0	0.3 - 2.3
Biomass burning	0.7	0.4 - 1.0
Agricultural soils	3.3	0.6 - 14.8
Total anthropogenic sources	6.5	1.5 - 21.1
<b>Total emission</b>	<b>18.2</b>	<b>8.3 - 39.3</b>

Table 2.3:  $N_2O$  natural and anthropogenic sources according to Mosier et al., 1998 [33] and Olivier et al., 1998 [34].

The main source is the microbial process of nitrification and denitrification, in natural aquatic and terrestrial systems, as explained in section 2.3.1 and 2.3.2 respectively. The main anthropogenic source of  $N_2O$  is agriculture. Mosier et al., 1998 explains that an increase of the nitrogen (N) minerals have enhanced the production of  $N_2O$ , as a course of an addition of fertilizers including these N minerals [33]. This explanation was confirmed by Forster et al., 2007, who states that "The primary driver for the industrial era increase of

N<sub>2</sub>O was concluded to be enhanced microbial production in expanding and fertilized agricultural lands.” [14]

The microbial processes emitting N<sub>2</sub>O can be identified through SP (as shown in figure 2.2). Research has shown that oceanic, terrestrial and other sources of N<sub>2</sub>O can be distinguished by SP-values. The terrestrial sources are presented in figure 2.2. Experiments have further been made with automobile and oceanic sources. N<sub>2</sub>O from automobiles has been characterised by  $\delta^{15}\text{N}^{bulk}$  values at  $-4.9 \pm 8.2 \text{ ‰}$ , SP values at  $12.2 \pm 9.1 \text{ ‰}$  and  $\delta^{18}\text{O}$  values at  $43.5 \text{ ‰}$  [52]. Oceanic N<sub>2</sub>O have been characterised by SP values at  $18.3 \text{ ‰}$ , bulk values at  $7.0 \text{ ‰}$  and  $\delta^{18}\text{O}$  values at  $14.5 \text{ ‰}$  for surface mixed layers [40] [11].

One should notice that all SP values presented are within the SP-range of nitrification and denitrification. For terrestrial nitrification the average values are  $\text{SP} = 33 \text{ ‰}$ ,  $\delta^{15}\text{N}^{bulk} = 0.9 \text{ ‰}$  and  $\delta^{18}\text{O} = 11.3 \text{ ‰}$ . For terrestrial denitrification the average values are  $\text{SP} = 0.1 \text{ ‰}$ ,  $\delta^{15}\text{N}^{bulk} = -23 \text{ ‰}$  and  $\delta^{18}\text{O} = -12.4 \text{ ‰}$ . [48]

## 2.2.4 Sink of nitrous oxide

Once N<sub>2</sub>O is produced, it has been found to have a lifetime of at least 114 years in the environment. When the N<sub>2</sub>O-gasses are released into the environment, they will be removed by a number of reactions in the stratosphere. The chemical decomposition done by the action of light (also called photo dissociation or photolysis) is accounting for 90 % of the total sink of N<sub>2</sub>O in the atmosphere. The photolysis is done through the reaction described in equation 2.15:



The last 10% of the sink is lost through the photo-oxidation reaction as shown in equation 2.16 and 2.17.



In these equations O(<sup>1</sup>D) is an expression for an O atom in an excited state, and  $h\nu$  is an expression for the energy of the light reacting with atom.[14]

Reaction 2.16 has a particular role in the atmospheric chemistry. This reaction is the largest natural source of NO (otherwise known as odd nitrogen)[58]. A production of NO in the upper stratosphere can enhance the destruction of ozone (O<sub>3</sub>) through reaction 2.18 and 2.19.



These two reactions result in the following net reaction, in which only ozone and oxygen react, leaving the odd nitrogen out of the equation.[58]



A significant imbalance between produced  $N_2O$  (natural and anthropogenic) and destruction in the stratosphere was presented by Kim and Craig, 1993 [25]. The imbalance is due to the heavy  $N_2O$  in the troposphere. These  $N_2O$  molecules are enriched in both  $^{15}N$  and  $^{18}O$  compared to both stratospheric and terrestrial/ oceanic produced  $N_2O$ . The conclusion to this imbalance is that a large back-mixing flux from the stratosphere has happened after enrichment by photolysis and chemistry.

This back-mixing flux can be described by the standard Rayleigh fractionation. The Rayleigh fractionation provides a relation between the isotopic enrichment and the fractionation. An approximation of the Rayleigh equation is presented in equation 2.21.

$$\delta = \delta_0 + \epsilon \times \ln(f) \quad (2.21)$$

In this equation  $\delta$  and  $\delta_0$  are the remaining and initial heavy-to-light isotope ratio respectively.  $\epsilon$  is the enrichment factor which can be denoted  $\epsilon = (\alpha_R - 1)$  ( $\alpha_R$  is the fractionation coefficient).  $f$  is the fraction of the remaining  $N_2O$ . Rahn et al., 1997 [41] presents derived enrichment factors of  $\epsilon = -14.5 \text{ ‰}$  for  $^{15}N$  and  $\epsilon = -12.9 \text{ ‰}$  for  $^{18}O$ .

All of the produced  $N_2O$  does not get out of the soil before it is used and converted. The  $N_2O$  not leaving the soil is used in the denitrification and nitrifier denitrification processes in the creation of  $N_2$ , as described in section 2.3.2 and 2.3.3 respectively.

## 2.3 Production of nitrous oxide

There are three primary biological pathways causing the nitrogen loss in the ecosystem. These pathways are converting different nitrogen compounds into gaseous nitrogen which can then be emitted from the soils and into the atmosphere as ammonia gas, di-nitrogen, nitric oxide and nitrous oxide. The three pathways are Ammonia volatilization, nitrification and denitrification. The work presented in this thesis is concentrated on the nitrification and the denitrification processes, since these are the ones leading to  $N_2O$  production.

### 2.3.1 Nitrification

Nitrification is the biological process in which ammonium ( $NH_4^+$ ) is oxidized with oxygen ( $O_2$ ) first into nitrite ( $NO_2^-$ ) and then into nitrate ( $NO_3^-$ ). Effectively the process is a loss

of electrons from the nitrogen atom to the oxygen atom. This nitrification is an important process in the soil, when undergoing the nitrogen cycle.

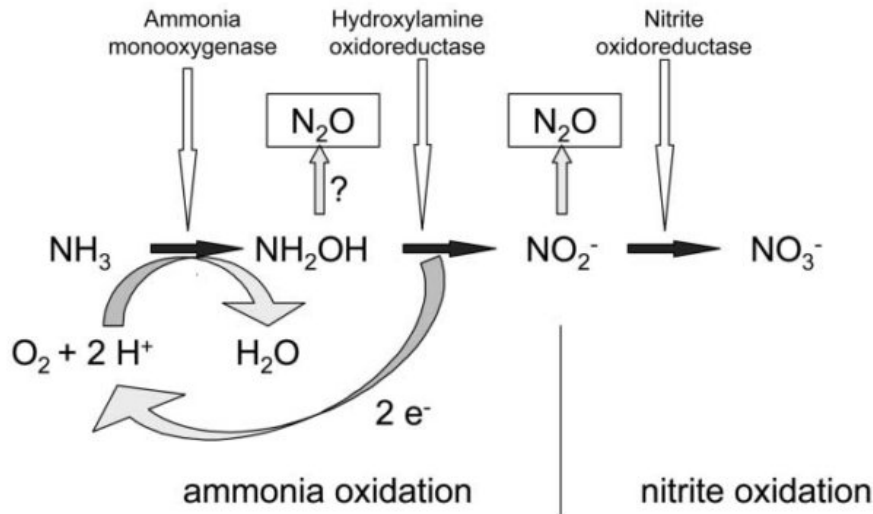
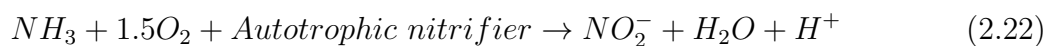


Figure 2.3: Outline of the nitrification pathways [59].

The nitrification process is an aerobic process which is carried out by Autotrophic nitrifiers (the dominating nitrifier) and Heterotrophic nitrifiers respectively. The Heterotrophic nitrifiers obtain energy from destruction of organic matter. Autotrophic nitrifiers are bacteria which use the energy gained from the  $\text{NH}_4^+$  oxidation to fix carbon, comparable to the way solar energy is used in photosynthesis. The autotrophic nitrifiers can be divided into two groups, depending on which oxidation they are "responsible" for. The nitrifiers converting  $\text{NH}_4^+$  to  $\text{NO}_2^-$  are known by starting their name with "Nitroso-", while the nitrifiers converting  $\text{NO}_2^-$  to  $\text{NO}_3^-$  have "Nitro-" as the beginning. Only nitrifiers of the "Nitroso-" group are used in the work presented here. The autotrophic nitrifier nitrification process is listed in equation 2.22.



Prior to this equation  $\text{NH}_4^+$  is converted into  $\text{NH}_3$ . For this project the interesting part is the production of  $\text{N}_2\text{O}$ .  $\text{N}_2\text{O}$  is produced during a nitrification process, as a chemical decomposition. The  $\text{N}_2\text{O}$  is produced as a bi-product from both  $\text{NH}_2\text{OH}$  and  $\text{NO}_2^-$ .

During the work presented here two different nitrifying bacteria were used. The two autotrophic nitrifiers used are called *Nitrosospira multififormis* and *Nitrosomonas europaea* respectively. [59] [20]

### 2.3.2 Denitrification

Denitrification is the biological process in which a stepwise reduction of  $\text{NO}_3^-$  first to  $\text{N}_2\text{O}$  and then to  $\text{N}_2$  takes place. During anaerobic conditions the denitrification bacteria use  $\text{NO}_3^-$  instead of oxygen as an electron acceptor in the respiration of organic matter.

The full denitrification process is:

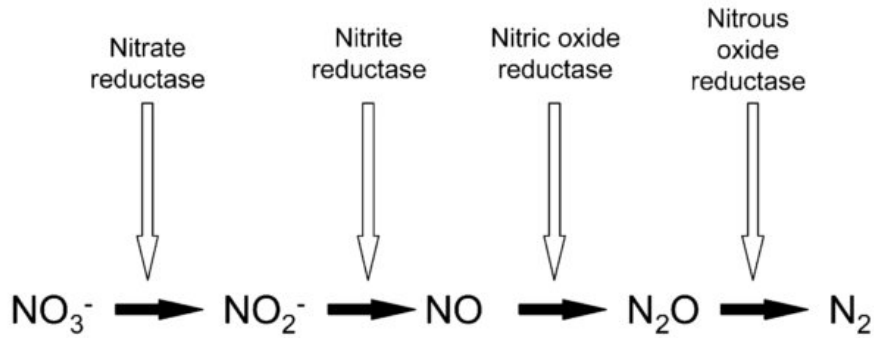
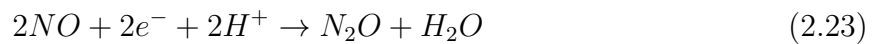


Figure 2.4: Outline of the denitrification pathways [59].

In comparison to the nitrification processes,  $\text{N}_2\text{O}$  is a natural and regular intermediate in the production of a nitrogen ( $\text{N}_2$ ) gas. The obligatory intermediate process of producing  $\text{N}_2\text{O}$  is primarily caused by the nitric oxide ( $\text{NO}$ ) as can be seen in equation 2.23.



In order for the denitrification process to happen it is conditional that the oxygen concentration is low, that the nitrate concentration is high and that an organic carbon supply is available. [59] and [20]

During the experiments described in this thesis, two different cultures of denitrifying bacterias were used. These two cultures are *Pseudomonas Flourescens* (culture 1) [7] and *Pseudomonas Chlororaphis* (culture 14) [8].

*Pseudomonas Flourescens* produce  $\text{N}_2\text{O}$  as the biproduct in the process of producing nitrogen ( $\text{N}_2$ ). When all of the nitrate is used by the bacteria, the nitrate reduction has produced only  $\text{N}_2$ .

The production of  $\text{N}_2\text{O}$  during such a process would in theory first lead to increasing concentration of  $\text{N}_2\text{O}$ . Then once all of the  $\text{NO}_3^-$  is used, the concentration of  $\text{N}_2\text{O}$  would decrease again, due to production of  $\text{N}_2$  gasses.[7]

*Pseudomonas Chlororaphis* on the other hand, has  $N_2O$  as the end-product. This bacterial species does not have the enzyme called "Nitrous oxide reductase" which causes the conversion of  $N_2O$  to  $N_2$ . This means that  $N_2O$  is accumulating up to the point when the bacteria becomes inactive (or runs out food). Ideally the concentration and isotope value become constant (like presented figure 2.5). This figure shows the  $N_2O$  production after an addition of  $NO_3^-$  at time zero. From this figure it is clear that the concentration of  $N_2O$  increases

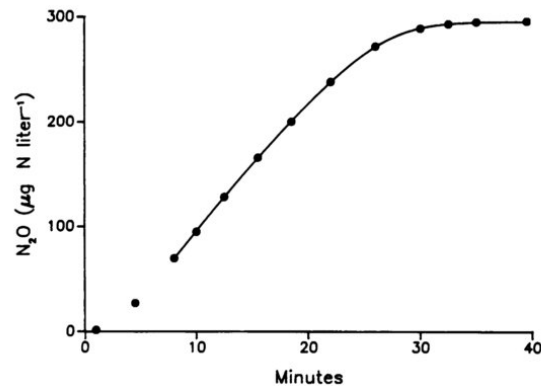


Figure 2.5:  $N_2O$  production rate after addition of  $NO_3^-$  at time 0 [8].

after the addition of  $NO_3^-$ . Once all of the  $NO_3^-$  has been used, the production of  $N_2O$  stops and the concentration stabilizes. [8]

### 2.3.3 Nitrifier denitrification

In order to close the circle of the nitrification and denitrification processes, the process known as nitrifier denitrification also need a short introduction. The nitrifier denitrification process is identified as a nitrification process, but it is a combination of the nitrification followed by denitrification. The difference between this process and the nitrification process, is that nitrifier denitrification only produces  $N_2O$  by reduction of nitrite. The sequence of reactions in a nitrifier denitrification process is carried out by the autotrophic  $NH_3$  oxidizers, as shown in figure 2.6. The nitrifier denitrification process has been found to occur both under anaerobic and aerobic conditions.

Since nitrifier denitrification is somehow a combination of the two basic processes (nitrification and denitrification), there will be no further reference to this process in this thesis.



two isotopically different molecules) of the two NO bonds, in the fractionation process.

The internal displacement caused by NOR-enzymes are not present during the autotrophic nitrifier nitrification. During the autotrophic nitrification process the reactions going from  $\text{NH}_2\text{OH}$  to  $\text{NO}_2^-$  are primarily occurring with help from the enzyme *Hydroxylamine oxidoreductase* (HOR). HOR is at the same time the enzyme responsible for the production of  $\text{N}_2\text{O}$  as shown in figure 2.7. This process is according to Hooper et al., 1979 [18] and McCarty,

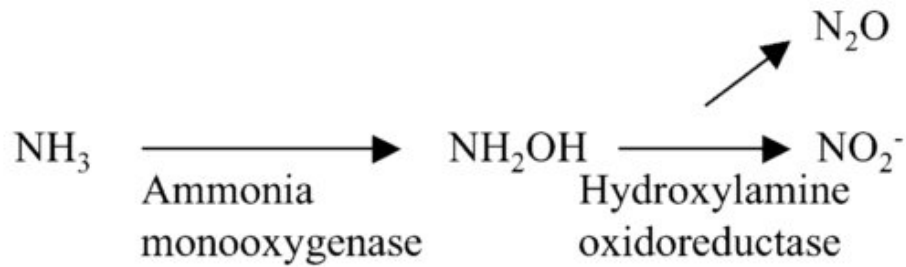


Figure 2.7: *Outline of the nitrification pathways, as done by autotrophic nitrification [47].*

1999 [31] among others, not completely described. Therefore it is not fully understood where exactly the emission of  $\text{N}_2\text{O}$  is originating. It is however agreed that HOR is the primary enzyme involved in the production of  $\text{N}_2\text{O}$ . [31] [18]

## Instrumental theory

A prototype of the Picarro G5101-i analyzer is used to analyze the N<sub>2</sub>O gasses. The background theory of the cavity ring-down spectroscopy used by this Picarro analyzer is presented in this chapter.

### 3.1 Absorption spectroscopy

Absorption spectroscopy is a spectroscopic technique for measuring the absorption of radiation. With absorption spectroscopy it is possible to measure and analyze trace gases. The measurements can be used to determine the concentration of the gasses and to distinguish different isotopologues and isotopomers.

Absorption spectroscopy is a measurement technique where a beam of light with an intensity of  $I_0$  and wavelength  $\lambda$  is passing through a gas filled volume of length  $z$ . Over time the light will be absorbed by the molecules and thereby lower the intensity of the light traversing. This absorption of light intensity is why the theory of absorption spectroscopy is based on Beer-Lambert's law of optical absorption (3.1). The purpose of Beer-Lambert's law is to quantify the absorption a beam of light is experiencing when passing through a volume of gas.

$$I = I_0 e^{-\alpha z} \quad (3.1)$$

In equation 3.1 the transmitted light has the intensity  $I$  given in watt per  $m^2$ . The last variable is the absorption coefficient ( $\alpha$ ) which is most often given in  $cm^{-1}$  ( $\frac{1}{length}$ ). Absorption is the process where radiative energy is transferred to kinetic energy, and the absorption coefficient is a quantification of the magnitude of the absorption per unit length [5]. To learn more about the absorption coefficient we need to go a bit deeper into the physics of the absorption spectroscopy. This will not be discussed further in this thesis, since the focus

of the work presented is on the experiments. A detailed description can be found in the Book by Bohren et al., 2007 [5].

The absorption can only happen at very specific intervals for each absorber gas. These intervals are determined by the corresponding wavelength ( $\lambda$ ) and transition energy between two quantum mechanical energy states. The energy states depend, among other things, on the mass of the atoms in the molecule. This is the reason that different isotopes of a molecule can be distinguished through absorption spectroscopy.

The specific intervals are called absorption lines. These absorption lines have four characteristics: a line position, a line strength (or height), a line shape and a line width. The line strength is proportional to the intensity (or concentration). The line width is proportional to the total pressure.

The line shape is in general terms a normalized non-dimensional function ( $f(x)$ ), resulting in different functions for the absorption coefficient depending on the distribution. The absorption coefficient depends on the frequency, the temperature ( $T$ ), and the pressure ( $p$ ). The line shape is a function of the value of the contribution from one absorption line to the absorption coefficient ( $\alpha$ ):

$$\alpha_G(\nu, p, T) = \frac{I}{\gamma} f\left(\frac{\nu - \nu_c}{\gamma}\right) \quad (3.2)$$

where  $\nu_c$  is the frequency at the center,  $I$  is the intensity,  $\gamma$  is the line width and  $G$  denotes the molecule of interest. This line function is normalized so that the area under the curve is 1. In practice this means that if a line is made broader it will be due to an increase in absorption at the sides and a decrease in absorption at the center. The full Intensity is therefore given as  $I = \int \alpha_G d\nu$ . [39]

The absorption lines are, as mentioned earlier, not always just straight lines. When a molecule is in motion it will experience line broadening from one or more of the following effects: *Pressure broadening*, *Doppler broadening* and *Dampening effect*.

On figure 3.1 the Lorentz broadening (Pressure broadening) and the Doppler broadening is shown in a graphical representation. The figure shows the difference in the effect of the two forms of broadening. Where the Lorentz broadening has the biggest effect at the sides, the Doppler broadening has the strongest effect in the center of the absorption line.

- The Damping effect is considered to be the normal effect, since it happens due to the loss of energy caused by emission from the molecule. Thus it is also known as the natural linewidth. This damping effect is very small when looking at the infrared spectrum.

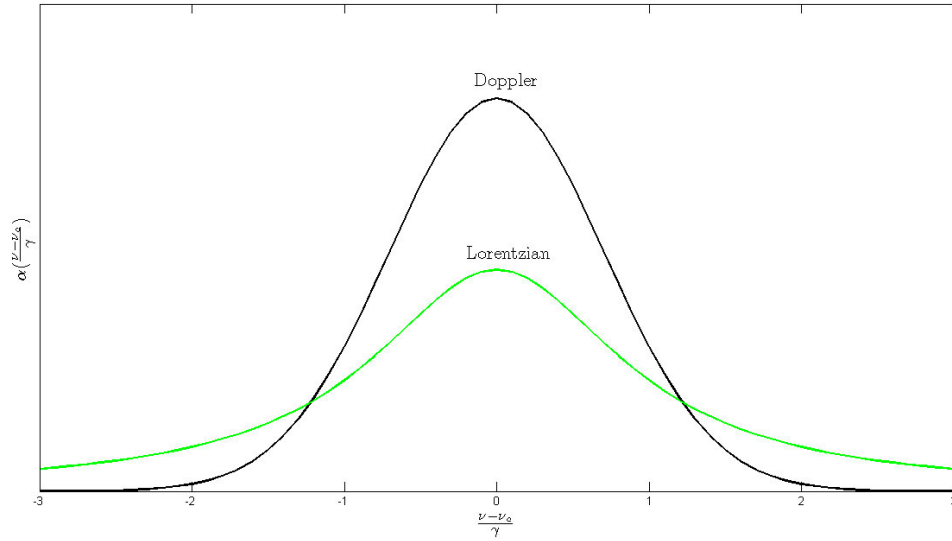


Figure 3.1: *Demonstrative Lorentz and Doppler line shapes for the same intensities and line widths. The profiles are made with a standard normal distribution.*

- The Pressure broadening is also known as the collisional broadening. When two molecules are moving around in the gas and collide, energy is transferred both between the two molecules but also within the individual molecule. This energy transfer may lead to a change in energy level. The change in energy level is leading to a broadening in the absorption lines and can be expressed with the Lorentz profile ( $\alpha_L$ ) (3.3). This profile is given as equation 3.2 where the Lorentz line shape is  $f(x) = \frac{1}{\pi \cdot (1+x^2)}$ .

$$\alpha_L = \frac{I}{\pi} \frac{\gamma_L}{(\nu - \nu_c)^2 + \gamma_L^2} \quad (3.3)$$

This equation calculates the absorption coefficient using the intensity ( $I$ ), the frequency ( $\nu$ ) and the half-width of the line at the half-maximum ( $\gamma$ ) which is given by (3.4)

$$\gamma_L = \gamma_c \frac{p}{p_0} \left( \frac{T_0}{T} \right)^n \quad (3.4)$$

Here  $\gamma_0$  is the width at the standard pressure  $p_0 = 1013$  hPa and temperature  $T_0 = 273$  K,  $p$  is the pressure and  $T$  is the temperature at the measuring position. The index  $n$  is an experimentally found number, which can vary between  $\frac{1}{2}$  and 1 depending on the molecule of interest. The index number is  $n = 0.75$  for  $N_2O$  [15].

Pressure broadening is the most important broadening effect in the lower part of the atmosphere, and therefore the most important line broadening effect in this thesis. [29]

- The Doppler effect is less important in the lower part of the atmosphere. This is because the molecules need to be in thermodynamic equilibrium for the Doppler broadening to take place. Doppler broadening is essentially happening because a molecule will encounter light-beams with higher frequencies when moving towards the source, and lower frequencies when moving away from it, thus leading to possible excitations. The absorption coefficient caused by the Doppler broadening is calculated using the gaussian distribution line shape  $f(x) = \frac{\exp(-x^2)}{\sqrt{\pi}}$  and equation 3.2.

$$\alpha_D = \frac{I}{\gamma_D \sqrt{\pi}} \exp \left[ - \left( \frac{\nu - \nu_c}{\gamma_D} \right)^2 \right] \quad (3.5)$$

In which the Doppler line width is

$$\gamma_D = \nu_0 \left( \frac{2k_B T}{mc^2} \right)^{\frac{1}{2}}, \quad (3.6)$$

and  $k_B$  is the Boltzmann constant, and  $m$  is the mass of the molecule. [29][39]

When making figures of the absorption spectroscopy, it is often more convenient to use the wavenumber  $\tilde{\nu}$ , which is defined as  $\tilde{\nu} = 1/\lambda$  [29].

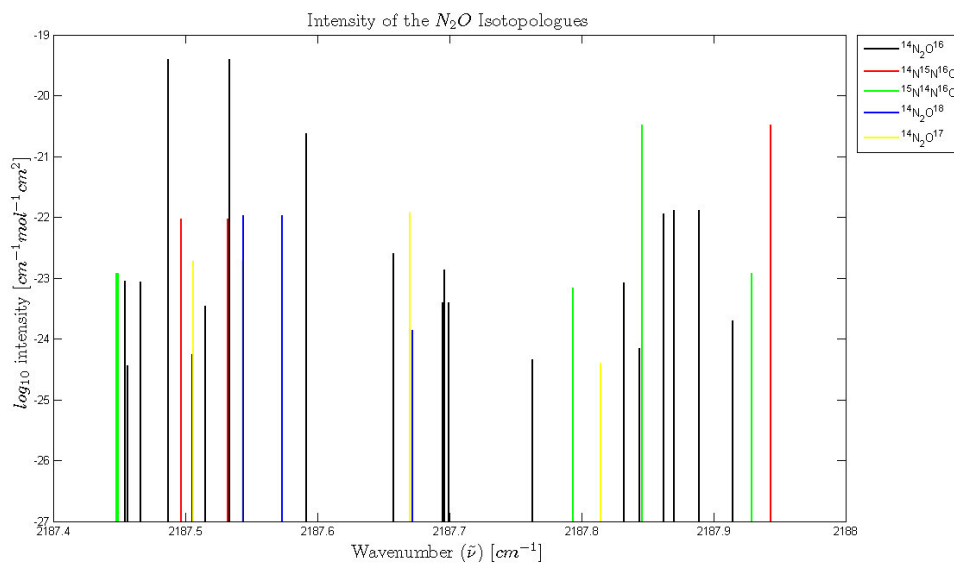


Figure 3.2: *The transition for the isotopologues of nitrous oxide in the spectral range used in the Picarro-analyzer [19].*

If either of the molecules are not moving or if the pressure is very low, then the absorption lines will be at the upper boundary for the Doppler-broadening. The lines would therefore have their natural thickness which is significantly thinner than the minimal thickness caused by the Doppler-broadening. The spectral lines shown in figure 3.2 refer to the strenght of absorption, as calculated by using equation 3.8. The spectral range in this figure is the same as the one used in the Picarro-analyzer.

## 3.2 Mid-infrared spectroscopy

Light is a well known and well described quantity. It is an accomplished fact that light consists of electromagnetic radiation and can be treated as a wave. A random beam of light will have a specific size of the characteristic wavelength from which the energy ( $E$  [J]) and the frequency ( $\nu$  [Hz]) of the beam can be determined. The range of all possible frequencies this beam can obtain, is known as the electromagnetic spectrum. In principle the electromagnetic spectrum is ranging infinitely. Though quantum theories predict a minimum length, known as the Planck length ( $1.616199 \cdot 10^{-35}$  m). The relation between the most important magnitudes for electromagnetic waves are given in equation 3.7. In this equation  $h$  is the Planck's constant in Joule seconds [Js].

$$\nu = \frac{c}{\lambda} = \frac{E}{h} \text{ or } E = \frac{hc}{\lambda} \quad (3.7)$$

However, not every wavelength in the electromagnetic spectrum is useful when studying different chemical compounds, in this case the Greenhouse gases. Using the infrared range of the spectrum is convenient, since it is possible to investigate the structure of the particular molecule and the correlation between the characteristics of a specific molecule and its tendency to absorb specific frequencies. Further research has shown that the infrared spectrum can be subdivided into three sections named after the distance from the visible light spectrum. Closest to the visible light is the near-infrared range spanning from  $4000 \text{ cm}^{-1}$  to  $12800 \text{ cm}^{-1}$ , then the Mid-infrared range going from  $200 \text{ cm}^{-1}$  to  $4000 \text{ cm}^{-1}$  and furthest away is the Far-infrared range which is going from  $10 \text{ cm}^{-1}$  to  $200 \text{ cm}^{-1}$ . The focus of this thesis will be on the Mid-infrared range of the electromagnetic range, since this is the spectral range used in the Picarro CRDS G5101-i isotopic  $\text{N}_2\text{O}$  instrument [3]. The Mid-infrared range is convenient for this instrument and this research because: "The vast majority of gaseous chemical substances exhibit fundamental vibrational absorption bands in the mid-infrared spectral region ( $\approx 2 - 25 \mu\text{m}$ ), and the absorption of light by these fundamental bands provides a nearly universal means for their detection." [50].

The spectral range used in the Picarro-instrument is only a small part of the entire Mid-infrared spectrum. That means some justifications had to be made in order to narrow down the spectral window used. These justifications and the reasons to make them are both of scientific and optical nature as described by Balslev-Clausen 2011 [3]. As a result of these justifications, the spectral range was adjusted to the first part of the mid-infrared spectra as shown in figure 3.3.

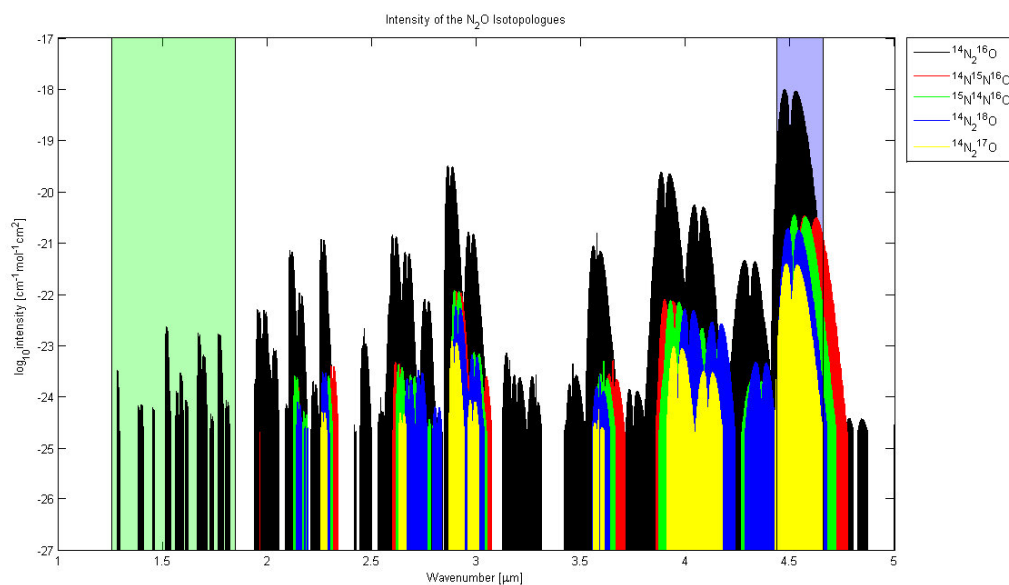


Figure 3.3: *The spectral range of the near-infrared and the first part of the mid-infrared spectrum. The Light-green area is the spectra used by the commercial products, whereas the light-blue area is the area used by the Picarro instrument [3].*

In figure 3.3 two different intervals are shown with a light-green color and a light-blue color respectively. The light-green interval represents a part of the near-infrared spectrum used in other commercial products. The light-blue interval is the one used in the  $\text{N}_2\text{O}$ -analyzer used in this work. This interval needed to be further decreased in length. This was done by analyzing the correlation between the spectrum and the isotopologues with respect to the following five criteria:

- The line intensity strength should be large, especially for the less abundant isotopologues.
- Minimal overlap with spectroscopic features of other molecules.
- The line absorption of the isotopologues should be of similar magnitude in order to achieve a large dynamic range.
- The distance between spectroscopic lines of interest should be appropriately small.
- Temperature and pressure dependence of the absorption lines should be minimal.

Now looking at the first criteria concerning the intensity strength. It is clear that all five isotopologues individually have the highest intensity and therefore also the highest absorption, over the light-blue spectral range shown in figure 3.3. After this determination,

and by using the spectral absorption coefficient expressed as a Lorentzian profile, the spectral range was narrowed down, and two small intervals were chosen. From applying the five criteria on these two small intervals and with the knowledge of the equipment available, the decision was made. The final range chosen for the instrument was from  $2187.45 \text{ cm}^{-1}$  to  $2188 \text{ cm}^{-1}$ , in which range the different isotopologues is located as shown in figure 3.4.[3]

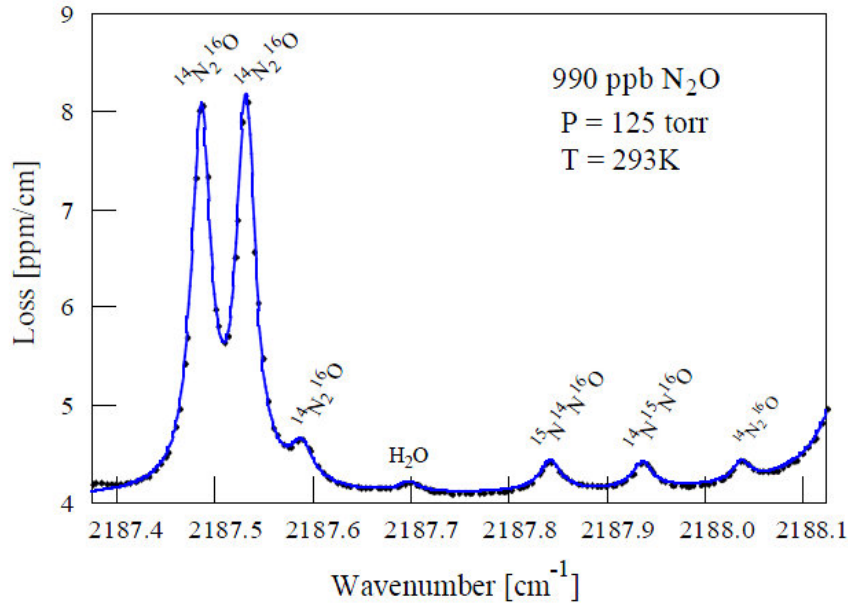


Figure 3.4: *The final chosen spectral range for use in the  $\text{N}_2\text{O}$ -analyzer with specification of the location of three of the five  $\text{N}_2\text{O}$ -isotopologues used in this thesis.*

Further comments and discussions on figure 3.4 will be given in section 3.3.

### 3.3 Cavity Ring Down Spectroscopy

From section 3.1 it is known that if a beam of light is sent through a cell filled with a composition of gasses, the isotopes can be determined together with their concentrations. This knowledge of the gas is determined from the wavenumber and the spectral line profile obtained by using the absorption spectroscopy principle.

The problem with this simple form of spectroscopy is that each absorption line does not necessarily give the same spectral profile, even when looking at profiles of the same "species". In order to solve this issue an equation was made to give the relation between the absorption profile and the gas-concentration:

$$\alpha_{i,l} = nI_{i,l}g_{i,l}(\lambda) \quad (3.8)$$

In this equation  $n$  is the absorbers concentration,  $g_{i,l}(\lambda)$  is the normalized spectral profile (calculated by using the normalization equation ( $\int_{-\infty}^{\infty} g_{i,l}(\lambda) d\lambda = 1$ )) and  $(i, l)$  is the indicators of the molecule and the specific absorption line respectively.[3]

This equation helps overcome the problems with the simple absorption spectroscopy, but it does not solve them. A problem of a more technical nature is that the spectral profile depends on the temperature, the pressure and the composition of the gas used in the setup.

Cavity Ring Down Spectroscopy or CRDS is a technique for dealing with the problem of the precision of the technical aspects. The CRDS analyzers have a build-in high precision temperature and pressure control of the gasses entering the instrument. This was done in order to secure a high stability of the measurements.

The work presented in this thesis was made with a trace gas ( $N_2O$ ) which generally had a low concentration. A lower pressure will almost give the same height in concentration level, while it will make the spectral profile thinner.

When dealing with other methods of infrared spectroscopy, the instruments have problems in measuring the very small contributions to absorption from the trace gasses, since the sensitivity is only in parts per million (at best). CRDS also has the solution to these limitations, due to the very long effective path length of the light. The effective path length can be more than 20 kilometers. This very long path length is made possible because a closed loop between two or three mirrors is present. The light beam will be reflected between the mirrors in a closed loop for about 100.000 times, as shown in the upper part of figure 3.5.

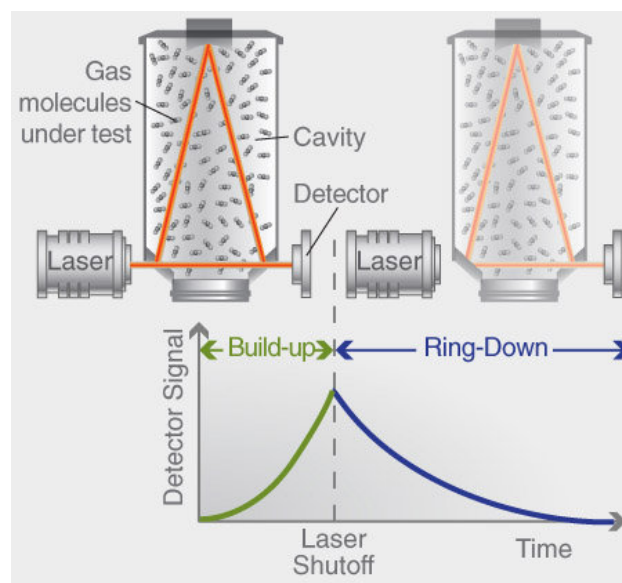


Figure 3.5: *The schematics of how the cavity of the Picarro CRDS is filled/emptied, and the contemporary ring down.*

The general length of the cavity in a Picarro analyzer is 25 cm long, but using the mirrors to reflect the light back and forth (about 100.000 times), makes the effective path length 25 kilometer [38]. The time it takes for the light to finish one full circle in the cavity is given as  $t_{rt} = \frac{L}{c}$ , where  $L$  is the distance travelled and  $c$  is the speed of light.

This ring down time is also known as the free spectral range (FSR). The FSR is a value of the difference in light frequency between the transmission resonances. When the light entering the cavity have the same frequency as the light traversing in the cavity, the two beams will be oscillating in phase with the wavelength  $\lambda_M = \frac{L}{M}$ , where  $M$  is an integer. In order to obtain this resonance, both cavity length and the laser wavelength need to be adjusted.

The laser used in this instrument is a tunable External Cavity - Quantum Cascade Laser (EX-QCL). Further information on the laser can be found in the Ph.D. thesis by Balselv-Clausen, 2011 [3].

While the laser is circulating inside the cavity, the photo detector placed on the outside of one of the mirrors is detecting the small amount of light leaking out. This detection of the escaping (loss) light produces a signal proportional to the intensity of light inside the cavity. When the photo detector reaches a threshold level the laser signal is stopped. At this point the light inside the cavity will circulate between the mirrors, which are reflecting 99.995 % of the light. The term "ring down" (or ring down time) is the exponentially decay of the light intensity inside the cavity. This decay is due to the lack of full reflection from the mirrors and absorption by molecules. The cavity ring down is shown schematically in figure 3.5.

Now, if some kind of gas is introduced into the cavity (compared to an empty cavity), the gas will absorb some of the light circulating the cavity. The amount of absorption ( $A_c$ ) will depend on the concentration of the gas, as described earlier. This absorption of light will lead to a decrease in the ring down time as shown in figure 3.6. [38]

Also shown is that the intensity of the light ( $I$ ) will decrease over time as  $\frac{dI}{dt}$ . This is schematically shown in figure 3.6. The intensity change over one round trip can be described as:

$$\frac{dI}{dt} = -\frac{A_c I}{t_{rt}} \quad (3.9)$$

where  $A_c$  is the cavity round trip absorptance and  $t$  is time measured in seconds.

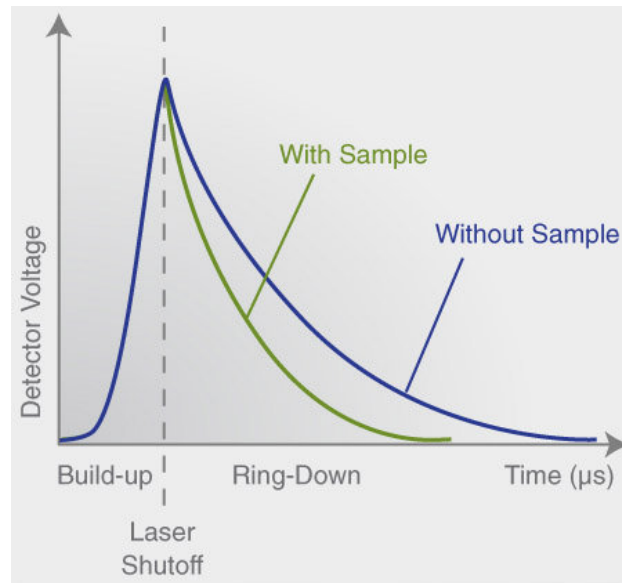


Figure 3.6: *The light intensity in the cavity over time when shutting down the laser. The green line is the ring down with a gas inside the cavity, whereas the blue line is with an empty cavity.*

The solution to this differential equation is Beer-Lambert's law in a slightly modified version of equation 3.1.

$$I = I_0 e^{-\frac{t}{\tau}}, \quad \tau = \frac{t_{rt}}{A_c} = \frac{1}{c\alpha_c} \quad (3.10)$$

where  $\tau$  is the ring down decay time and  $\alpha_c$  is the effective absorption coefficient per round trip in the cavity in  $\text{cm}^{-1}$ .

The ring down time is used directly by the Picarro analyzer. These continuous measurements make it possible to distinguish between the two forms of intensity loss. Furthermore this continuous measurements of the ring downs and their differences end up in gas concentrations which are then independent of the laser intensity. The Picarro analyzer fits the spectral lines and uses known gasses measured at the time of calibration for comparison. [3]

The effective absorption coefficient per round trip in the empty cavity, is found from measurements and calculations using equations 3.9 and 3.10. When knowing the absorption from the empty cavity ( $A_c$ ), the effective absorption coefficient per round trip in the empty cavity is given by equation 3.11.

$$\alpha_c = \frac{A_c}{L}. \quad (3.11)$$

Knowing this and knowing that the sum of the absorption ( $A_c$ ) and the transmittance ( $T_c$ ) in the cavity always equals 1 ( $A_c + T_c = 1$ ) (since no scattering is present in the cavity

( $S_c = 0$ )), gives the opportunity to find the effective absorption coefficient of the cell ( $\alpha_g$ ).

$$A_c = 1 - T_c \quad , \quad \text{where} \quad T_c = R^3 \exp(-\alpha_g L) \quad (3.12)$$

The cavity mirror reflectivity ( $R$ ) is raised to the power of three, because there are three mirrors in the CRDS-analyzer used in this thesis. [62]

In order to isolate the effective absorption coefficient from the gas the Taylor expansion  $\ln(x) = x$  and equation 3.11 is used.

$$\alpha_c L = 1 - R^3 - \alpha_g L \quad (3.13)$$

↓

$$\alpha_g = \alpha_c - \frac{1 - R^3}{L} \quad (3.14)$$

The baseline absorption is never zero, as shown for example in the spectral plots from the CRDS-analyzer used in this thesis (figure 3.4). This is because the mirrors are not fully reflecting the light. This deviation from a full reflection, can be found by setting  $\alpha_g = 0$  in equation 3.14:

$$\alpha_{c0} = \frac{1 - R^3}{L} \quad (3.15)$$

Another reason for a deviation in baseline absorption could be that absorption of the light is happening from spectral lines further away from the range of interest. This could especially be the case for a higher pressure.[3]

Other than this CRDS is "...a non destructive analysis, and so a measurement can be repeated on the same sample as many times as desired, if the sample is kept statically in the cell." [3]

## 4

**Experimental setup**

The Picarro analyzer is a part of a recirculation setup. The circulating path of the gas is from a closed chamber, through multiple drying units, into the Picarro analyzer and back into the closed chamber. The work presented in this thesis is a combination of long-term closed chamber experiments and relative short-term standard gas sample experiments. An external flushing setup was made and placed in series with the analyzer, in order to obtain the best possible results in all experiments. The analyzer used is the prototype of the Picarro G5101-i analyzer.

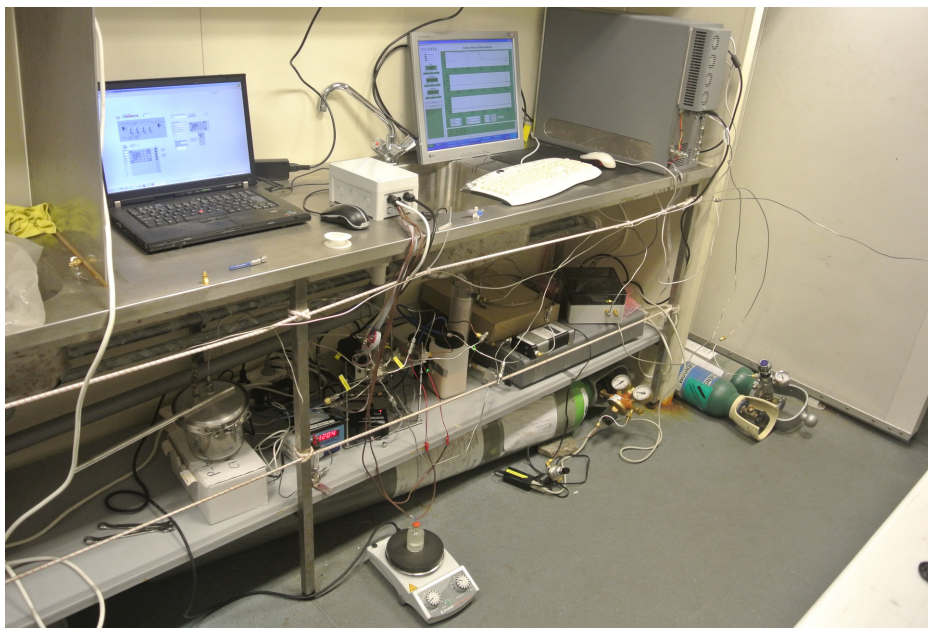


Figure 4.1: *Picture of the Picarro G5101-i analyzer placed in a loop with the external measuring setup. The optics unit is the one on the table to the right, and the host unit is the one on the shelf to the right. The analyzer is controlled from the screen next to the optics unit. The external setup is controlled by the laptop on the table.*

## 4.1 Picarro G5101-i analyzer

The Picarro analyzer measures gas samples using the principles of CRDS in the Mid-IR range as described in the previous sections. The analyzer consists of two units, a host unit and an optics unit. The optics unit has the following dimensions:  $W \times H \times D = 37 \text{ cm} \times 28 \text{ cm} \times 58 \text{ cm}$ . The optics unit contains all optics, data acquisition cards, driver electronics and the cavity. The host unit has the following dimensions:  $W \times H \times D = 44 \text{ cm} \times 23 \text{ cm} \times 62 \text{ cm}$ . This unit contains host computer, laser driver, liquid cooling system, and an acousto-optic modulator (AOM). [3]

Originally a pump was also located in the host unit, but a new external pump has been connected since the internal pump was leaking. The focus in this thesis is the measurements. Therefore only the cavity and a few other parts which are in physical contact with the gas will be discussed in this chapter.

### 4.1.1 The cavity

The cavity placed in the Picarro analyzer is a ring-shaped high-finesse optical cavity. The cavity has been made from a cylinder of stainless steel invar. Invar is nickel-iron alloy (36 % nickel and 64 % iron) which is known to have a very low thermal expansion coefficient. Using the invar cavity results in a cavity in which the thermal fluctuations have no influence. [42]

Figure 4.2 shows a cross section of the cavity. The gas inlet and outlet are shown in each respective end as the dotted lines. The laser beam (red) enters the cavity in the left end, through one of the two high-reflectivity plane mirrors (blue). The beam is traversing around in a triangle between the two plane mirrors in the left end and a high-reflectivity concave (bulging inward) mirror mounted at the right end. The plane mirrors are glued onto the cavity, while the concave mirror is attached to the cavity body via a piezoelectric element (dark red). This piezoelectric element allows that the concave mirror can be adjusted. The internal cavity length is about 24.1 cm and the width is 2.5 cm. This gives an effective

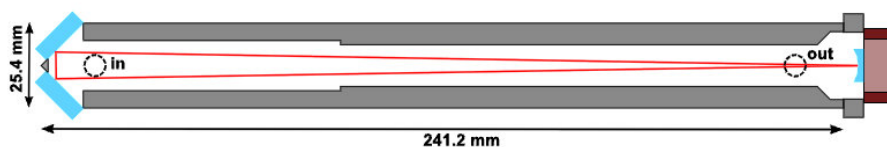


Figure 4.2: Schematic cross section of the cavity used in the prototype of the Picarro G5101-i analyzer. The laser beam (red line) is traveling between the mirrors (blue).

round-trip length for a beam of light of 48.5 cm. The internal volume of the cavity is

approximately 35 cc. As explained in section 3.3 it is crucial that the full path length for the beam is significantly longer than that of one round trip. This increased path length is possible because of the properties of the high-reflectivity mirrors. Each of the two plane mirrors has a flat surface with an anti-reflective coating on the outside and a high-reflective coating on the inside. This results in a reflectivity of 99.995 %. The concave mirror has a 1 meter radius of curvature and an effective reflectivity of 99.989 %. In this way a relatively small part of the incident laser beam will penetrate the mirror and enter the cavity. Once the light is inside it will hardly ever get out again. This results in a buildup of the laser intensity, which over time creates a very high intensity inside the cavity. Because of this high reflectivity the effective path length of the laser beam in the cavity will be 6000 m when the cavity ring down time is 10  $\mu$ s. The greater part of the incident beam is reflected on the inner mirror and therefore never enters the cavity. The optical feedback to the laser is reduced (a lot) because of the 45° entry angle and an external blackbody (with a known absorption range, adequate to the used wavelength). This is compared to the feedback when using a linear cavity. This is the biggest advantage of using a round cavity instead of the linear cavity. The cavity used in this thesis is round, mostly because of the reduced optical feedback, but also because of the boundary condition for the ring resonator. The boundary condition for the ring resonator is like that of a traveling wave. This results in uniform light intensity and in uniform sample excitations. The only caveat about the ring-shaped cavity is that more mirrors are needed to line up the laser beam. This leads to a more difficult line-up of the laser.[3]

The optical ring cavity is another name for a optical ring resonator (ORR). The theory behind the ORR is that it is a set of waveguides which in a closed loop are coupling light inputs and outputs. The light is traversing the hollow space inside the device.

## 4.2 The flushing system

We made an external system in order to re-circulate the gas samples measured with the Picarro G5101-i analyzer. This system has two different modes depending on the situation needed. The two modes are for flushing the system and for measuring the sample. The schematics of the two modes are shown in figure 4.3 and figure 4.4, respectively.

The flushing setup mode is made in order to flush all parts of the system with a known gas composition. This is done to make sure that the same starting concentration and isotopic composition is present in the system every time. In this setup there are two paths of flushing. The first path (green arrows in figure 4.3) is the one going through the Picarro analyzer. The

gas enters the system from a gas bottle filled with  $N_2$  or a synthetic mixture of atmospheric air, depending on the experiment. The gas flows through a mass flow controller (MFC), before entering the 8-port valve directing the gas through the drying setup. The drying setup consists of a nafion unit and an ascarite trap. The driers make sure that no water or  $CO_2$  enter the analyzer (as described in section 5.1.1 and 5.1.2 respectively). After the drying setup the gas flows into the Picarro analyzer, where the concentration and isotopic composition are measured. Hereafter the gas continues out of the system into the lab as waste.

The second path of the flushing mode (red arrows in figure 4.3) is through the container containing the source of the  $N_2O$  production. The gas enters from the same gas bottle as used in the other part of the flushing setup. The gas flows directly into the big glass container. From here it streams through a pressure gauge (PG), a membrane pump, and continues as the purge gas used in the nafion unit. After the nafion unit, the gas goes out to waste.

The path of the purge gas as used in the nafion unit is shown with the purple arrows in figure 4.3.

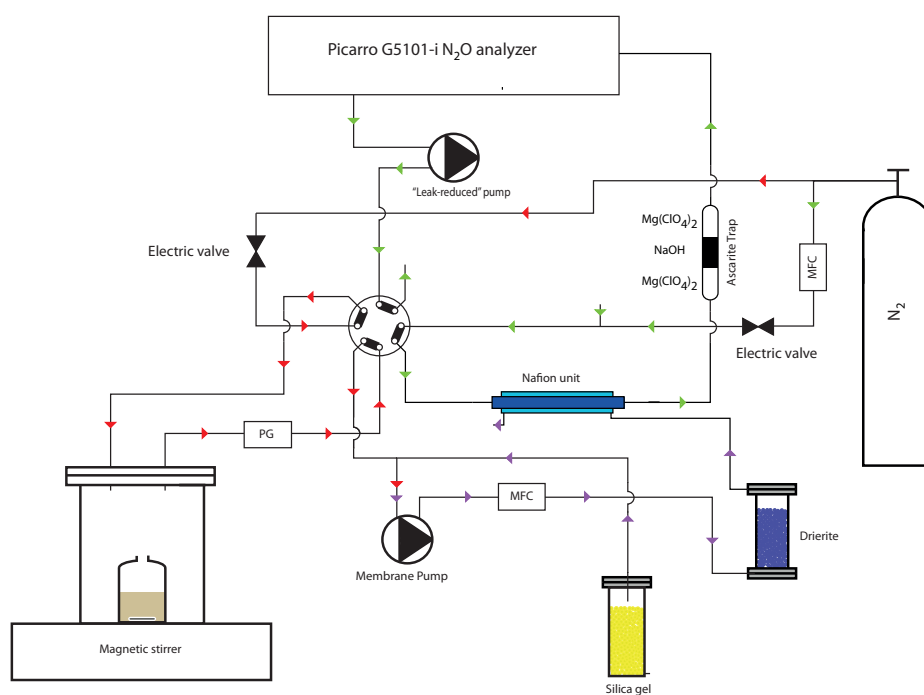


Figure 4.3: *Schematic of the flushing mode of the external  $N_2O$  setup. The green arrows show the gas flow when flushing the Picarro analyzer. The red arrows show the gas flow when flushing the source (container). The purple arrows show the gas flow in the drying system.*

The flushing procedure is fully automated to ensure reproducibility in the measurements. This means that the two electric valves, the 8-port valve and the membrane pump are automatically operated. The automatic setup is in such a way that the 8-port valve should be in the flushing mode for a total of 335 seconds (5 min 35 sec). The first part of the flushing setup is flushed during the entire 335 seconds. The second part is flushed for 290 seconds, before the membrane pump shuts down. After another 30 seconds, the electric valve is closed and kept like that for 15 seconds before the measuring mode is turned on. This in-term shutdown is made to ensure that an "ambient" pressure is reached.

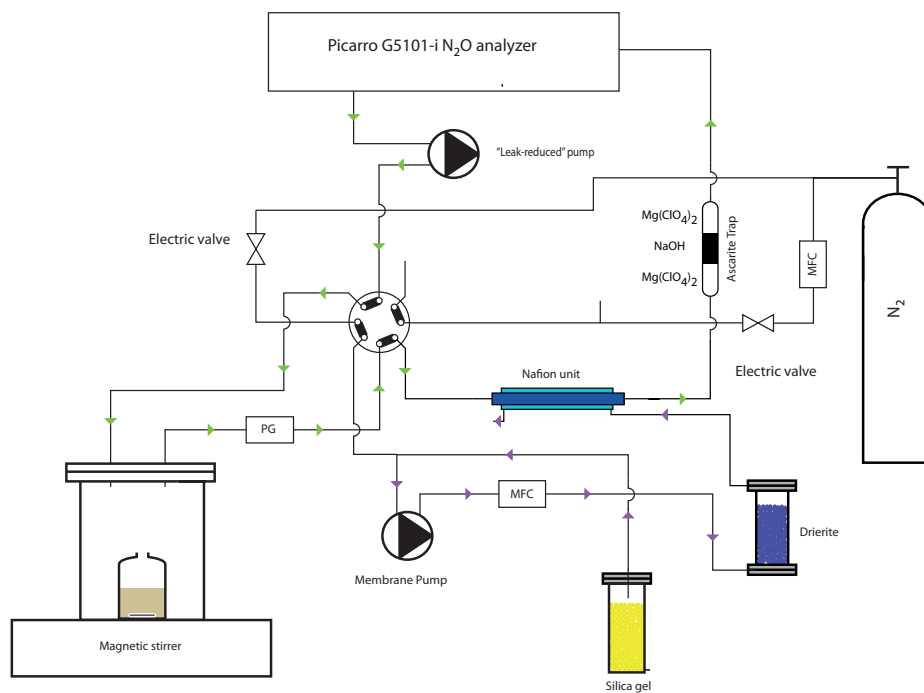


Figure 4.4: Schematic of the measuring mode of the external  $N_2O$  setup. The green arrows show the flow of the measuring gas - going from the source through the drier and into the analyzer. The purple arrows show the flow of the drying system.

The second mode is the measuring mode. When for example a mono-culture is placed in the big glass container, a gas will emit from the culture and flow through the system in the direction of the green arrows. This gas will first flow through the 8-port valve in which it will be directed to the Picarro analyzer, via the nafion unit and then through the ascarite trap. After the gas has been measured it will continue back into the glass container and be mixed with the emitted gas. By using a re-circulation setup like this, it is possible to measure the change over time both in concentration and in isotopic composition of the gasses emitted from the source (in this case the mono-culture).

The flow of the purge gas, used in the nafion unit, is shown with purple arrows. The role of both the ascarite and nafion is described in section 5.1.

### 4.3 The sample bag measuring setup

A large part of the measurements presented in this thesis were made using gas sampling bags. We therefore adopted the system for analyzing the gasses inside these bags. This system is shown in figure 4.5.

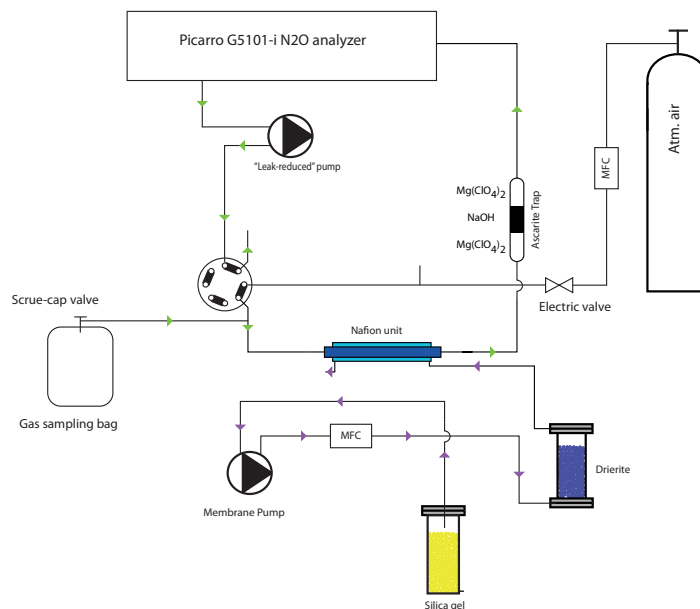


Figure 4.5: *Schematic of the measuring mode when using the gas sampling bags. The green arrows show the flow of the measuring gas and the purple arrows show the flow of the drying system.*

This setup is similar to the one just explained. The only difference is that the gas flows out of the gas sampling bag, and goes out to waste.

When one bag is empty, the bag is removed and replaced. While the bags are being changed the system pulls in laboratory air - but not used in further analysis.

### 4.4 Gas collection setup

We collected samples from natural environments i.e. soils. Both the measuring sites and the method for accumulating a mixture of gasses emitted directly from the ground (as described in chapter 8) were discovered by Professor Søren Christensen from the terrestrial ecology department at the Institute for Biology, University of Copenhagen. As stated in this chapter, it is required that the gas samples are transferred from the test site through a needle into a sample bag.

An efficient method for collecting the gasses from the soil was needed in order to ensure

successful experiments. In the process of ensuring reliable gas samples the following considerations were taken into account:

- A minimal contamination from atmospheric air.
- Both of the destinations for field experiments are far away from any power supplies.
- The amount of gas needed for getting measurements in steady state.
- Number of samples desired.

After consideration of these aspects, the following setup was chosen:

The principle of this gas collection setup is that, first of all a gas sampling bag is placed



Figure 4.6: *Gas collection setup.*

inside a leak tight plastic box. The bag is then connected with a plastic tube through the lid to a needle, intended to be pushed into the rubber top of the chamber. Even when the sample bag is open, no atmospheric air is entering the bag and contaminating it. Now, in order for the bag to be filled with the gas from the chamber, vacuum is applied inside the box (but outside the bag). When air is sucked out of the box, the bag will inflate with gas from the chamber. Vacuum is produced with a pump which is sucking out air from the box through a plastic tube connected to the box.

At Buresoe we used a foot pump while at Disko Island an electrical battery driven pump (as is shown in figure 4.6) was used to produce vacuum.

## Setup components

The measuring methods described in chapter 4, demand a couple of external components as well as a couple of different gasses for both calibration and background measurements.

### 5.1 Gas drying components

Before the gas sample of interest enters the Picarro G5101-i analyzer, it needs to be as clean as possible. This means that water vapor ( $\text{H}_2\text{O}$ ) and carbon dioxide ( $\text{CO}_2$ ) need to be removed from the gas before entering the analyzer. The water vapor needs to be removed from the gas primarily in order to protect the mirrors. If too much water enters the cavity will the water vapor condense on the mirrors. This will cause the laser beam to scatter. Both  $\text{CO}_2$  and  $\text{H}_2\text{O}$  have been found to absorb light in the ranges used by the Picarro G5101-i analyzer. The absorption by these molecules would therefore interfere the measurements of the  $\text{N}_2\text{O}$  molecules. This would result in inaccurate absorption values.

In order to gain the best possible result, two units were placed upstream from the analyzer.

#### 5.1.1 Nafion unit

Going from the inlet of the gas and downstream towards the analyzer, the first unit is a nafion unit.

A nafion unit consists of an outer stainless steel tube and an inner nafion tube. The nafion tube is a penetrable membrane tube. The sample gas flows in the inner tube, whereas the gas in the outer tube is a counter flowing purge gas. The drying happens because of the counter flowing purge gas which is transferring the water vapor molecules through the membrane tube into the purge gas stream. This process of drying a gas is called pervaporation and it is driven by the water concentration differential (humidity gradient) between the two gas



Figure 5.1: *The nafion unit used in the setup.*

streams. This causes the gas to diffuse from the high humidity gas to the low humidity gas. An important aspect for drying a gas using the nafion tube is that the preferred velocity of the purge gas should be at least twice that of the gas sample velocity. The exact flow rate depends on the water vapor saturation level of the sample gas. In the literature the flow rate has therefore been found to be 10 times that of the sample gas [26]. This is because even a small humidity gradient will cause a reaction, since the evaporated water is already further downstream from the inlet of the sample gas. In this thesis the flow rate of the purge gas was approximately 10 times that of the sample gas.

The purge gas needs to be dried before entering the nafion tube. This drying and cleaning is done by Drierite and Silica gel. It is done in order to ensure that the purge gas has a considerable lower concentration of water vapor than the gas of interest. [26] [35] [55]

### **Silica gel**

The first part of the drying process is to lead the purge gas through a container with Silica gel. Silica gel is a purified and processed version of the naturally occurring mineral called silicon dioxide ( $\text{SiO}_2$  or silica) [16].

The chemical compound of silica was discovered in ancient times and is today used in several different forms and for a large variety of products, though primarily in the production of glass [13]. When silica is processed correctly it can obtain a relatively tough and hard granular form with an average pore size of 2.4 nanometers, giving each granular a very large surface area. This granular form is referred to as silica gel and it is a strong desiccant of water molecules. Silica gel is used in for example food productions and in laboratory experiments as a desiccant. This desiccant can absorb up to 40 % of its weight in moisture. Silica gel has one of the highest moisture absorption rates of the desiccants available. [45] This high absorption rate is possible since the gel absorbs moisture onto the large surface



Figure 5.2: *Silica gel granular as used for drying the purge gas*

of each granular.

In this work, the purge gas is obtained by first leading atmospheric air through the container with silica gel as for example shown in figure 5.2. The bulk of the water vapor of the air, used for drying the sample gas, is trapped on silica gel.

The silica gel used is yellow in contrast to the original silica gel which is white or blue (mixed with cobalt chloride). This orange color is for indication of the moisture contents of the silica gel, since the gel is changing color while absorbing moisture. [45]

### **Drierite**

The second part of the drying process is to lead the purge gas through a drierite gas drying unit (figure 5.3). This second step lowers the water content significantly.

Drierite is a desiccant primarily consisting of the chemical compound called Calcium Sulfate ( $\text{CaSO}_4$ ). Calcium sulfate has many applications and forms depending on the pre-work. The drierite works as a moisture indicator, due to the impregnation with Cobalt (II) chloride. The colored cobalt chloride works as an indicator due to its blue color when dry, versus pink color when wet.

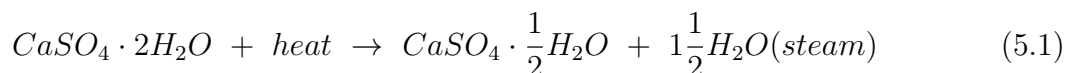
Drierite can work as a dryer for all purposes, gasses, air, liquids, solids and even refrigerators. Therefore drierite is also used in various products both of commercial and private nature.



Figure 5.3: *Drierite*

Drierite is not as efficient a dryer of gasses as silica gel, but the drierite granular has a water capacity of 10 to 14 weight percent. The absorption rate of drierite depends on the percentage size of the pore space volume, just as with silica gel. The granular used in this work has a pore space volume of 38 %. [57] [12]

When drierite is exhausted it can be dehydrated by heating the granular. When heating drierite, the following chemical reaction takes place and partially dehydrated granular returns after heating.



### 5.1.2 Ascarite Trap

After concentration of water vapor has been lowered by leading the gas through the nafion tube, the sample gas is flowing through an ascarite trap. An ascarite trap is both a water trap and a CO<sub>2</sub> trap.

Ascarite is another name for Sodium Hydroxide (NaOH) originally absorbed on Asbestos. The ascarite used in this thesis is NaOH absorbed on silica based granular form. When NaOH reacts with a sample gas including CO<sub>2</sub>, it will react as follows:



From this reaction it is clear that a new portion of water vapor is produced. Therefore the ascarite trap is constructed in such a way (see figure 5.4) that the granular of NaOH is packed with Magnesium Perchlorate Hydrate (Mg(ClO<sub>4</sub>)<sub>2</sub>·H<sub>2</sub>O) on both sides. Some glass wool is placed between the two different chemicals in both ends to prevent dirt to enter the trap and to prevent reactions between the two chemicals. The Mg(ClO<sub>4</sub>)<sub>2</sub>·H<sub>2</sub>O in front of the NaOH is placed there to prevent water to condensate and thereby block the CO<sub>2</sub> trap. The Mg(ClO<sub>4</sub>)<sub>2</sub>·H<sub>2</sub>O after the NaOH is intended to react with the water produced by the NaOH reaction. [54]



Figure 5.4: *The ascarite trap as used in this thesis. The black powder is Magnesium Perchlorate hydrate (Mg(ClO<sub>4</sub>)<sub>2</sub>·H<sub>2</sub>O) and the white powder is Sodium Hydroxide (NaOH)*

After these two traps (Nafion tube and Ascarite trap) the sample gas is clean enough to measure the N<sub>2</sub>O concentration and isotopic composition.

## 5.2 Leak-reduced pump

In the original prototype of the Picarro G5101-i N<sub>2</sub>O analyzer (used for the work presented in this thesis) a four head diaphragm pump (KNF, N84.4 ANDC) was installed, to pump the sample gas through both the setup and the analyzer. The leak rate of this pump is too high, the original diaphragm pump was therefore replaced. For the experiments presented in this thesis the pump is ment to be as leak-tight as possible.

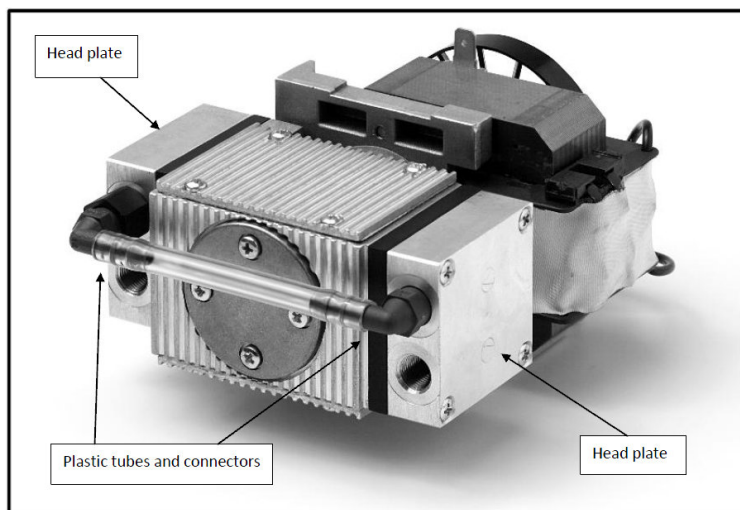


Figure 5.5: *The new mini Diaphragm vacuum pump (N 84.4 ANE), made into the leak-reduced pump used in the Picarro-analyzer setup.*

Instead of the old pump a new mini diaphragm vacuum pump (N 84.4 ANE) (figure 5.5) was ordered. This pump is stated to be operating gas-tight, by KNF (the company selling the pump). In practice such a thing as a 100 % leak tight pump is very unlikely. The new mini diaphragm vacuum pump was as well tested to have a too high leak rate.

A reduction of the leak rate was therefore needed:

- The metal pieces (head plates) on the sides of the pump was moved. Grease coated O-rings were placed on the inlets and outlets.
- The head plates were put back on their original position.
- All of the metal-joints and the membrane were sealed with vacuum sealant (Celvaseal high vacuum leak sealant, Myers vacuum repair service,inc.).
- The original plastic tubes and connectors were replaced by some of stainless steel.
- The pump was placed in a plastic box, to stabilize and protect the pump from dust.
- To be able to automate 230 V the pump was connected via solid state relay.

After the pump was finished it needed to be tested for leak rate. This test was conducted using the setup shown in figure 5.6. In the setup the Picarro-CH<sub>4</sub> analyzer and a pure N<sub>2</sub> gas was used. In the N<sub>2</sub> gas bottle the concentration of CH<sub>4</sub> was close to zero. Introducing N<sub>2</sub> directly taken from the bottle into the analyzer showed a CH<sub>4</sub> concentration of approximately 2 ppb.

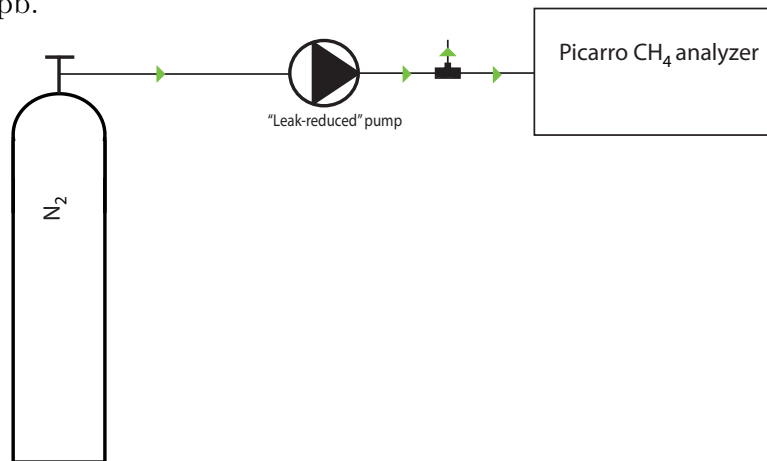


Figure 5.6: *Schematic setup for testing the new leak-reduced pump. The tube between the N<sub>2</sub> bottle and the pump is a capillary and so is the small tube going away from the T-connector. This way will there by a low pressure going into the pump, causing the pump to suck in more lab-air if the pump is not leak-tight.*

The leak test was performed at both high pressure and low pressure (compared to atmospheric air pressure). The most efficient way to see the leak rate is to measure the leak when a stream of N<sub>2</sub> gas is flowing through the pump at low pressure. When the incoming gas is at low pressure, it will cause the pump to suck in more lab-air if the pump is not tight. During this low-pressure test, the Picarro showed CH<sub>4</sub> concentrations of less than 3ppb in the measurements with the improved leak-reduced pump. It can therefore be concluded that leak rate of the pump was reduced due to the explained leak-reducing procedures.

### 5.3 External gases used

During the work presented here, two gasses were used for flushing the system (bottled atmospheric air and pure nitrogen). Two standard gasses (CIC-MPI-1 and CIC-MPI-2) were used for calibrating the system.

As previously stated, in chapter 2.3.2, is the denitrifying bacteria preferred under anaerobic conditions, where no oxygen is available. When flushing the system with 99.9999 %

nitrogen, an optimal environment with anaerobic conditions is created for the denitrifying bacteria.

For the nitrifying processes an aerobic environment is essential. A flush with gas from the nitrogen bottle would therefore result in a bad experimental environment. Therefore a bottle with a synthetic mixture of atmospheric air is used for the experiments in which nitrifying bacteria is present. There needs to be  $N_2O$  in this bottle of atmospheric air. Having a certain concentration of  $N_2O$  present in the gas bottle, gave us the possibility of using the measurements to calculate the the drift of the instrument.

Figure 5.7 shows the measurements of the  $N_2O$  concentration from the bottle with atmospheric air. These measurements were conducted over half a year. More precise is figure 5.7 showing all of the time-steps in which the atmospheric air bottle has been used between March 2013 and August 9th. 2013. In the beginning of the period was a leak detected. This leak resulted in measurements of the bottled atmospheric air at concentrations of approximately 0.33 ppm (atmospheric concentration). These measurements are therefore removed from figure 5.7. A lot of the measurements lasted for 5 minutes and 35 seconds (one flush sequence). The time axis has been merged, to remove all the time gaps and thereby smooth out the profile. From looking at the concentration variation over time it is possible to tell whether the instrument is stable over time.

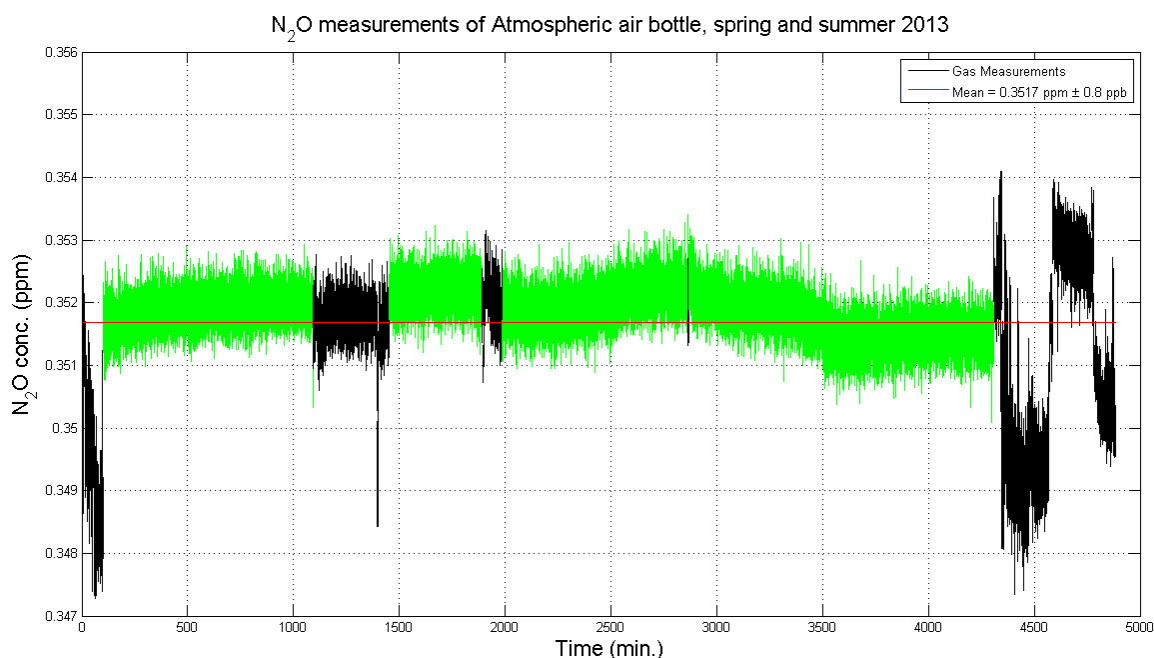


Figure 5.7: *Measurements of the bottled atmospheric air over six months. A total of 167 measurements (primarily short measurements) have been merged. The green profiles represents the longer measurements. The black profiles are the flush sequences.*

Over the time frame of the experiments there have been some fluctuations in the concentrations measured from the atm. air bottle, as can be seen in the figure. But a few comments must be made to this observation. First of all, was it discovered that the 5 minutes and 35 seconds of flushing were not sufficient for getting stable measurements for each flush. If all of the flush-measurements were discarded, only the longer measurements (four measurements of minimum 1 hour) would be present and the standard deviation would thereby decrease. From figure 5.7, it appears that there is a small long term drift in the measurements. However, for each of the four longer measurements, the scattering is less than 1 ‰. This does indicate that the short-term drift of the instrument is relatively small.

### 5.3.1 Standard gasses and calibration

Two standard gasses were used during the experiments presented here. The two gasses are called CIC-MPI-1 and CIC-MPI-2. Both of the standards are mixtures of the original MPI-1 and MPI-2, respectively. These gasses were given from Jan Kaiser [Pers. comm. between J. Kaiser and D. Balslev-Clausen]. The MPI-standards have previously been measured as presented in table 5.1 and 5.2 respectively.

MPI-1	
$\delta^{15}N$ -mean	$1.01 \pm 0.03$ ‰ vs. Air-N <sub>2</sub>
$\delta^{18}O$	$38.45 \pm 0.22$ ‰ vs. VSMOW
$\delta^{15}N^{\beta}$	$1.3 \pm 0.9$ ‰ vs. Air-N <sub>2</sub>
$\delta^{15}N^{\alpha}$	$0.7 \pm 0.9$ ‰ vs. Air-N <sub>2</sub>

Table 5.1: Content of the MPI-1 standard, provided by Jan Kaiser. [Pers. comm. between J. Kaiser and D. Balslev-Clausen]

The CIC-MPI-1 standard is a mixture of MPI-1 in 20.1 % O<sub>2</sub> and 79.9 % N<sub>2</sub>. After the mixing the N<sub>2</sub>O concentration of the CIC-MPI-1 is  $\approx 1.92$  ppm. The CIC-MPI-2 standard is a mixture of MPI-2 in 20.1 % O<sub>2</sub> and 79.9 % N<sub>2</sub> and after mixing the N<sub>2</sub>O concentration of the CIC-MPI-2  $\approx 1.828$  ppm.

The accurate values of the content in the two standards might not be the same as in the MPI standards due to the mixing. A confirmation of the values is therefore needed. This is currently being done in Japan and the values are therefore not confirmed yet. The MPI standard values are therefore assumed to be accurate and used for calibration of the data presented in this thesis.

MPI-2	
$\delta^{15}N$ -mean	$-1.78 \pm 0.03$ ‰ vs. Air-N <sub>2</sub>
$\delta^{18}O$	$40.47 \pm 0.22$ ‰ vs. VSMOW
$\delta^{15}N^{\beta}$	$-15.9 \pm 0.9$ ‰ vs. Air-N <sub>2</sub>
$\delta^{15}N^{\alpha}$	$12.4 \pm 0.04$ ‰ vs. Air-N <sub>2</sub>

Table 5.2: Content of the MPI-2 standard, provided by Jan Kaiser. [Pers. comm. between J. Kaiser and D. Balslev-Clausen]

In figure 5.8 three measurements of the CIC-MPI-1 standard gas are shown. And in figure 5.9 four measurements of the CIC-MPI-2 standard gas are shown. In both of these figures is the top plot presenting the concentration of N<sub>2</sub>O. The middle plot presents the  $\delta^{15}N^{\alpha}$

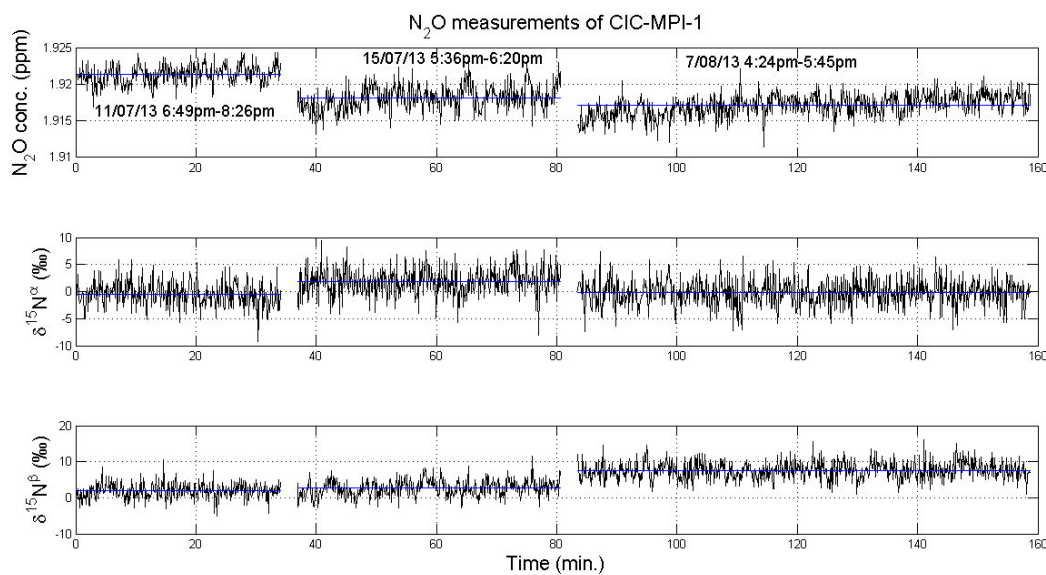


Figure 5.8: Measurements of the standard gas CIC-MPI-1. The blue lines show the mean of the respective measurement series. The top plot present the three measured N<sub>2</sub>O concentration with standard deviations of 1.3 ppb, 1.7 ppb and 1.6 ppb respectively. The middle plot is the  $\delta^{15}N^{\alpha}$  values with standard deviations of 2.25 ‰, 2.49 ‰ and 3.38 ‰ respectively. The third plot is the  $\delta^{15}N^{\beta}$  values with standard deviations of 2.24 ‰, 2.44 ‰ and 2.58 ‰ respectively.

From these two figures it look like there is a long term drift over days. This is especially clear from the concentration plot in figure 5.8. The concentration of N<sub>2</sub>O in the CIC-MPI-1 gas is found to be drifting with 4.3 ppb over 28 days. Over the same period is the  $\delta^{15}N^{\alpha}$

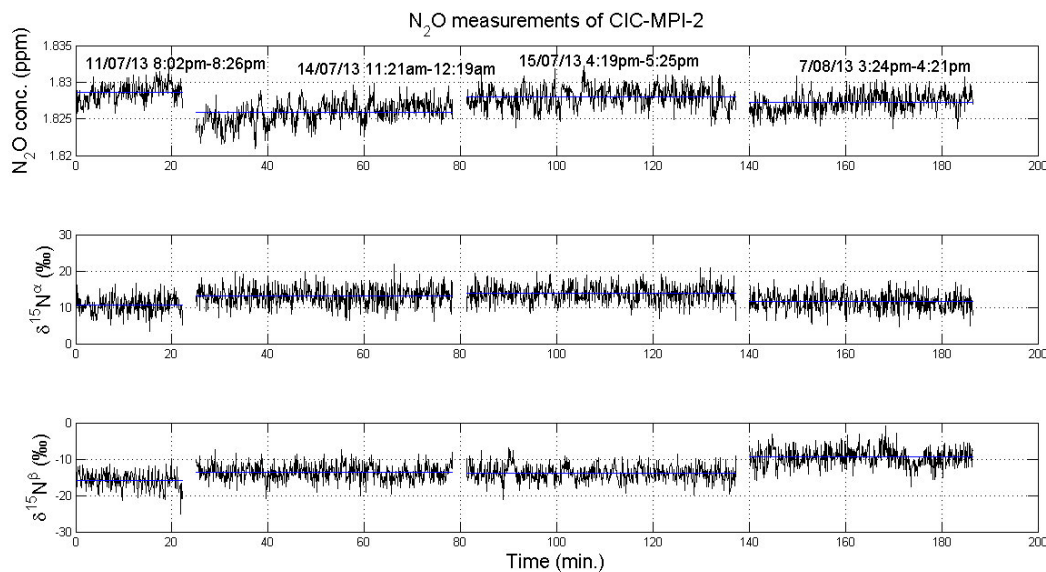


Figure 5.9: *Measurements of the standard gas CIC-MPI-2. The blue lines show the mean of the respective measurement series. The top plot presents the four measured  $N_2O$  concentration with standard deviations of 1.2 ppb, 1.6 ppb, 1.4 ppb and 1.3 ppb respectively. The middle plot presents the  $\delta^{15}N^\alpha$  values with standard deviations of 2.45 ‰, 2.62 ‰, 2.44 ‰ and 2.48 ‰ respectively. The third plot presents the  $\delta^{15}N^\beta$  values with standard deviations of 2.37 ‰, 2.25 ‰, 2.21 ‰ and 2.57 ‰ respectively.*

drifting with 0.24 ‰ and the  $\delta^{15}N^\beta$  with 5.72 ‰. The drift of the CIC-MPI-2 gas is a little less pronounced. From figure 5.9 the concentration,  $\delta^{15}N^\alpha$  and  $\delta^{15}N^\beta$  are found to be drifting with 1.4ppb, 0.95 ‰ and 6.47 ‰, respectively. All of these drifts are relatively large and it is therefore clear that a calibration is important for getting accurate results. This long term drift does not affect the measurements, since calibration is done every day (and for every measurement).

However, over one concentration measurement (as presented in figure 5.8 and 5.9) the instrument is stable within  $\pm 1$  ppb for both CIC-MPI-1 and CIC-MPI-2. The instrument can therefore still be set to remain stable over the time frame of one measurement. The same conclusion of the stability over time can be made from both the concentration the SP and the bulk measurements of the  $N_2O$ .

A total of four measurements were done using the CIC-MPI-2 standard gas. The results from these measurements are presented in figure 5.9. From the four measurements of CIC-MPI-2, the same comment as with the CIC-MPI-1 standard gas can be told.

As already stated was a calibration (using the MPI standards presented in figure 5.1 and 5.2) of the measurements needed. The calibration was done for each isotope ( $\delta^{15}N\alpha$  and  $\delta^{15}N\beta$ ). It was done by linearly fitting the MPI-standards with the measured CIC-MPI standards. From this a linear expression was found. The expression was then used to calibrate the measured data from non-standard gasses.

## Mono-Culture experiment

Park et al., 2011 [37] state that the SP differentiates between the source of the  $N_2O$  isotopomers from a nitrifying bacteria or a denitrifying bacteria. The data published in the paper represents a series of different experiments all measuring the SP from non-continuous measurements. Non-continuous measurement only give a snapshot of the measurements. It does not show what the trend is and it is therefore impossible to tell how far in the process the measurement is. The following experiment was made with the purpose of making continuous measurements of the  $N_2O$  production produced from mono-cultures of nitrifying bacteria and denitrifying bacteria. The bacteria was placed inside the measuring setup and continuously measured. The measurement from the time when food was added and lasted until the production was stabilized (at least five hours).

### 6.1 Nitrification bacteria experiment

A total of four different mono-cultures were used in this experiment (as described in section 2.3.1 and 2.3.2 respectively).

The first step of the nitrifying experiment, is to pour the culture of interest into a petri dish. This is done to increase the surface of the liquid-to-air face and thereby increase the emittance of gas from the liquid. In order to further increase this surface, a magnet is placed at the bottom of the petri dish. The petri dish is then placed in the glass-container in the flushing system. The glass container is placed on top of a magnetic stirrer.

A flush (with atmospheric air) of the system starts just seconds before the petri dish is placed in the glass container. The flush prior to measurement is essential to secure a known and reproducible gas composition in the system.

The first measurement of each mono-culture is a measurement of the gas emitted from the pure nitrification bacteria. This measurement should not show any increase in  $N_2O$

concentration - other than the very small leak-rate. The experiment can continue after approximately 90 minutes, if no potential increase of  $N_2O$  concentration can be identified. If a production is visible this needs to be flushed out before proceeding.

The experiment proceeds by starting a flush of the system, and meanwhile add 3mL of ammonium (3 mL of 220 mg  $NH_4Cl$  per liter) into the petri dish. After the end of the flush, the measurement of the production of  $N_2O$  from the nitrification culture takes place.

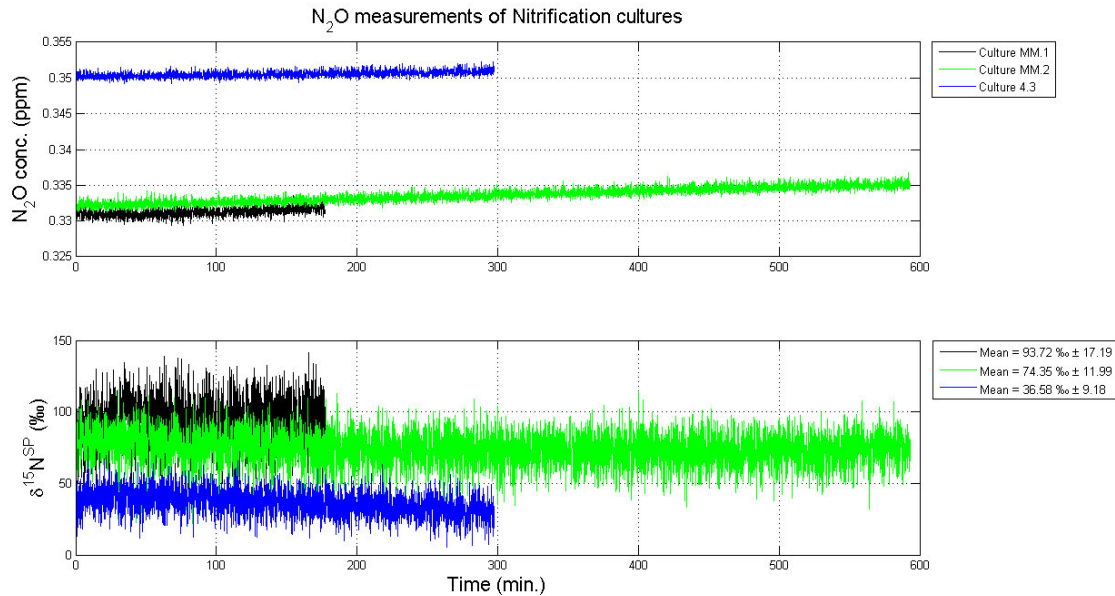


Figure 6.1: The  $N_2O$  concentration and SP from the tests with nitrifying bacteria culture 4. The green and black profiles represent measurements of *Nitrosospira multiformis*. The blue profile represents a measurement of *Nitrosomonas europaea*.

Multiple experiments have been made in order to produce a significant concentration of  $N_2O$  during a nitrification process. In figure 6.1 three measurements of nitrification production are shown. The green and black profile were measured in spring 2013 in Copenhagen. These two profiles represents measurements of *Nitrosospira multiformis*. A significantly leak were found after these measurements were made. The significance of this leak can be seen in the low starting concentration. New bacterias were not available before the field season at Disko, because of a relatively long growth period of new bacteria. The blue profile was measured in July 2013 on Disko Island. This profile represents a measurement of *Nitrosomonas europaea*. In the bottom figure the measured SP variability is shown. From these profiles it can be seen that the SP-value is different for each of the three measurements. The mean of the SP ranges from 36.6 ‰ up to 93.7 ‰. This large difference can be explained from the fact that two different nitrifying cultures were used and because of the leak.

In figure 6.2 the full evolution of the  $N_2O$  concentration and SP, during the nitrification process of *Nitrosomonas europaea*, is shown. This measurement is from Disko Island. In this figure, the red part represents the flush of the system and the black part the actual measurement.

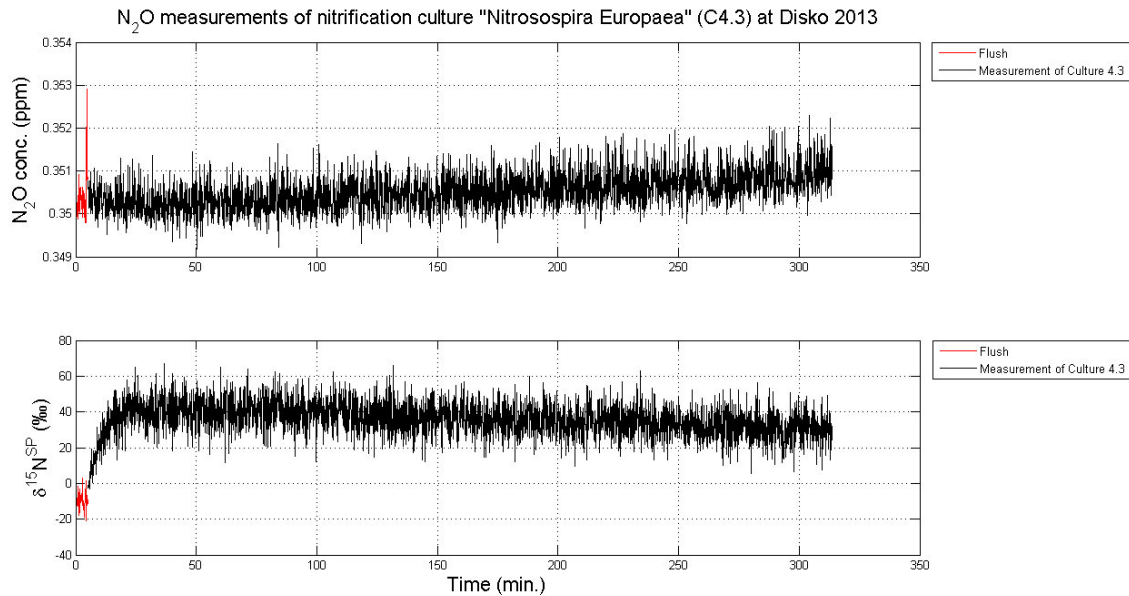


Figure 6.2: *The evolution of  $N_2O$  concentration and site preference of nitrification bacteria culture 4.3*

The most interesting part of this figure is the evolution of the  $N_2O$  concentration. Compared to figure 6.1 it is easier to see the small variations over time in figure 6.2. The conclusion on this is revealed later in chapter 10.

## 6.2 Denitrification bacteria experiment

The experiments with denitrifying bacteria start out with a degassing of the denitrification bacteria with the bottled  $N_2$ . This needs to be done in order to secure that the glass flask containing the denitrifying bacteria, are free of  $N_2O$  prior to the measurements. This degassing was done by bubbling  $N_2$  through the water for approximately 12 hours (over night). This degassing will cause an uptake of any other dissolved gas in the water.

After the degassing the glass-flask is placed in the big glass container in the flushing setup.  $KNO_3$  is added (2.5 mL of 45 mg  $KNO_3$  per liter) to the flask just before it is placed in the container. A flush of the system starts when the flask is placed in the setup. The flush is performed with the bottled  $N_2$  since the denitrifying bacteria works under anaerobic conditions. When the flush is finished, the measurement of the  $N_2O$  production from denitrifying bacteria starts.

As already stated, two different denitrifying bacteria were measured during the work presented. The profiles presented in figure 6.3, show the results of the measurements of *Pseudomonas Chlororaphis* (culture 14). This culture misses the last step of denitrification caused by the enzym called "Nitrous oxide reductase". This means that the produced  $N_2O$  never converses to  $N_2$ . A more detailed description can be found in section 2.3.2.

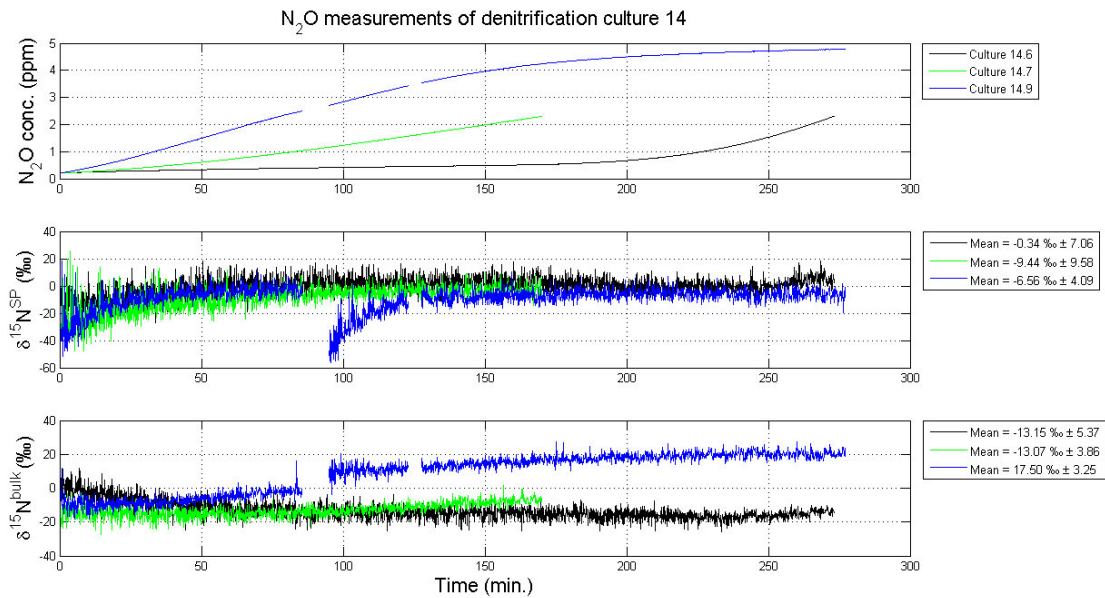


Figure 6.3: *The  $N_2O$  concentration, the SP and the Bulk from the tests with denitrifying bacteria culture 14.*

In this figure three different measurements of the culture are shown. The green and black profiles represent one continuous measurement, from the addition of  $KNO_3$  and until approximately a concentration of 2.3 ppm is reached. The blue profile represents the "full" profile as it looks if all of the  $KNO_3$  is used. This profile is a stitched together profile, in which two measurements are stacked. This stacking was needed since the concentration of the gas becomes too high (concentrations above approximately 2.3 ppm.) for a reliable measurements. Therefore a flush of the system was done between the first and second part of the profile. The concentration of  $N_2O$  starts from close to zero after a flush, allowing the production to continue within the reliable range. The profile is stiched by chosing the intervals of interest (with gabs in between). The first part is plotted normally. The second part (from 95 minutes and foward) is corrected for the flush. This means that the zero point (starting point) of the second part is corrected and moved to the end concentration of the first part. All of the values measured in the second part is then multiplied with the new zero point. The second gap is because of a transient failure in the instrument. In the analysis the data was corrected for the flush and failure, and placed as it would have looked like if

the measurements were continuous.

In the middle part of this figure the SP is plotted. From these profiles it can be seen that the SP is increasing in the beginning. The profiles level out and become stable after approximately 50 min. This level of stability in SP is for all of the profiles just below a SP-value of 0. For the three profiles the exact values are: black =  $-0.3 \text{ ‰} \pm 7.1 \text{ ‰}$ , green =  $-9.4 \text{ ‰} \pm 9.6 \text{ ‰}$  and blue =  $-6.6 \text{ ‰} \pm 4.1 \text{ ‰}$ .

The lowest part of the figure presents the bulk values of the measurements. These bulk values are all stabilizing over the time frame of the measurements. The green and black profiles are stable almost instantly whereas the blue profile increases for approx. 220 minutes before it stabilizes. That the bulk values are stabilizing is another indication that the isotopic composition is stable.

In figure 6.4 the results of the measurements of *Pseudomonas Fluorescens* (culture 1) are presented. This culture is the full denitrifying bacteria. This means that  $\text{N}_2\text{O}$  is produced when food ( $\text{NO}_3^-$ ) is available. When the  $\text{NO}_3^-$  is used the consumption of  $\text{N}_2\text{O}$  takes over and produces  $\text{N}_2$ . This is also described in section 2.3.2.

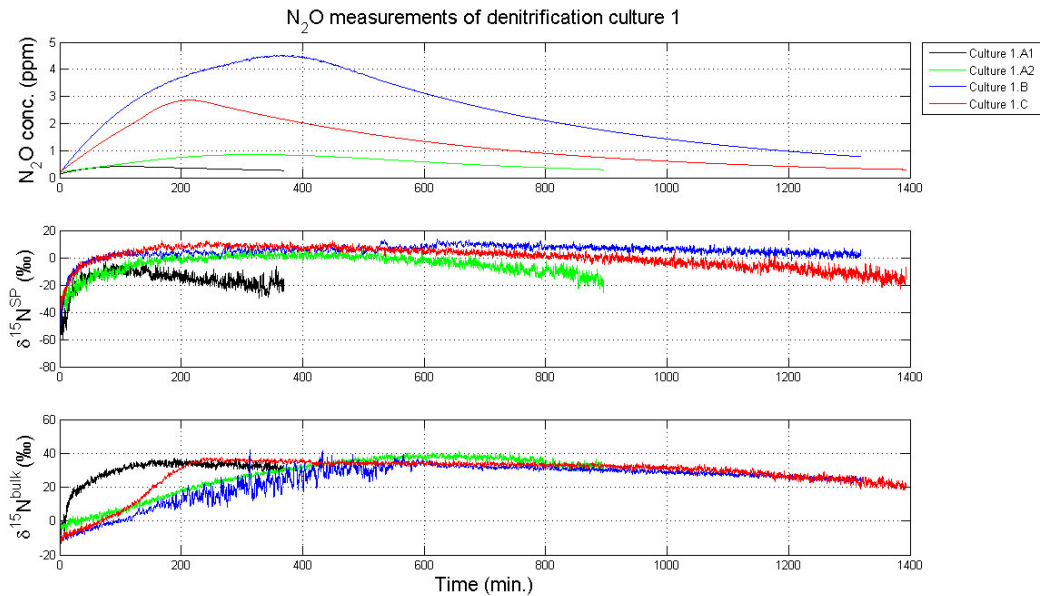


Figure 6.4: *The  $\text{N}_2\text{O}$  concentration, the SP and the Bulk from the tests with denitrifying bacteria culture 1.*

This figure consists of three plots, showing the concentration, the SP and the bulk respectively. In the top-plot, four profiles of three different samples of the culture are shown. The black profile represents the first measurement, in which only a small addition of  $\text{KNO}_3$  was added. Once the  $\text{N}_2\text{O}$  concentration was back to reference, a second (small) addition of

$\text{KNO}_3$  was added. The second measurement is represented by the green profile. The blue profile represents the third measurement, in which 10 times more  $\text{KNO}_3$  was added than in the first measurement. The red profile represents the fourth measurement. This profile is (for this instrument) the best profile, since the concentration stays below 3 ppm.

One very interesting feature of these measurements compared to those of culture 14, is the path of the concentration e.g., first half of the experiment production dominates leading to an increase when  $\text{NO}_3^-$  is being consumed. In the second half uptake dominates and a decrease is therefore observed.

The middle-plot shows the change in SP over the time of measurements. Over the time frame of the measurements all of the profiles have a similar tendency to follow the concentration up and down, around a maximum. A significant difference between the concentration curve and the SP curve is the stability of the maximum values. The SP stays at the maximum value for a longer period. This top part is shown in figure 6.5.

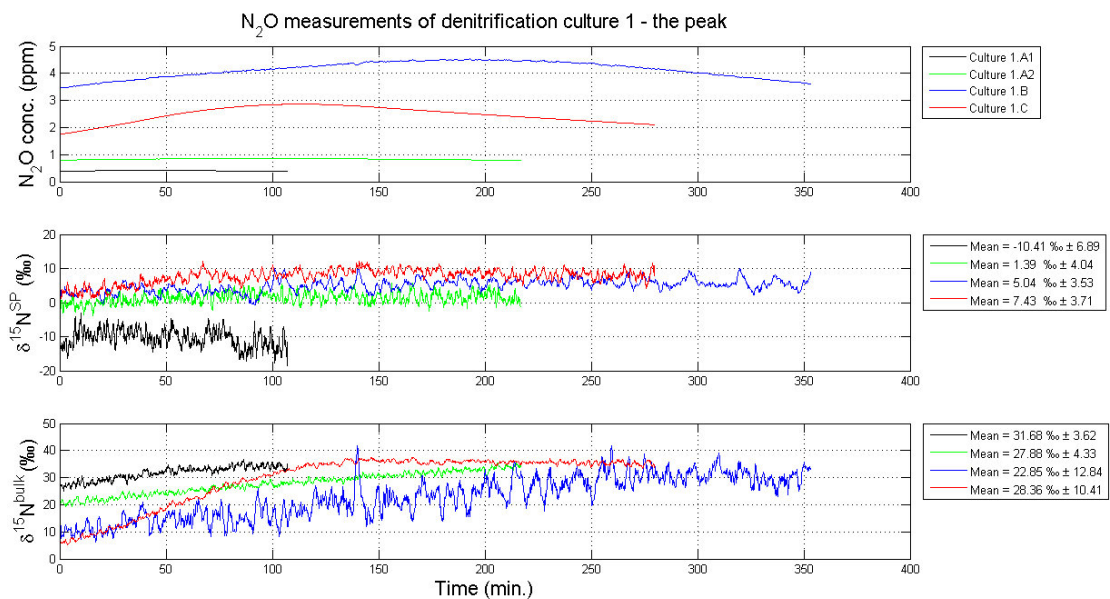


Figure 6.5: *The  $\text{N}_2\text{O}$  concentration, the SP and the Bulk from the tests with denitrifying bacteria culture 1.*

In figure 6.5 the maximum SP-values presented are obtained during the denitrification process of culture 1. The mean SP values over the top of the curves are as follows: black =  $-10.4 \text{ ‰} \pm 6.9 \text{ ‰}$ , green =  $1.4 \text{ ‰} \pm 4.0 \text{ ‰}$ , blue =  $5.0 \text{ ‰} \pm 3.5 \text{ ‰}$  and red =  $7.4 \text{ ‰} \pm 3.7 \text{ ‰}$ .

After the maximum in SP-value, the values decrease again for the rest of the measurement.

### 6.3 Validation of mono-culture experiments

For both the nitrifying and denitrifying bacteria experiments, an independent experiment was made for validating the measurements.

The validation experiments consist of measurements of clean water followed by a measurement in which  $\text{KNO}_3$  or  $\text{NH}_4\text{Cl}$  has been added to the water. This way the water will be exposed for the same chemical solution as the bacteria. It is therefore possible to tell if the changes found in the mono-culture experiments are because of a bacterial growth/destruction of the  $\text{N}_2\text{O}$ -molecules or just because of the added chemicals. For this reason the experiment is called a blank test.

The water used in both of these experiments was deionized and UV-filtered before it was poured into a glass flask and autoclaved. This leaves water in which all potential bacteria is killed.

In figure 6.6 and figure 6.7 the blank test with  $\text{KNO}_3$  and  $\text{NH}_4\text{Cl}$  are shown. In both of these experiments the amount of chemical solution added prior to the test, is identical to the amount added in the mono-culture experiments.

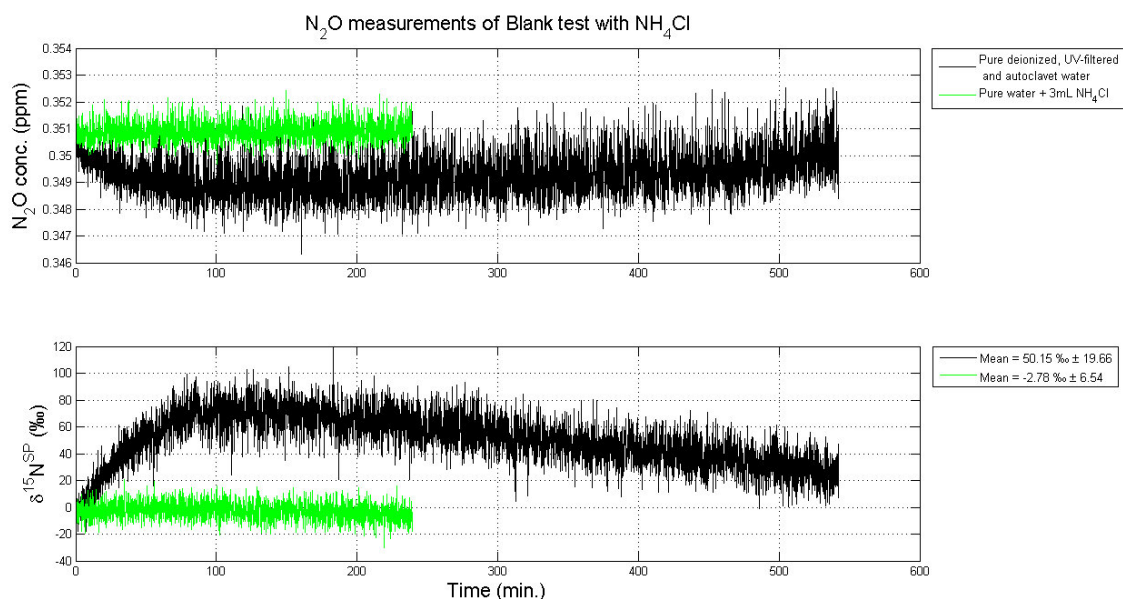


Figure 6.6: *The  $\text{N}_2\text{O}$  concentration and SP from the blank test with  $\text{KNO}_3$ .*

In both of these figures the black profile represents the pure water and the green profile represents the water after addition of the respective chemical solution. The important profile is in both cases the green. Since there is no  $\text{N}_2\text{O}$  present in either the water nor in the chemical solution, there should not be any changes in either the concentration or in the SP.

It is clear that a slight change in both concentration and SP is detected from the pure

water as shown in figure 6.6. This is probably due to a small amount of  $N_2O$  in the water, due to the exposure to the atmospheric air. The green profiles, on the other hand, are very stable both in concentration and SP. This denotes that there is no  $N_2O$  bonded in the  $NH_4Cl$  solution. The results given in the nitrifying experiments are therefore due only to production and destruction from the bacteria.

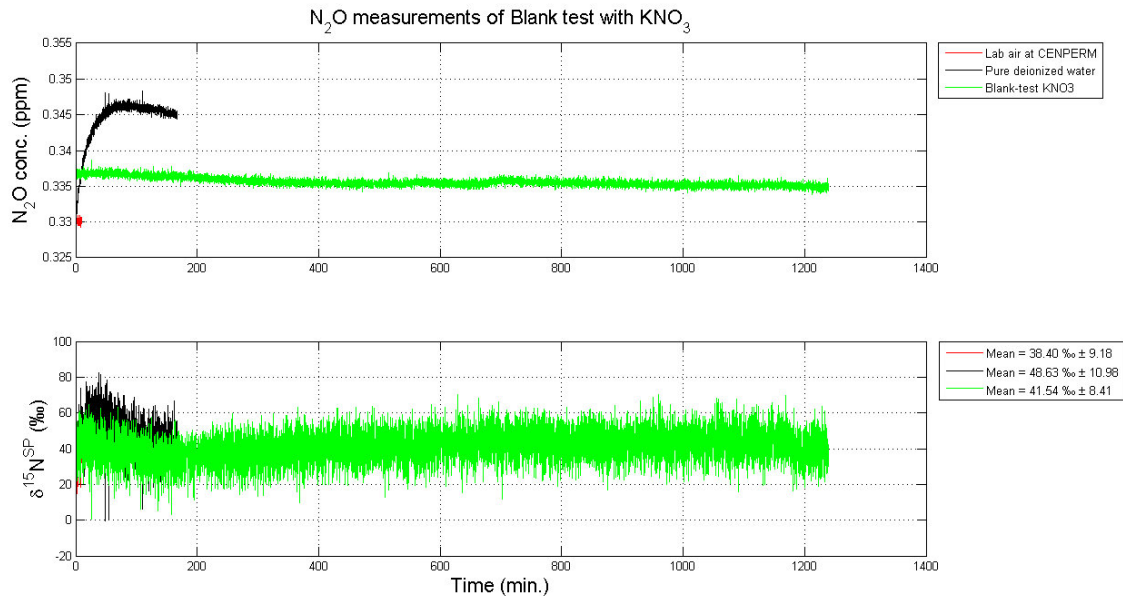


Figure 6.7: *The  $N_2O$  concentration and SP from the blank test with  $KNO_3$ .*

The shape of the profiles in figure 6.7 is the same as in figure 6.6, but the starting concentration and SP are different. This is because of the leak in the setup (as explained previously). An extra profile (red) is shown in this figure. This profile represents the laboratory air around the instrument. The reason that this profile is in the figure, is because it can be assumed that a significant amount of lab air was flushed into the system during the flush. The offset in starting concentration and SP can therefore be concluded to be due to a flush with a mixture of the atmospheric air (on bottle) and the air from the laboratory. Both the concentration and the SP are more or less constant after the addition of the  $KNO_3$  solution. It is therefore safe to believe that the  $KNO_3$  solution is free of  $N_2O$ . The results given in the denitrifying experiments are trustworthy.

## Incubation experiment

This first experiment is an incubation of  $\text{N}_2\text{O}$  from the bacteria in a soil sample from a natural ecosystem from the minerotrophic wetlands called Maglemosen.

### 7.1 Experimental description

A soil core of dimensions  $W \times H \times D = 20 \text{ cm} \times 20 \text{ cm} \times 20 \text{ cm}$  with growing vegetation was taken from Maglemosen and brought back to the laboratory. Maglemosen is a nonmanaged minerotrophic wetland located at  $(55^\circ 51' N, 12^\circ 32' E)$  approximately 20 km north of Copenhagen (as shown in figure 7.1). The soil sample used in this experiment was a small



Figure 7.1: *Picture of the site in Maglemosen from which the soil sample was taken.*

part of this intact soil core. The core is a sample of the top 20 cm in the root zone. It can

therefore be treated as a full functional ecosystem. The sample was dug up after a period of approximately 3 weeks with a water level approximately 30 cm below the surface. This dry period resulted in an oxidization of the soil sample. These conditions resulted in perfect conditions for nitrifying bacteria. A detailed description of the soil and site can be found in the paper by Jørgensen et al., 2012 [22].

In the laboratory the soil was placed in a glass-cylinder without a lid. The soil was standing on a table in the lab (filled with normal atmospheric air) for a week before it was used. During this period the soil was damped and kept in a natural light-cycle, so that any natural process would continue as if it had not been moved.

Prior to the measurements the soil was moved into the glass container and placed in the flushing setup with the Picarro analyzer. The experiment started with a flush of the system with atmospheric air (on bottle). Hereafter the dirt was left for 40 hours while measuring the production/destruction of the  $N_2O$ . In figure 7.2 these continuous measurements are shown.

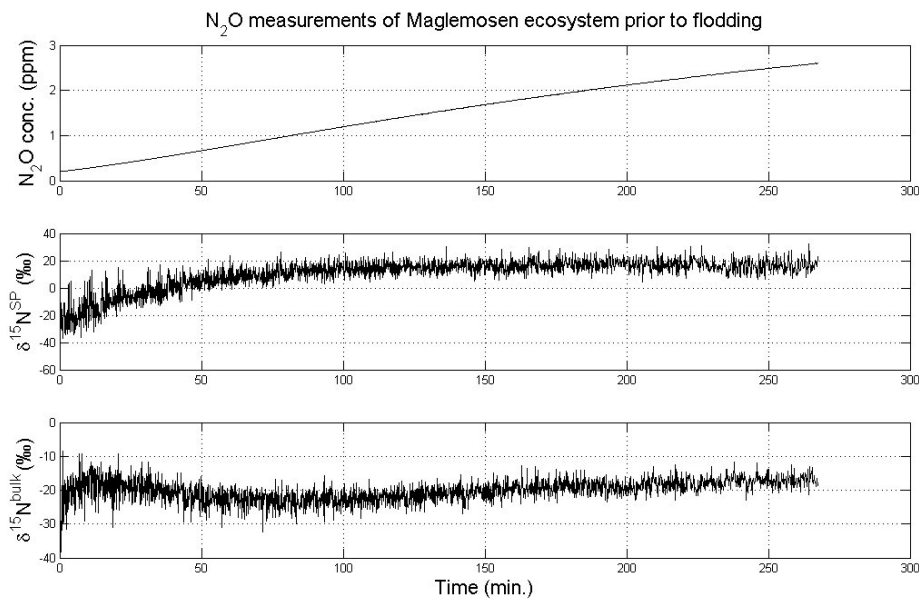


Figure 7.2: *The  $N_2O$  concentration, the SP and the Bulk from the dirt flooding test - prior to the flooding.*

The top plot represents the concentration of  $N_2O$ , the middle plot represents the SP and the last plot represents the bulk changes over time. The concentration of  $N_2O$  is clearly increasing at an almost constant rate over the time frame of this experiment. In the beginning the SP is increasing. Then after approximately 100 minutes the SP is stabilizing at approximately 18 ‰. The bulk values are oscillating a bit more, but it is still relative stable

around -15 ‰. This indicates that the relative difference between the isotopomers is more or less stable.

While the dirt sample was measured a bottle of deionized water was degassing with  $N_2$ . This was done in order to make sure that no additional  $N_2O$  was left to be added to the soil through the water. This degassing lasted over night (approximately 10 hours).

After the measurement of the soil (as shown in the figure), the sample was flushed several times with  $N_2$ . This was done until there was no production or destruction of  $N_2O$ . Once no activity was detectable, the dirt sample was flooded with the degassed water, then flushed and measured. The measurement of the flooded sample is shown in figure 7.3.

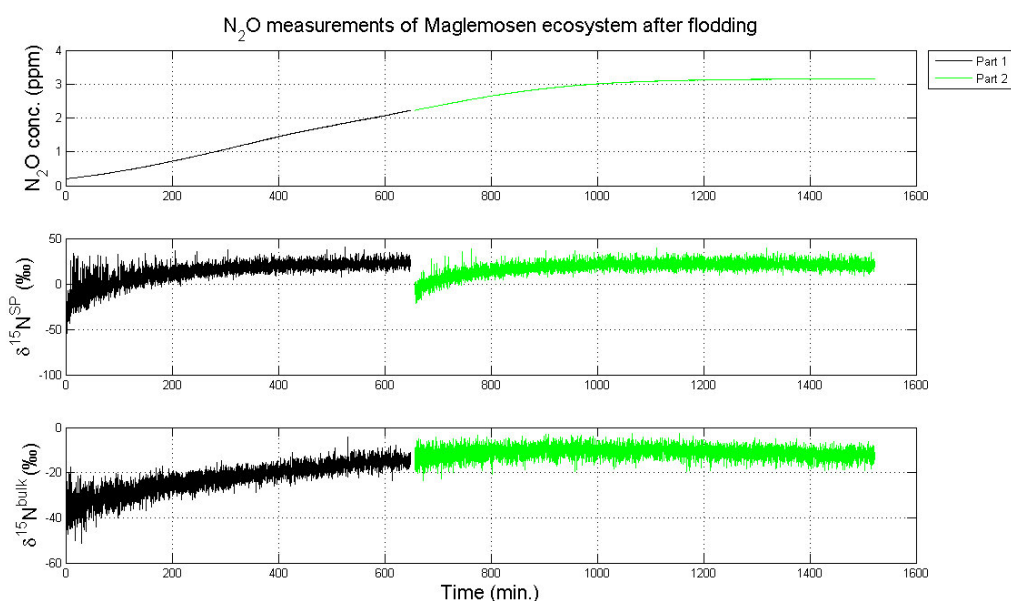


Figure 7.3: *The  $N_2O$  concentration, the SP and the Bulk from the dirt flooding test - after the flooding.*

In this figure two profiles are shown. Both of the profiles are measurements of the same sample (the flooded dirt sample). A flush of the system was needed since the instrument is not accurate at concentrations above ca. 2.5 ppm. The black profile represents the first measurement and the green profile represents the second measurements.

The concentration profiles indicate that a very nice and smooth upsurge in  $N_2O$ , until it levels out at approximately 3.2 ppm. The slope of the concentration profile is less steep than in figure 7.2. Both of the SP profiles indicate that the SP of the sample is 20 ‰. These SP curves are not immediately at that level of SP, since the gas emitted from the samples needs to mix with the flushing gas. The bulk values are as well increasing until they reach a constant level at approximately -10 ‰ after approximately 800 minutes.

## Field experiment at Buresoe

Production of  $N_2O$  is primarily done through nitrifying and denitrifying processes. The first field experiment is testing the change in isotopic composition of  $N_2O$  as a result of the changing environments on a slope towards swamp.

### 8.1 Site description and location

The first field experiment presented in this thesis was done between September 2012 and April 2013 at a test site in Buresoe. Buresoe is a forest with both lakes and swamps. It is located 30 km to the north-west of Copenhagen at  $55^\circ 49'$  N,  $12^\circ 15'$  E.

The test site is 6 meters  $\times$  15 meters in dimensions, and consists of 20 measuring points as shown in figure 8.1. The first row (sites 1, 6, 11 and 16) is placed a few meters from a trail, at the top of an upward slope. The following four rows are then placed down slope, until row no. 5 (sites 5, 10, 15 and 20) which is located just next to a swampy area. The change in elevation from the first row to the last row is approximately 3 meters.

The position of the rows were chosen in such a way that there is a difference in the elevation of each row, as well as an increasing humidity of the soil at each row. The con-

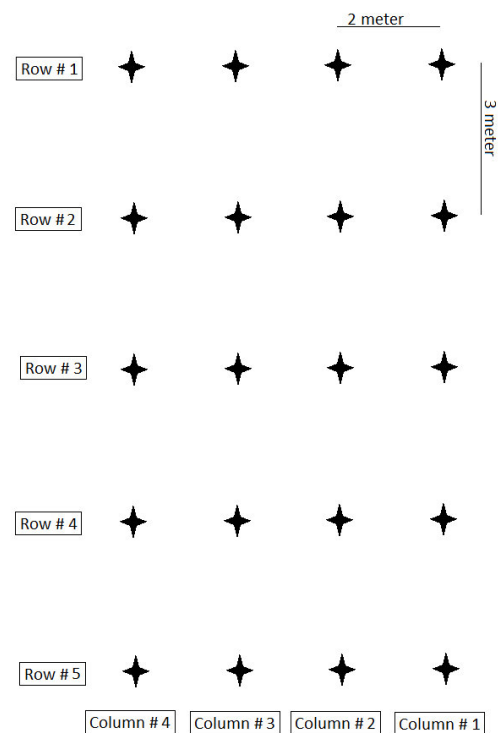


Figure 8.1: *Schematics of the test-site at Buresoe, with the stars representing the measuring points.*

ditions of the soil at the measuring points, are going from an aerobic environment at the first row, towards a more anaerobic environment at the last row. The intention with this is to carry out a study of the effect on  $N_2O$  production from the nitrifying bacteria versus the denitrifying bacteria.

## 8.2 Experimental description and results

The experiments made at this test site, were to collect gasses emitted from the ground using the gas collection setup as described in section 4.4. At each of the 20 measuring points a plastic tube (with an inner diameter of 10 cm) was pushed approximately 15 cm into the soil. The plastic tubes were pushed into the soil in the summer of 2012. This was done in order for the microorganisms not to be effected by the disturbance of pushing the tubes into the soil (the microorganisms needs at least 48 hours between being disturbed and measuring). The experiment started by placing a lit on top of each plastic tube. Before the gas samples were collected the lit had to be on for about 20 minutes. This way the gas inside the tube would have the signature of the microorganisms emitting the gas from the ground. At each test-site approximately 1.5 L of gas was collected in gas sample bags. Once a sample from each site was collected the gas was transported back and analyzed using the "sample bag measuring setup" (as described in section 4.3) in the laboratory. The samples were collected four times; in September 2012, October 2012, November 2012 and April 2013 respectively.

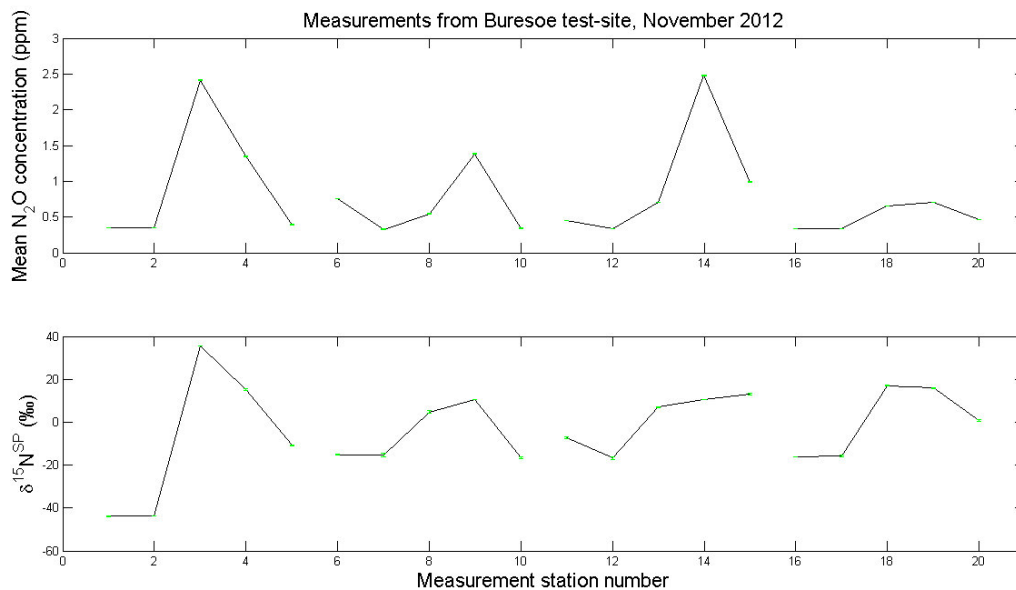


Figure 8.2: *Third measurement at Buresoe, November 27th 2012.*

The results from the measurements done on November 27th 2012 are shown in figure 8.2. The values plotted in this figure are the mean values of a 45 minutes measurement of each sample bag. The values indicate that both the highest concentrations of  $N_2O$  and some of the highest SP-values are emitted from the sites in row four. Also the sites in row three are emitting  $N_2O$  with higher SP-values, than row one and two. Both the lowest concentrations and SP-values are emitted from row one and two just as expected.

All of the 20 sites were not measured at each measuring campaign, because of difficulties with the sample bags and the gas collection setup. The tendency of all the successful measurements are the same as found in figure 8.2. The mean values of all successful measurements in each of the five rows are:

Row No.	$N_2O$ concentration [ppm]	SP [‰]
1	$0.487 \pm 0.164$	$-9.56 \pm 7.88$
2	$0.363 \pm 0.047$	$-14.31 \pm 2.69$
3	$3.995 \pm 3.437$	$15.74 \pm 8.92$
4	$4.016 \pm 5.229$	$16.72 \pm 7.08$
5	$0.542 \pm 0.182$	$0.6717 \pm 13.40$

Table 8.1: Mean  $N_2O$  and SP measurements from Buresoe.

## Field experiments at Disko Island

A series of experiments were conducted during a field campaign on Disko Island, Greenland, in July and August 2013. The experiments all had the common cause of identifying the isotopic composition of the  $N_2O$  emitted from different sites. In the following chapter the results from these experiments are presented.

### 9.1 Site description and location

The second field experiment presented in this thesis, was done in July 2013 at a test site approximately 3 km to the east from the Arctic Station, on the south coast of the Disko Island in central West Greenland ( $69^{\circ}15' N$ ,  $53^{\circ}34' W$ ). The test site was made by the CENPERM group during the summer periods in the years 2012 and 2013. The sites are located with a geographical position leading to a low arctic coastal climate. Furthermore the test site is placed in an area called "wind valley" because of the strong winds blowing through the valley, especially throughout the winter. The test site consists primarily of a



Figure 9.1: *Photograph of the test-side on Disko island, Greenland. The measuring blocks are located to the left in this picture.*

total of 12 blocks (north-south turning) each divided in two by a snow-fence in the middle. The snow fences are constructed for experiments to clarify the treatment effects on the natural ecosystems. The snow fences should clarify the effect caused by a change in snow accumulation on top of the test ground. The wind primarily blows from the north to the south during the winter months. This results in an accumulation of snow on the south side of the fence, and a thinner layer of snow on the north side. This variation in snow results in two different conditions. On the north side where the snow accumulation is less, the period without snow is longer and therefore is the growth-period for the underlying soil and plants longer. The opposite is the case on the south side, leading to a shorter growth-period. Each side of the snow fence is divided into 4 plots with the treatment as listed below.

- Plot A: No treatment - Surves as a standard plot.
- Plot B: ITEX (International Tundra Experiment) - ITEX is a six-sided plastic chamber without a roof, serving the same purpose as a greenhouse.
- Plot C: Shrub removal - Removing plants which are known to be sensitive to the climate changes makes it possible to investigate the changes caused by the change in vegetation.
- Plot D: ITEX and shrub removal - a combination of B and C.

Therefore, each block has 8 plots with different treatments. The only difference between the north and the south side is the difference in conditions caused by the snow fences. The 12 blocks can be divided into 6 blocks placed at higher and drier locations, and 6 blocks placed at lower wetter locations. It is therefore possible to measure changes caused by these different environments.

## 9.2 Experimental description and results

Several experiments were made during the field campaign on Disko Island. The experiments all had the same primary scientific objective. Namely to identify the concentration and the site preference of the  $N_2O$  gasses. The difference between the experiments is the location and the biological and geographical conditions of the measuring sites. The different locations have been chosen to detect a handful of different theories about the  $N_2O$  production in the arctic. These locations can be differentiated in humidity of the soil and the elevation of the site.



Figure 9.2: *Photograph of the snow fences at one of the dry sites. Both sides of the snow fence is similar with only a difference in the distribution of the four plots (since they are distributed randomly).*

### 9.2.1 Dry snow-fence site

The first location is the dry snow-fence sites. These sites were chosen since they are both located at a higher elevation above sea level and the ground underneath is drier than the surrounding areas. It is expected that a nitrification process is the most dominant producer of the  $N_2O$  gasses because of this drier conditions. This is also expected since we know that these sites overlaying a very ammonium-rich permafrost-layer [From oral conversation with Professor Bo Elberling, CENPERM].

In practice the measurements of emission of  $N_2O$  gasses from the dry snow-fence sites, were done using the gas collection setup (section 4.4), and the chamber system made by the CENPERM group.

This chamber system consists of a 20 cm x 20 cm square metal frame which is placed a couple of centimeters in the ground, at the area of interest. The top part of the frame is above the ground and is split up into an inner and an outer frame (creating a small "canal"). The gas collection starts out with filling some water into the "canal". This water prevents a leak of gas while the gasses are accumulating inside the plastic chamber. The plastic chamber is approximately 30 cm high and has a rubber plug (1 cm in diameter) at the top. An 1/8" tubing goes through the plug, serving as the connection between the chamber and the gas collection setup. The chamber was placed on top of the frame for 20 minutes before the collection of the gas was started.

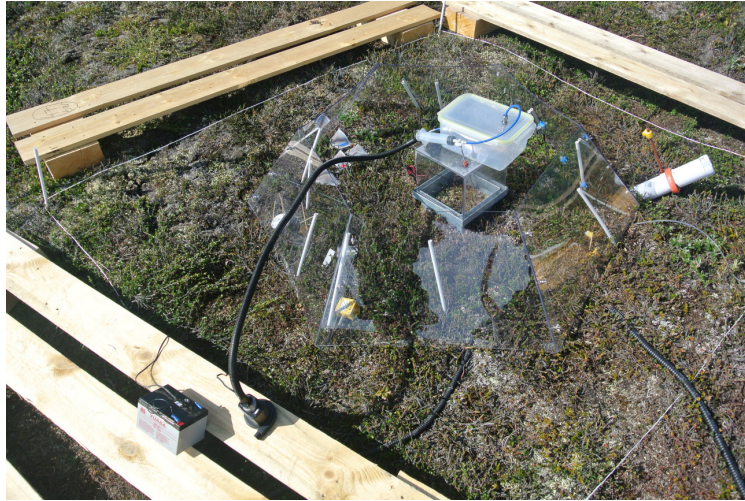


Figure 9.3: Photograph of the gas extraction setup, with the chamber system made by the CENPERM group.

There are a total of 6 dry snow-fence sites. The measurements conducted at these sites showed significant differences in SP and as well very low concentrations of  $N_2O$ . The large spread in SP combined with a low concentration of  $N_2O$  is most probably due to a sink in  $N_2O$  at some of the plots (this will be discussed further in the chapter 10). Measurements of the atmospheric air was performed in order to distinguish the sites of production from those of causing a sink in  $N_2O$ . The atmospheric air samples were taken from ca. 2.5 meter above the ground at one of the dry snow-fence site. The plots producing  $N_2O$  were chosen to be those with an average concentration above the average concentration of the atmospheric air (as presented in figure C.1). Plot number 1, 2 and 3 have an average concentration above this value. It is therefore only plot 1, 2 and 3 which is presented in this thesis.

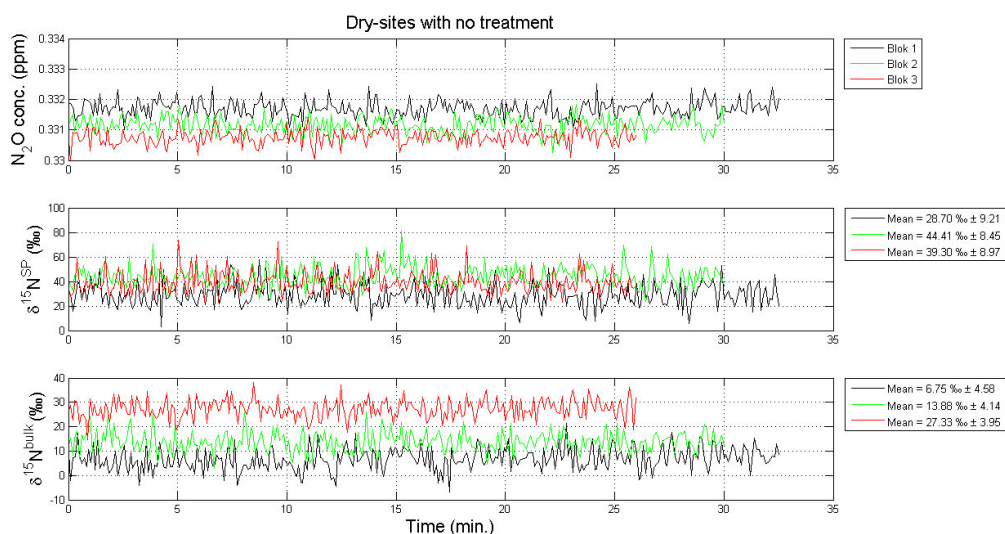


Figure 9.4: The  $N_2O$  concentration, site preference and Bulk-value from measurements of the plots with no treatment.

The measurements conducted at the dry snow-fence site is used in both the slope and the treatment effect experiment. The different measurements are therefore presented in groups of equal treatment. All of the 8 treatment plots can be found in appendix D. It is clear from these figures that the effect of the different treatments is very limited. It was therefore chosen that only the control sites and the sites with only snow-fence as treatment should be presented here.

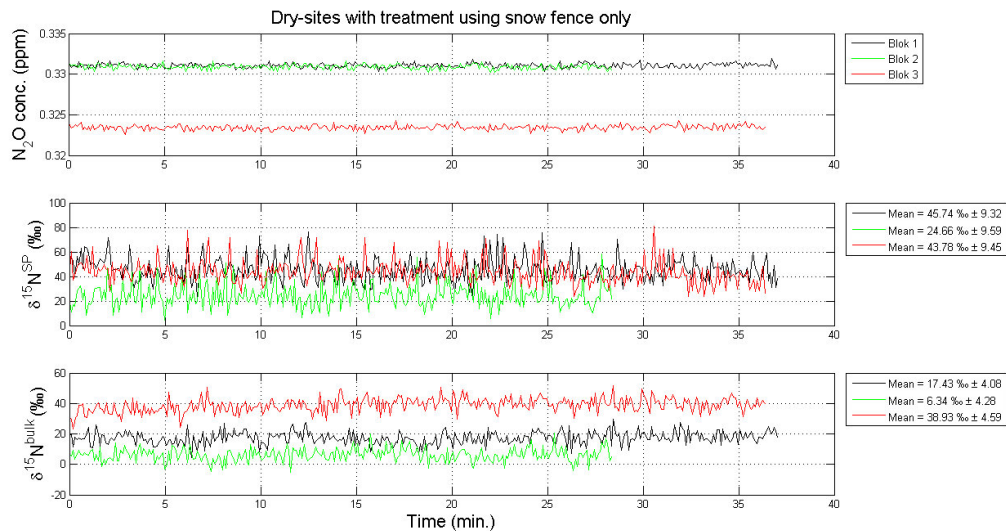


Figure 9.5: *The  $N_2O$  concentration, site preference and Bulk-value from measurements of the plots with the effect of the snow-fence as the only treatment.*

The top graph in both figure 9.4 and 9.5, shows the concentration as collected from each of the three blocks. These concentrations all show values around the atmospheric concentration found at Disko (see appendix C for verification). The most interesting graph is the second graph in each figure, since it shows the SP from each of the three blocks. All of the profiles presented in these two figures are ranging between a SP of 24 ‰ and 46 ‰. The average SP value (as measured at the control plots) presented in figure 9.4 is  $37.5 \text{ ‰} \pm 8.9$ . The average SP value (for the plots with snow-fence treatment) presented in figure 9.5 is  $SP = 38 \text{ ‰} \pm 9.5$ .

## 9.2.2 Wet snow-fence site

The second location is the wet snow-fence site. The wet site is located in a small valley between a mountain ridge and the higher leveled dry site. This site is very wet, because of all the melting water flowing down the mountain as the snow and ice melts. Since a lot more water is present at this site, a denitrification process is expected to dominate.

The measuring method is identical to the one used at the dry snow-fence site.

The  $N_2O$  concentrations at this site are in the area of that of the atmospheric air, just as

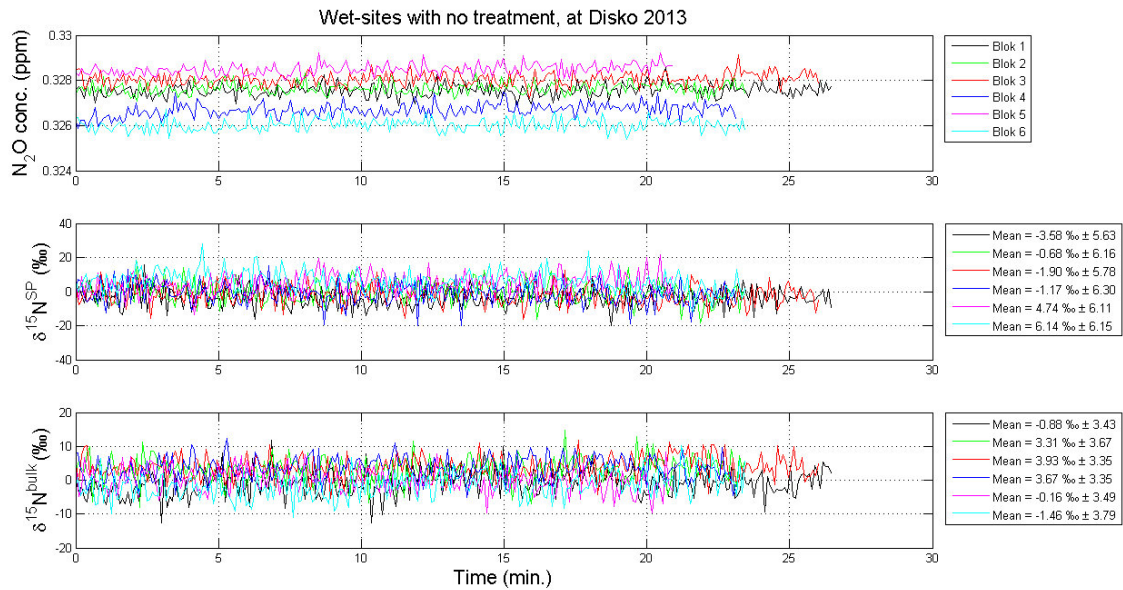


Figure 9.6: The  $N_2O$  concentration, the SP and the Bulk from the wet test sites at Disko.

was the case at the dry site. The interesting part of figure 9.6 is the second graph. This graph shows that the SP measured in all of the six blocks are equal to zero, within the standard deviation. This can further be demonstrated by looking at the average of the six wet sites. The average SP-value of the wet sites are  $SP = 0.6 \text{ ‰} \pm 6.0$ .

### 9.2.3 Transportation of Nitrous Oxide

The fourth arctic  $N_2O$  identification experiment was performed to make a test of the  $N_2O$ -gas transport from the source through the soil and into the atmosphere.

The motivation for this experiment is due to previous experiments by Askaer et al., 2011 [2]. The results presented in that paper show the importance of *Phalaris arundinacea* as a  $CH_4$  transporter from soil to atmosphere. At the sites on Disko Island, the plants of interest are *Carex stans* and *Eriophorum scheuchzeri*. These plants are both similar to the ones used in the paper by Askaer et al., 2011. The reason for this very effective gas transport is first of all that the plants have a very long root system (figure 9.7). This means that the roots can penetrate



Figure 9.7: *Carex stans*

deep into the ground to a depth of (10-30 cm), where the production of methane happens. Phalaris is an extremely good gas transporter due to the root construction. These roots are built in such a way that there are vertical channels going from the end of the root all the way through the plant. These long channels must always be filled with gasses in order to keep water from entering and thereby drowning the plant. The gasses entering these channels are therefore filled with whatever gasses are produced below the surface of the ground. These gasses are transported through the plant and into the atmosphere. Jørgensen et al., 2012 [22] presented results indicating that this gas transport inside Phalaris also occurs with  $N_2O$ .

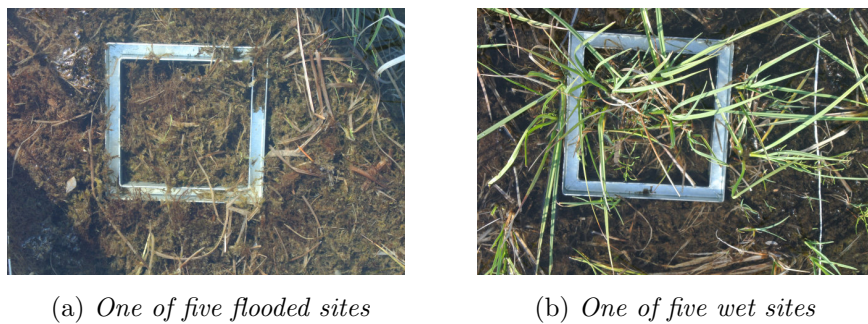


Figure 9.8: Pictures taken next to the wet snow-fence site, at the new sites where the ground is flooded in large areas.

The purpose of this experiment is to see if the  $N_2$  gas-transport in this arctic region is similar to that presented by Jørgensen et al., 2012 [22] and Askaer et al., 2011 [2]. This experiment is in other words to measure the gas transport/emission from two different types of sites. One in which only a few plants are present (figure 9.8a). One in which there are no plants above the water level (figure 9.8b). The experiment is conducted with the use of the CENPERM chamber and the gas collection setup. If the transport of  $N_2O$  is similar to that previously published it would, be possible to clearly distinguish the two sites from each other. This difference will be visible when looking at the concentrations and/or the SP. The results from the gas transportation-test are shown in figure 9.9.

The top graph shows the  $N_2O$  concentrations. It is clear that the gas concentrations are about the same order as the concentrations of the atmospheric air measured at the test site. Other than this the graph shows that the concentrations of  $N_2O$  are a bit larger for the sites including plants than the one with only water. When looking at the SP in the middle graph only a very small difference appears. This indicates that a small fractionation is possibly occurring at the sites with plants compared to the site with only water. The bulk values

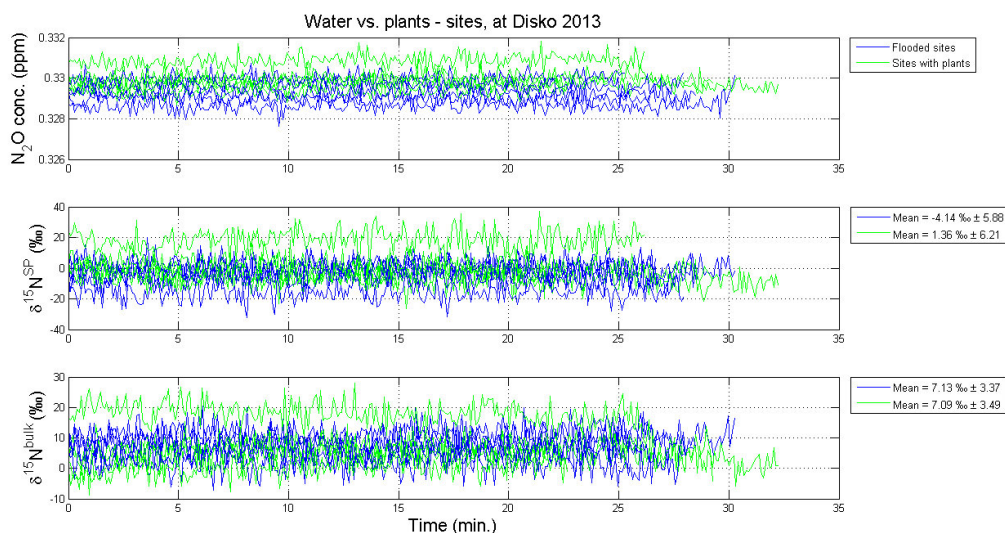


Figure 9.9: The  $N_2O$  concentration, the SP and the Bulk from the "Water vs. plant site", at Disko.

(plotted on the last graph) do not show any difference of significance.

#### 9.2.4 Arctic active layer production

The last experiment on Disko Island is the "Arctic active layer emission" experiment. The purpose of this experiment was to measure the emission of  $N_2O$  from different depths in the active layer.

Four dirt samples were dug out from a "random" spot next to one of the wet sites. The samples all came from the same column of dirt. The volume of this column was approximately 10 times that needed. This was done in order to secure undisturbed samples. The dirt samples were placed in sample bags for storage before being transported back to the lab and measured.

In figure 9.10 and 9.11 the measurements from the top and the third layer are presented. In both of the figures two profiles are shown in each of the three plots. The black profile is the pure dirt sample measured. The green profile is a flooded dirt sample. These two layers have been chosen because they show some interesting features compared to the other two. The results from the second and fourth layer measurements can be found in appendix E.

The story is the same for all of the four dirt samples prior to flooding. Namely that the dirt alone is not producing any  $N_2O$  of significance. This can be seen from the top plot, showing the concentration variation over time. The middle plot shows the SP. From these plots the same conclusion can be made. Namely that not much is happening in the pure

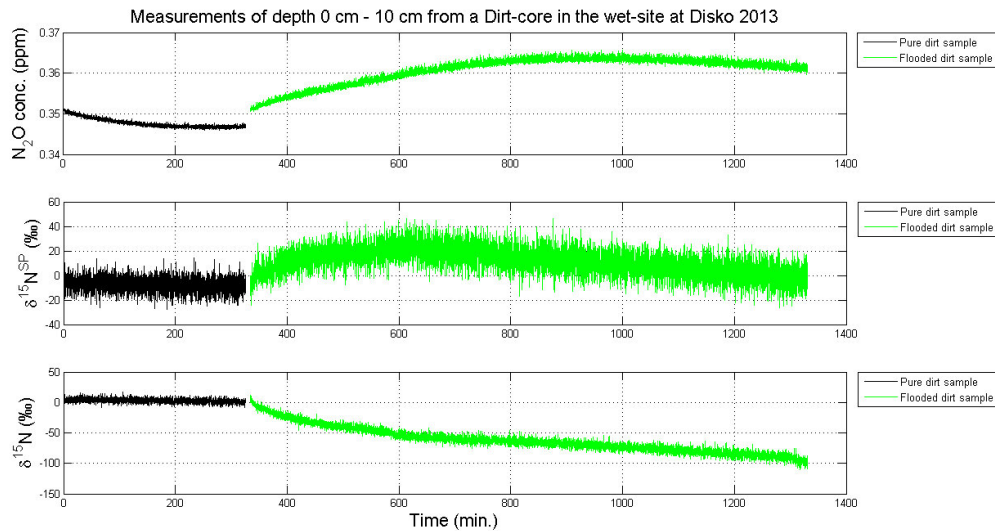


Figure 9.10: *Measurements of the first layer (0-10 cm) at a wet site.*

dirt sample. In the third plot the two figures show a difference. The measurement of the top layer show a constant  $\delta^{15}\text{N}$  variation over time. Whereas the third layer shows that the gas emitted from the sample is getting heavier.

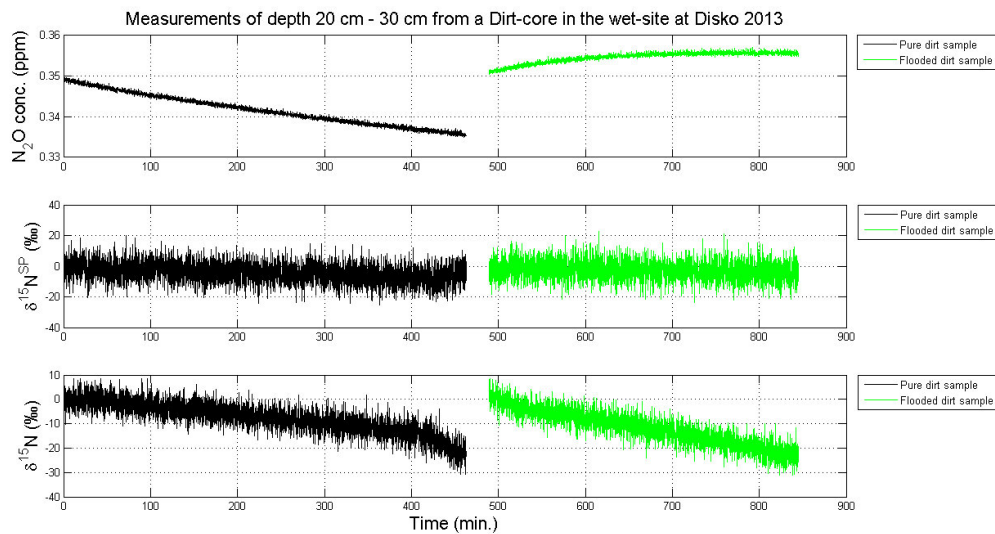


Figure 9.11: *Measurements of the third layer (20-30 cm) at a wet site.*

The story is somewhat different after the dirt has been flooded. In the two layers presented here the green profiles show that both the concentration and the SP are increasing a little in the beginning. After while the SP decreases towards negative values again. The concentration profile increases for a bit longer before it starts to decrease. These effects can be seen more easily in figure 9.10. Though the trend is the same in figure 9.11.

The  $\delta^{15}\text{N}$  profile indicates that the gas emitted from the flooded sample is getting heavier over time.

## 10

## Discussion

**The Picarro G5101-i analyzer**

The work presented in this thesis is some of the first continuous measurements of  $N_2O$ . The measurements were made possible because of the creation of the prototype of the Picarro G5101-i CRDS analyzer. The general conclusion on the analyzer is that it is working as it should. A few difficulties arose and adjustments were needed throughout the work of this thesis. Most importantly, it was found that the stability of the measurements is highly dependent on stable temperatures. This was most obvious during the campaign at Disko Island. Here the instrument was located in a cooling container on an iron table. This provided the perfect opportunity for adjusting the temperature as desired. We were therefore able to have a constant (within approximately 1-2 °C) temperature for the entire campaign (31 days). Therefore the measurements have no significant oscillating temperature profile as a course of temperature variations during the day.

Bacteria (unprovoked increase of  $N_2O$ ) appeared two times inside the instrument, during the work of this thesis. This unprovoked  $N_2O$  production was found to be either inside the tubes going into the analyzer or (most probable) in the Picarro analyzer itself. The solution was found to be a flush of the entire system with chloroform.

The unprovoked  $N_2O$  production was hardest to eliminate the first time (when the setup was in the laboratory at CENPERM). At this point a glass flask with chloroform was opened and placed inside the big glass container in the measuring setup (section 4.2). The chloroform evaporated from the flask and recirculated in the setup. This procedure was very inefficient and the flush was needed for several days before the unprovoked production was eliminated. The second time (on Disko Island), a new method for flushing the setup with chloroform was used. The glass flask with chloroform was combined through a needle (through the rubber lid on the flask) with the setup upstream from the nafion tube. This direct uptake

of gas from the small flask caused the chloroform to evaporate a lot faster due to the low pressure in the flask (a small needle was placed to ensure a minimal intake of air). After flushing the system (using this method) over night the bacteria were eliminated and the experiments could continue.

### **The mono-culture experiments**

For this thesis a suite of different experiments have been executed. The interpretation of these results are all more or less relying on the mono-culture experiments. The mono-culture experiment is divided in two sections. The first experiment concerns nitrifying bacteria and the second concerns denitrifying bacteria.

The experiments made with nitrifying bacteria were partially successful. First of all because no visible  $N_2O$  production was found from the bacteria. A significant production of  $N_2O$  is necessary in order to identify the source causing the changes. If no production occur, a change in the isotopic composition can not be identified as coming from a single source. It is therefore necessary to provoke a production for this experiment to be a succes.

In the beginning of each measurement a change in SP is visible. The SP-values from the two (black and green profile) measurements, with *Nitrosospira multiformis*, were very high (mean values of 86 ‰ and 67 ‰ respectively). The measurement of *Nitrosomonas europaea* showed on the other hand a significant lower SP (mean value of 33 ‰). This difference in SP-values can partly be explained by the fact that two different bacterial streams were used and partly by the discovered leak.

The rest of the explanation of the nitrifying measurements arises from figure 6.2. The evolution of the concentration profile has a general upward gradient. For the *Nitrosospira multiformis* the general growth rate is 0.26 ppb per hour, whereas the general growth rate for the *Nitrosomonas europaea* is 0.2 ppb per hour. This suggests that a continuation of the measurements for a longer period of time would increase the gradient even more. This is in good accordance with Sutka et al., 2003 [47] and Sutka et al., 2006 [48]. It is stated in these two papers that the required (time needed for the bacteria to produce  $N_2O$  from the  $NH_4^+$ ) incubation time was 3 days and 6 days respectively for measurements of *Nitrosomonas europaea*.

The final conclusion to the nitrification experiment is therefore that we most likely are measuring the nitrifying bacteria with a usable setup. The intention of the flushing and measuring setup seems to be working. However, no succesfull experiments with nitrifying bacteria confirm this. We found an increase in SP when measuring both bacterial streams.

These increased values are in good accordance with Park et al., 2011 [37]. But further continuous measurements need to be done.

Additionally any future measurements will need an incubation time of probably 6 days in order to gain reliable and valid measurements of both the concentration and the isotopic composition.

The experiment with the denitrifying bacteria, *Pseudomonas Chlororaphis* and *Pseudomonas Flourescens* were both very successful. We found that the measurement of the  $N_2O$  production from the mono-cultures gave very nice concentration profiles (figure 6.3 and figure 6.4). The measurements of *Pseudomonas Chlororaphis* showed some accurate and stable SP-values over more than five hours. A general SP below 0 ‰ was measured from all three measurements.

The measurements of *Pseudomonas Flourescens* showed as well some very nice concentration profiles. Especially the blue and red profiles which clearly show both the production and destruction of  $N_2O$ . The SP-values are also changing over the course of the experiment. The SP-values around the top point are especially interesting. From figure 6.5 the SP-values are found to be between 0 ‰ and 10 ‰. The SP-values are increasing to the top of concentration and then decreasing when  $N_2O$  is taken up again. The increase prior to the top is linked to the mixing of the original gas-composition and the emitted gas. The decrease after the top is a lot smaller and is linked to the destruction of the  $N_2O$  molecules. It can therefore be assumed that the destruction is causing a fractionation of the  $N_2O$  molecules. All of the presented denitrifying mono-culture experiments are in very good accordance with the ones presented by Park et al., 2011 [37].

### **Ecosystem experiments**

During the work presented here, several experiments were conducted in natural ecosystems. These experiments were all done with the purpose of tracing  $N_2O$  production and the sources from different parts of the ecosystem through identification of the isotopic composition.

The experiment with soil samples from Maglemosen (as presented in figure 7.2 and 7.3) was thought to present two different processes. Namely nitrification and denitrification. The profile presented in figure 7.2 shows a very nice production of  $N_2O$ . The isotopic composition of these  $N_2O$  molecules was found to have an average SP of approximately 18 ‰. This value is in the high end, between the values measured in the mono-culture experiments. It is therefore an indication that the primary process of  $N_2O$  production is nitrification. This

is exactly as expected since the soil is relatively dry.

The profiles presented in figure 7.3 should in theory show a relatively rapid increase in  $N_2O$  concentration (compared to the first figure). This increase should happen because of the limited amount of oxygen caused by the flood. With a limited amount of oxygen available the primary process should shift to denitrification ( $SP \approx 0 \text{ ‰}$ ). This is not what we see in figure 7.3. In this figure it is clear that the SP first increase and then stabilizes at a value of about 20 ‰. This is approximately the same value as before the flood. Furthermore the inclination is less steep. It must therefore be assumed that the soil sample from Maglemosen is not representative for an ecosystem with both nitrifying and denitrifying bacteria. Another conclusion could be that the denitrifying bacteria in Maglemosen are producing  $N_2O$  with high SP. The theory that SP can be used for identification of the sources of  $N_2O$  would in that case be proven wrong. Though this is very unlikely, when looking at the other results presented in this thesis.

The measurements of gas samples from Buresoe were primarily conducted to measure the potential change in SP caused by the slope. From table 8.1 can the significant change in SP, depending on the position of the row, be found. We found that the SP at the first two rows were in the lower part of the denitrifying SP-range. The mean concentration at these rows was found to be only slightly larger than the atmospheric air. This is exactly as expected. The concentration and SP-values of the gas emitted, increased significantly moving down slope to row no. 3 and 4. There is a band in which the amount of available  $NH_4^+ / NH_3$  has increased significantly. This makes perfectly good sense. The water will wash out the  $NH_4^+ / NH_3$  when moving down slope. The  $NH_4^+ / NH_3$  will then accumulate when the terrain flattens. An increase in available  $NH_4^+ / NH_3$  will lead to a more nitrifying environment. At the last row (row no. 5) a small production of  $N_2O$  was found. The SP of the gas collected here was again in the range of denitrifying bacteria. This can be explained from the increased amount of water (increased anaerobic environment). The final conclusion to this experiment is therefore that we have found a significant change in the isotopic composition, depending on the location on the slope.

Multiple experiments were conducted during the field campaign at Disko Island.

One of the most interesting experiments is the one comparing the activity at the wet and dry snow-fence sites. As shown in figure 9.4, 9.5 and 9.6 the difference between the two locations is fairly obvious. The measurements from the wet sites show that the SP at all of the 6 plots are  $0.6 \text{ ‰} \pm 6 \text{ ‰}$ . It is known from the theory of denitrifying bacteria that

these bacteria prefer anaerobic environments. It is therefore indicated from both theory and measurements that the wet sites are dominated by denitrifying bacteria.

The dry sites show a lot more variation in the measurements conducted at six blocks. This variation is primarily in SP values above 0. Most of the measurements from the 48 plots show SP-values between +15 ‰ and +30 ‰. This indicates that the environment of the dry snow-fence sites is dominated by nitrifying bacteria. That the dry-sites is dominated by nitrifying bacteria is as expected. It is a well known fact that nitrifying bacteria prefer aerobic and ammonia rich environments. The dry sites are definitely aerobic environments, and it is known, from previous experiments (conducted by the group of Bo Elberling) that ammonia is available in the soil at these sites [Pers. comm. with Bo Elberling].

No significant treatment effect can be seen from the measurements of the dry snow-fence sites. This is even though the experimental sites were made prior to this field season. The reason for this missing treatment effect can very well be because of a too late measuring campaign. The measurements took place about a month and a half after the snow was melted. At this point the amount of water can be assumed to be at a lower level than right after the melting of the snow. This can be assumed simply because the sites are on a downward slope which will lead the water away from the sites.

It can be assumed that the best conditions for production of  $N_2O$  is right after the snow has melted. At this time more water is available and the temperature at night is above the freezing point. A production of  $N_2O$  is therefore more likely. This assumption is made from the fact that the largest amount of  $N_2O$  produced is from lands at tropical latitudes [32]. The tropical latitudes are known to have a humid and warm environment.

The conclusion is therefore, that the treatment effect only can be found when the production of  $N_2O$  from the specific site exceeds the concentration found in the surrounding atmosphere.

The determination of the dominant  $N_2O$  transporter from the soil to the atmosphere was examined in section 9.2.3. Especially the concentration-plot (in figure 9.9) shows some interesting results. The profiles presenting the gas emission from plants seem to have a slightly higher  $N_2O$  concentration. It was not expected that the difference would be very large. The ecosystem is expected to use a few days to stabilize the "new" system after the removal. These measurements were conducted about 3 days after the removal and it is therefore not expected that a large change can be seen. The small difference detected is therefore a very positive result. Due to the results presented by Jørgensen et al., 2012 [22], it can therefore be assumed that a significant difference would have been measured at a later point in time.

However, further measurements need to be conducted to prove this assumption.

The last experiment presented in this thesis concerns the emission of  $N_2O$  from different depths of the active layer. These experiments were partly successful. Figure 9.10 and 9.11 show the top and the third section of the depth sample. These two depths are the most interesting ones. Let us start with the top part. Before the addition of water the concentration decreases a little. The SP measured from both of these soil samples are stable at approximately 0 ‰. According to the mono-culture experiments this means that denitrifying bacteria are dominant here. This was expected since the sample was taken from a wet site. The reason for the changes found after the addition of water can be found when looking at the  $\delta^{15}N$ . It is known that the water used was cleaned prior to addition. The  $\delta^{15}N$  measured of this clean water is presented in figure 10.1.

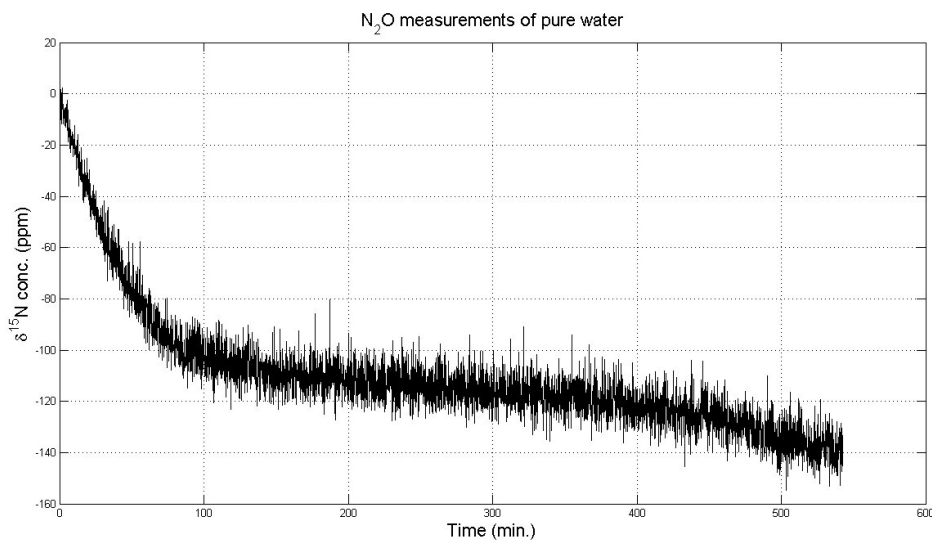


Figure 10.1:  $\delta^{15}N$  measurements of the clean water.

The conclusion of this figure is that a certain amount of  $N_2O$  molecules were in the water. The molecules in the water will reach an equilibrium state with the molecules in the gas phase. The amount of  $N_2O$  molecules in the water is less than in the gas phase. Therefore, fractionation will occur between the two phases. The heavy ( $^{15}N$ ) isotope will be enriched in the water phase. This will result in a relative increase of light ( $^{14}N$ ) isotope in the gas phase. This is exactly what is shown in figure 10.1.  $\delta^{15}N$  also decreases when the two soil samples are flooded. The  $N_2O$  molecules emitted from the water undergo fractionation. This causes an increased concentration. The change in SP happens while the steady state is achieved.

The difference between the first and the third sample is caused by the depth of the sample. There are less  $O_2$  and nutrients available at the depth of the third sample. Furthermore, the temperature of the soil decrease with depth.

# 11

## Conclusions

In this thesis the prototype of the Picarro G5101-i analyzer has been tested and used for several experiments. The analyzer has proven to be both stable and consistent in the measurements performed. This was especially the case after the optics unit was adjusted and set on the site in a temperature controlled container.

The experiments conducted are all more or less depending on the results from the mono-culture experiment. The final conclusion to the mono-culture experiments is that continuous measurements were successfully produced of two different denitrifying bacteria. The experiments show that  $N_2O$  produced from denitrifying bacteria have a SP below 10 ‰. Continuous measurements were also conducted with nitrifying bacteria. These measurements show promising results but further experiments need to be conducted in order to make final conclusions on these. The  $N_2O$  produced from nitrifying bacteria seems to have a SP above 20 ‰. It can be concluded that the SP has been demonstrated as a good tool for identifying the sources of  $N_2O$ .

Continuous measurements of the production/destruction of  $N_2O$  from soil samples with growing vegetation are presented. It is shown that the Picarro analyzer is capable of measuring changes in both concentration and isotopic composition of  $N_2O$  caused by natural emission.

Several measurements have shown that the SP varies depending on the surrounding local environment. Field experiments in Buresoe have shown a change in the isotopic composition of the emitted  $N_2O$ , depending on the location on the slope. It was found that a band dominated by nitrifying bacteria was present just above the swampy area in which denitrifying bacteria dominated. This conclusion is made on the basis of the results presented in the

experiments of mono-cultures. A similar conclusion is drawn from experiments with the dry and wet snow-fence sites measured on Disko Island. These experiments showed that the dry sites (located at a higher elevation) are dominated by nitrifying bacteria. The wet sites (located at a lower and wetter elevation) are dominated by denitrifying bacteria.

Through the measurements conducted at Disko Island, the data hints that the primary growth period of  $N_2O$  is just after the meltdown of the snow and in the upper part of the active layer. The results also indicate that the transport of  $N_2O$  from the source to the atmosphere in the arctic is through plants like *Carex stans* and *Eriophorum scheuchzeri*.

## 12

**Outlook**

The work presented in this thesis is some of the first measurements with a continuous analysis of the isotopic composition of  $N_2O$ . The production of  $N_2O$  from denitrifying bacteria was proved to have a variability of SP. The nitrifying experiments conducted were not completed due to a lack of time. Therefore, it could be very interesting to conduct multiple new experiments, primarily with nitrifying mono-cultures but also with new cultures of denitrifying bacteria.

The work done at Disko Island showed interesting results, it would therefore be interesting to continue and develop new measurements of  $N_2O$  production in the arctic region (at Disko Island).

The ultimate goal would be to measure and investigate the signature of  $N_2O$  in deep ice cores. This could lead to a possible understanding of the processes leading to the changes in  $N_2O$  from past to present.

## Bibliography

- [1] K K Andersen, N Azuma, J-M Barnola, M Bigler, P Biscaye, N Caillon, J Chappellaz, H B Clausen, D Dahl-Jensen, H Fischer, J Flückiger, D Fritzsche, Y Fujii, K Goto-Azuma, K Grønvold, N S Gundestrup, M Hansson, C Huber, C S Hvidberg, S J Johnsen, U Jonsell, J Jouzel, S Kipfstuhl, a Landais, M Leuenberger, R Lorrain, V Masson-Delmotte, H Miller, H Motoyama, H Narita, T Popp, S O Rasmussen, D Raynaud, R Rothlisberger, U Ruth, D Samyn, J Schwander, H Shoji, M-L Siggard-Andersen, J P Steffensen, T Stocker, a E Sveinbjörnsdóttir, a Svensson, M Takata, J-L Tison, Th Thorsteinsson, O Watanabe, F Wilhelms, and J W C White. High-resolution record of Northern Hemisphere climate extending into the last interglacial period. *Nature*, 431(7005):147–51, September 2004.
- [2] Louise Askaer, Bo Elberling, Thomas Friberg, Christian J. Jørgensen, and Birger U. Hansen. Plant-mediated CH<sub>4</sub> transport and C gas dynamics quantified in-situ in a *Phalaris arundinacea*-dominant wetland. *Plant and Soil*, 343(1-2):287–301, February 2011.
- [3] David Morten Balslev-clausen. *Application of cavity ring down spectroscopy to isotopic bio- geo- & climate-sciences & the development of a mid-infrared CRDS analyzer for continuous measurements of N<sub>2</sub>O isotopomers*. PhD thesis, University of Copenhagen, 2011.
- [4] T Blunier, J Chappellaz, J. Schwander, A. Dällenbach, B. Stauffer, T. F. Stocker, D. Raynaud, J. Jouzel, H. B. Clausen, C. U. Hammer, and S. J. Johnsen. Asynchrony of Antarctic and Greenland climate change during the last glacial period. *Nature*, 394:739–743, 1998.

- 
- [5] CF Bohren and DR Huffman. *Absorption and scattering of light by small particles*. Wiley-VCH Verlag GmbH, Weinheim, Germany., 2007.
- [6] H. Braun and J. Kurths. Were Dansgaard-Oeschger events forced by the Sun? *The European Physical Journal Special Topics*, 191(1):117–129, February 2011.
- [7] S. Christensen and G. J. Bonde. Seasonal variation in numbers and activity of denitrifier bacteria in soil. Taxonomy and physiological groups among isolates. *Danish Journal of Plant and Soil Science*, 89:367–372, 1985.
- [8] S. Christensen and J. M. Tiedje. Sub-parts-per-billion nitrate method: Use of an N<sub>2</sub>O-producing denitrifier to convert NO<sub>3</sub><sup>-</sup> or <sup>15</sup>NO<sub>3</sub><sup>-</sup> to N<sub>2</sub>O. *Applied and environmental microbiology*, 54(6):1409–1413, 1988.
- [9] D. Dahl-Jensen. Eemian interglacial reconstructed from a Greenland folded ice core. *Nature*, 493(7433):489–94, January 2013.
- [10] W Dansgaard and SJ Johnsen. Evidence for general instability of past climate from a 250-kyr ice-core record. *Nature*, 364:218–220, 1993.
- [11] JE Dore, BN Popp, DM Karl, and FJ Sansone. A large source of atmospheric nitrous oxide from subtropical North Pacific surface waters. *Nature*, 396(November):63–66, 1998.
- [12] Drierite. <https://secure.drierite.com/catalog3/page5.cfm?>
- [13] Maryann Feldman and Pierre Desrochers. Research Universities and Local Economic Development: Lessons from the History of the Johns Hopkins University. *Industry & Innovation*, 10(1):5–24, March 2003.
- [14] P Forster, V Ramaswamy, P Artaxo, T Berntsen, R Betts, D. Fahey, J. H. J Lean, D Lowe, G Myhre, J. N. R Prinn, G Raga, M. Schulz, and R. V. Dorland. Climate Change 2007: The Physical Science Basis. Contribution of Working Group I to the Fourth Assessment Report of the Intergovernmental Panel on Climate Change, chapter Changes in Atmospheric Constituents and in Radiative Forcing. *Cambridge University Press, Cambridge, United Kingdom and New York, NY, USA.*, pages 130–217, 2007.
- [15] Qiang Fu and K. N. Liou. On the Correlated k-Distribution Method for Radiative Transfer in Nonhomogeneous Atmospheres. *Journal of Atmospheric science*, 49(22):239–256, 1992.

- [16] Norman N. Greenwood and Alan Earnshaw. *Chemistry of the Elements*. 1984.
- [17] M. K. Hellerstein and R. A. Neese. Mass isotopomer distribution analysis at eight years: theoretical, analytic, and experimental considerations. *American Journal of Physiology - Endocrinology and Metabolism*, 276, 1999.
- [18] AB Hooper and KR Terry. Hydroxylamine oxidoreductase of *Nitrosomonas*: Production of nitric oxide from hydroxylamine. *Biochimica et Biophysica Acta (BBA)-Enzymology*, 571(1):12–20, 1979.
- [19] [Http://www.spectralcalc.com/spectral\\_browser/db\\_intensity.php](http://www.spectralcalc.com/spectral_browser/db_intensity.php). Spectral Calculator: High resolution spectral modeling, 2013.
- [20] F. S Chapin III, Pamela A Matson, and Harold A Mooney. *Principles of terrestrial ecosystem ecology*. 2002.
- [21] J Imbrie, EA Boyle, and SC Clemens. On the structure and origin of major glaciation cycles 1. Linear responses to Milankovitch forcing. *Paleoceanography*, 7(6):701–738, 1992.
- [22] Christian Juncher Jø rgensen, Sten Struwe, and Bo Elberling. Temporal trends in N<sub>2</sub>O flux dynamics in a Danish wetland - effects of plant-mediated gas transport of N<sub>2</sub>O and O<sub>2</sub> following changes in water level and soil mineral-N availability. *Global Change Biology*, 18(1):210–222, January 2012.
- [23] J Jouzel, V Masson-Delmotte, O Cattani, G Dreyfus, S Falourd, G Hoffmann, B Minster, J Nouet, J M Barnola, J Chappellaz, H Fischer, J C Gallet, S Johnsen, M Leuenberger, L Loulergue, D Luethi, H Oerter, F Parrenin, G Raisbeck, D Raynaud, a Schilt, J Schwander, E Selmo, R Souchez, R Spahni, B Stauffer, J P Steffensen, B Stenni, T F Stocker, J L Tison, M Werner, and E W Wolff. Orbital and millennial Antarctic climate variability over the past 800,000 years. *Science (New York, N.Y.)*, 317(5839):793–6, August 2007.
- [24] J. Kaiser, T. Röckmann, and C. A. M. Brenninkmeijer. Temperature dependence of isotope fractionation in N<sub>2</sub>O photolysis. *Physical Chemistry Chemical Physics*, 4(18):4420–4430, September 2002.
- [25] KR Kim and H Craig. Nitrogen-15 and oxygen-18 characteristics of nitrous oxide: A global perspective. *Science*, 262, 1993.

- [26] K J Leckrone and J M Hayes. Efficiency and temperature dependence of water removal by membrane dryers. *Analytical chemistry*, 69(5):911–8, March 1997.
- [27] M. Leuenberger, S. Borella, T. Stocker, M. Saurer, R. Siegwolf, F. Schweingruber, and R. Matyssek. *Stable isotopes in tree rings as climate and stress indicators*. vdf Hochschulverlag AG an der ETH Zürich, 1998.
- [28] Markus Leuenberger and Thomas Blunier. *Stable Isotopes*. Technical report, 2008.
- [29] KN Liou. *An introduction to atmospheric radiation*. Academic Press, second edition, 2002.
- [30] A Mariotti, JC Germon, P Hubert, and P Kaiser. Experimental determination of nitrogen kinetic isotope fractionation: some principles; illustration for the denitrification and nitrification processes. *Plant and soil*, 430(1981):413–430, 1981.
- [31] GW McCarty. Modes of action of nitrification inhibitors. *Biology and Fertility of Soils*, pages 1–9, 1999.
- [32] JM Melillo, PA Steudler, and BJ Feigl. Nitrous oxide emissions from forests and pastures of various ages in the Brazilian Amazon. *Journal of Geophysical ...*, 106(2000):179–188, 2001.
- [33] Arvin Mosier, Carolien Kroeze, and Cindy Nevison. Closing the global N<sub>2</sub>O budget: nitrous oxide emissions through the agricultural nitrogen cycle. *Nutrient Cycling in Agroecosystems*, 52(2-3):225–248, 1998.
- [34] J.G.J Olivier, A. F. Bouwman, K.W. Van der Hoek, and J.J.M. Berdowski. Global air emission inventories for anthropogenic sources of NO<sub>x</sub>, NH<sub>3</sub>, and N<sub>2</sub>O in 1990. *Environmental Pollution*, 102:135–148, 1998.
- [35] S. J. O'Shea, S. J.-B. Bauguitte, M. W. Gallagher, D. Lowry, and C. J. Percival. Development of a cavity-enhanced absorption spectrometer for airborne measurements of CH<sub>4</sub> and CO<sub>2</sub>. *Atmospheric Measurement Techniques*, 6(5):1095–1109, May 2013.
- [36] P. A. de Groot. *Handbook of Stable Isotope Analytical Techniques Vol. 2*. Elsevier, first edition, 2009.
- [37] S. Park, T. Pérez, K. a. Boering, S. E. Trumbore, J. Gil, S. Marquina, and S. C. Tyler. Can N<sub>2</sub>O stable isotopes and isotopomers be useful tools to characterize sources and microbial pathways of N<sub>2</sub>O production and consumption in tropical soils? *Global Biogeochemical Cycles*, 25(1):GB1001, January 2011.

- [38] Picarro. [http://www.picarro.com/technology/cavity\\_ring\\_down\\_spectroscopy](http://www.picarro.com/technology/cavity_ring_down_spectroscopy), 2013.
- [39] Raymond T. Pierrehumbert. *Principles of Planetary climate*. Cambridge University Press, The Edingbergh building, Cambridge CB2 8RU, UK, 2010.
- [40] Brian N. Popp. Nitrogen and oxygen isotopomeric constraints on the origins and sea-to-air flux of N<sub>2</sub>O in the oligotrophic subtropical North Pacific gyre. *Global Biogeochemical Cycles*, 16(4):1–10, 2002.
- [41] T. Rahn. Stable Isotope Enrichment in Stratospheric Nitrous Oxide. *Science*, 278(5344):1776–1778, December 1997.
- [42] Mark Van Schilfhaarde, IA Abrikosov, and B Johansson. Origin of the Invar effect in iron-nickel alloys. *Nature*, 400(July), 1999.
- [43] Adrian Schilt, Matthias Baumgartner, Jakob Schwander, Daphné Buiron, Emilie Capron, Jérôme Chappellaz, Laetitia Louergue, Simon Schüpbach, Renato Spahni, Hubertus Fischer, and Thomas F. Stocker. Atmospheric nitrous oxide during the last 140,000years. *Earth and Planetary Science Letters*, 300(1-2):33–43, November 2010.
- [44] Hanns-Ludwig Schmidt, Roland a Werner, Naohiro Yoshida, and Reinhard Well. Is the isotopic composition of nitrous oxide an indicator for its origin from nitrification or denitrification? A theoretical approach from referred data and microbiological and enzyme kinetic aspects. *Rapid communications in mass spectrometry : RCM*, 18(18):2036–40, January 2004.
- [45] Silicagelpacket.com. <http://www.silicagelpackets.com/silica-gel-packets/loose-bulk-silica-gel-non-indicating-and-indicating-white-orange>.
- [46] Lisa Y. Stein and Yuk L. Yung. Production, isotopic composition, and atmospheric fate of biologically produced nitrous oxide. *Annual Review of Earth and Planetary Sciences*, 31(1):329–356, May 2003.
- [47] R L Sutka, N E Ostrom, P H Ostrom, H Gandhi, and J a Breznak. Nitrogen isotopomer site preference of N<sub>2</sub>O produced by *Nitrosomonas europaea* and *Methylococcus capsulatus* Bath. *Rapid communications in mass spectrometry : RCM*, 17(7):738–45, January 2003.
- [48] RL Sutka and NE Ostrom. Distinguishing nitrous oxide production from nitrification and denitrification on the basis of isotopomer abundances. *Applied and environmental microbiology*, 72(1):638–644, 2006.

- [49] M. H. Thiemens. Mass-Independent Isotope Effects in Planetary Atmospheres and the Early Solar System. *Science*, 283(5400):341–345, January 1999.
- [50] FK Tittel, Dirk Richter, and Alan Fried. Mid-infrared laser applications in spectroscopy. *Solid-State Mid-Infrared Laser Sources*, 516(7):445–516, 2003.
- [51] S. Toyoda and N. Yoshida. Determination of nitrogen isotopomers of nitrous oxide on a modified isotope ratio mass spectrometer. *Analytical Chemistry*, 71(20):4711–4718, 1999.
- [52] Sakae Toyoda, Sei-ichiro Yamamoto, and Shinji Arai. Isotopomeric characterization of N<sub>2</sub>O produced, consumed, and emitted by automobiles. *Rapid Communications in Mass Spectrometry*, 22:603–612, 2008.
- [53] Sakae Toyoda, Naohiro Yoshida, Tatsuya Miwa, Yohei Matsui, Hiroaki Yamagishi, and Urumu Tsunogai. Production mechanism and global budget of N<sub>2</sub>O inferred from its isotopomers in the western North Pacific. *Geophysical Research Letters*, 29(3):5–8, 2002.
- [54] B.H. Vaughn, J. Miller, D.F. Ferretti, and J.W.C White. *Handbook of stable isotope analytical techniques*. Elsevier, 2004.
- [55] L. R. Welp, R. F. Keeling, R. F. Weiss, W. Paplawsky, and S. Heckman. Design and performance of a Nafion dryer for continuous operation at CO<sub>2</sub> and CH<sub>4</sub> air monitoring sites. *Atmospheric Measurement Techniques*, 6(5):1217–1226, May 2013.
- [56] R. A. Werner and W. A. Brand. Referencing strategies and techniques in stable isotope ratio analysis. *Rapid communications in mass spectrometry : RCM*, 15(7):501–19, January 2001.
- [57] Craig R White, Steven J Portugal, Graham R Martin, and Patrick J Butler. Respirometry: anhydrous drierite equilibrates with carbon dioxide and increases washout times. *Physiological and biochemical zoology : PBZ*, 79(5):977–80, 2006.
- [58] L.M. Wingen and B.J. Finlayson-Pitts. An upper limit on the production of N<sub>2</sub>O from the reaction of O(1D) With CO<sub>2</sub> in the presence of N<sub>2</sub>. *Geophysical research letters*, 25(4):517–520, 1998.
- [59] N. Wrage, G. L. Velthof, M. L. V. Beusichem, and O. Oenema. Role of nitrifier or denitrification in the production of nitrous oxide. *Soil Biology and Biochemistry*, 33:1723–1732, 2001.

- [60] N. Yoshida and S. Toyoda. Constraining the atmospheric N<sub>2</sub>O budget from intramolecular site preference in N<sub>2</sub>O isotopomers. *Nature*, 405(6784):330–4, May 2000.
- [61] E. D. Young, A. Galy, and H. Nagahara. Kinetic and equilibrium mass-dependent isotope fractionation laws in nature and their geochemical and cosmochemical significance. *Geochimica et Cosmochimica Acta*, 66(6):1095–1104, 2002.
- [62] Piotr Zalicki and RN Zare. Cavity ringdown spectroscopy for quantitative absorption measurements. *The Journal of chemical physics*, 102(August 1994):2708–2717, 1995.

*A***Abbreviation****Chemical compounds**

CO <sub>2</sub>	Carbon Dioxide
CH <sub>4</sub>	Methane
N <sub>2</sub>	Nitrogen
O <sup>-</sup>	Oxygen (unstable)
O <sub>2</sub>	Dioxygen
O <sub>3</sub>	Ozone
H <sub>2</sub> O	Water
H <sup>+</sup>	Hydrogen
N <sub>2</sub> O	Nitrous Oxide
NO	Nitric Oxide
NO <sub>2</sub> <sup>-</sup>	Nitrite
NO <sub>3</sub> <sup>-</sup>	Nitrate
N <sub>2</sub> O <sub>2</sub>	Dinitrogen Dioxide
NH <sub>4</sub> <sup>+</sup>	Ammonium
NH <sub>3</sub>	Ammonia
NH <sub>2</sub> OH	Hydroxylamine
NH <sub>4</sub> Cl	Ammonium Chloride
KNO <sub>3</sub>	Potassium Nitrate

## Physical magnitudes and instrumental names

$I_0$	Initial intensity
$I$	Intensity [ $\frac{Energy}{m^2}$ ]
$\lambda$	Wavelength [ $m$ ]
$z$	Light beam traveling distance
$N$	Number of energy states
$\nu_0$	Frequency at the center
$\nu$	Frequency [ <i>Hertz</i> ]
$c$	Speed of light [ $\frac{m}{s}$ ]
$T$	Temperature [ <i>Kelvin</i> ]
$p$	Pressure [ <i>hPa</i> ]
$h$	Planck's constant [ <i>Js</i> ]
$n$	Absorbers concentration
$\gamma$	Lorentz line width
$\gamma_D$	Doppler line width
$K_G$	Line shape
$k_B$	Boltzmann constant [ $1.3806488 \cdot 10^{-23} \frac{J}{K}$ ]
$\tilde{\nu}$	Wavenumber [ $cm^{-1}$ ]
$m$	Mass of molecule [ <i>Kg</i> ]
$M$	Integer in wavelength calculations
$L$	Distance travelled by the light, inside the cavity
$A_c$	Absorption from the cavity
$T_c$	Transmittance from the cavity
$S_c$	Scattering from the cavity
$\alpha_c$	Effective absorption coefficient of the cavity
$\alpha_g$	Effective absorption coefficient of the gas
$R$	Cavity mirror reflectivity, [99.999%]
$t_{rt}$	Cavity round trip time
$\tau$	Ring down decay time
$A_c$	Amount of absorption
IR	Infrared
Mid-IR	Mid-Infrared
CRDS	Cavity Ring Down Spectroscopy
CW	Continuous wave



## Derivation of Beer-Lambert's law

In section 3.3 it is stated that the solution to the intra cavity light intensity (equation 3.9), is a formulation of Beer-Lambert's law given as  $I(t)$ . In the following I have made the derivation from the solution ( $I(t)$ ) (as stated in the thesis). In the derivation I have made the calculations under the assumption that the calculations should be made with all frequencies, therefore the integral.

$$I(t) = \int_0^{\infty} I(\nu) \exp\left(-\frac{t}{\tau(\nu)}\right) d\nu \quad (\text{B.1})$$

where:

$$\tau(\nu) = \frac{d}{c[(1-R) + \kappa(\nu)l]}$$

In this last equation we have that  $R = 99.99 \approx 1$  and  $l = d$ , which means that

$$\tau \propto \frac{1}{c\kappa(\nu)}$$

therefore equation B.1 becomes:

$$\begin{aligned} I(t) &= \int_0^{\infty} I(\nu) \exp\left(-\frac{t}{\frac{1}{c\kappa(\nu)}}\right) d\nu \\ &= \int_0^{\infty} I(\nu) \exp(-t \cdot c \cdot \kappa(\nu)) d\nu \\ &= \int_0^{\infty} I(\nu) \exp(\kappa(\nu) \cdot x) d\nu \end{aligned}$$

$$I(\nu) = I_0(\nu) \cdot \exp(-\kappa(\nu) \cdot x)$$

From Zalicki et al., 1994, we know that  $\kappa(\nu) = \alpha$ , and since  $x = -t \cdot c$  it must be correct that  $x = 2L$ . Therefore equation B.1 must be a version of Beer-Lambert's law.



# Atmospheric air measurements at Disko

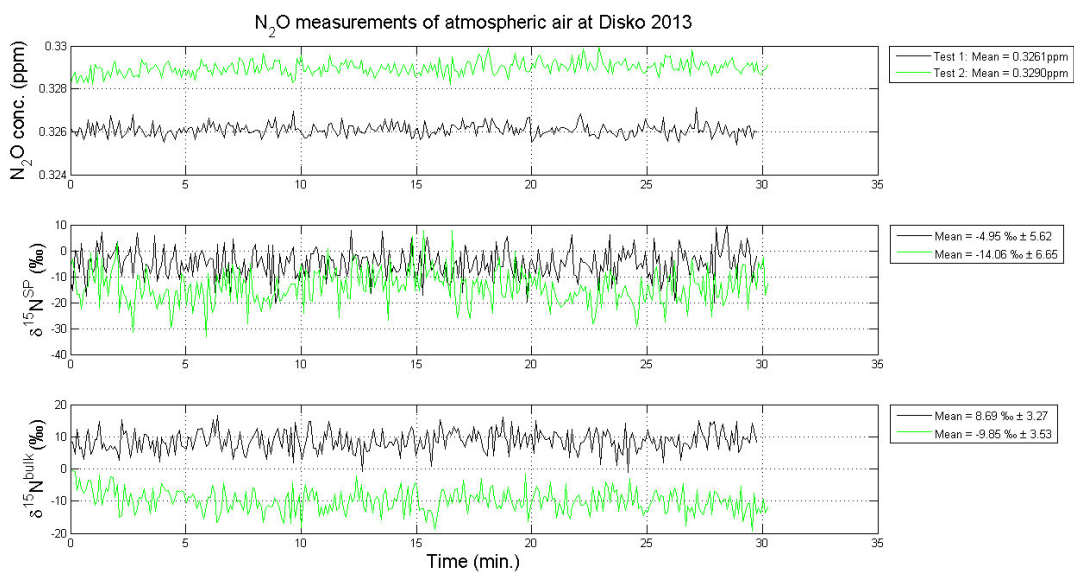


Figure C.1: *The N<sub>2</sub>O concentration Site preference and Bulk-value from measurements of the atmospheric air 2.5 meter above the dry snow-fence site.*



## Dry snow-fence site experiment plots

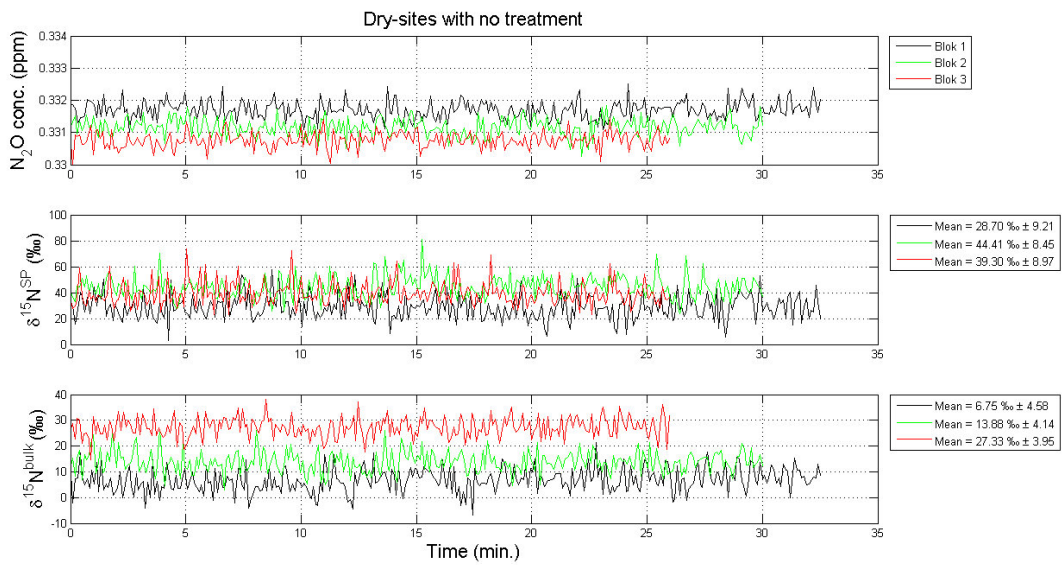


Figure D.1: The  $N_2O$  concentration Site preference and Bulk-value from measurements of the plots with No treatment.

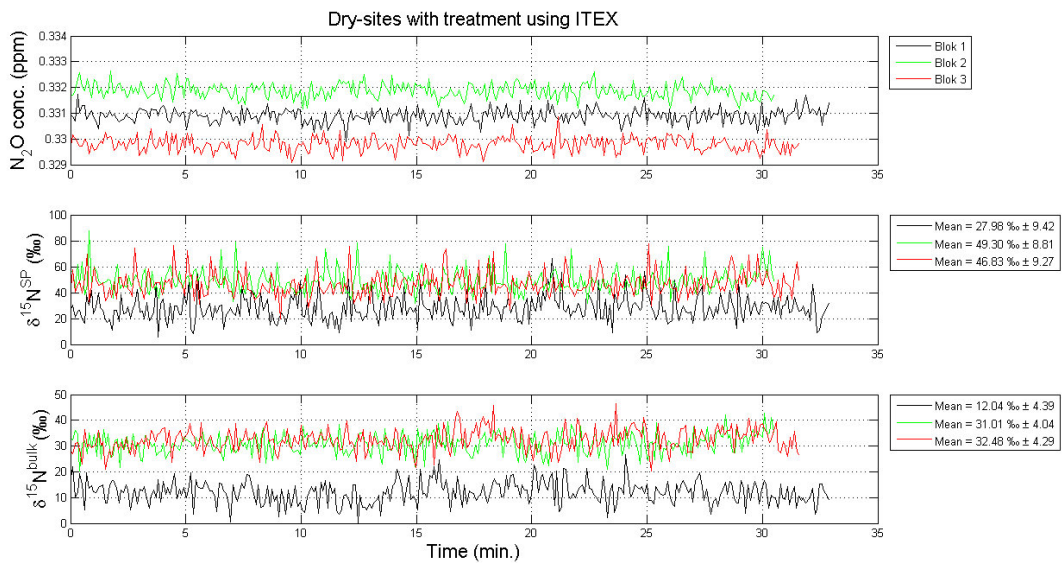


Figure D.2: The  $N_2O$  concentration Site preference and Bulk-value from measurements of the plots with ITEX treatment.

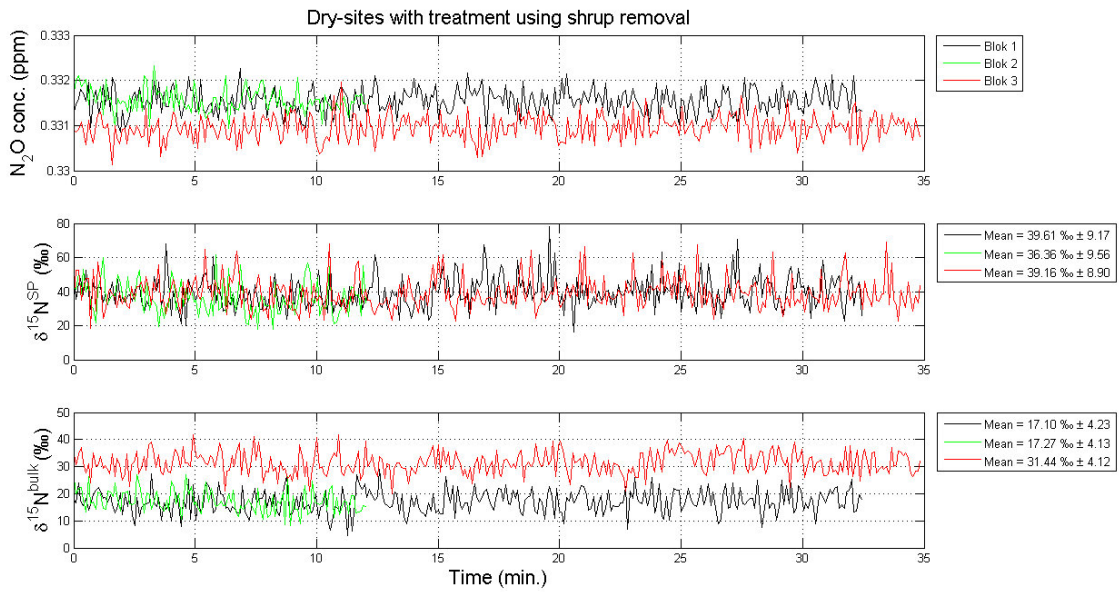


Figure D.3: The  $N_2O$  concentration Site preference and Bulk-value from measurements of the plots with shrub removal treatment.

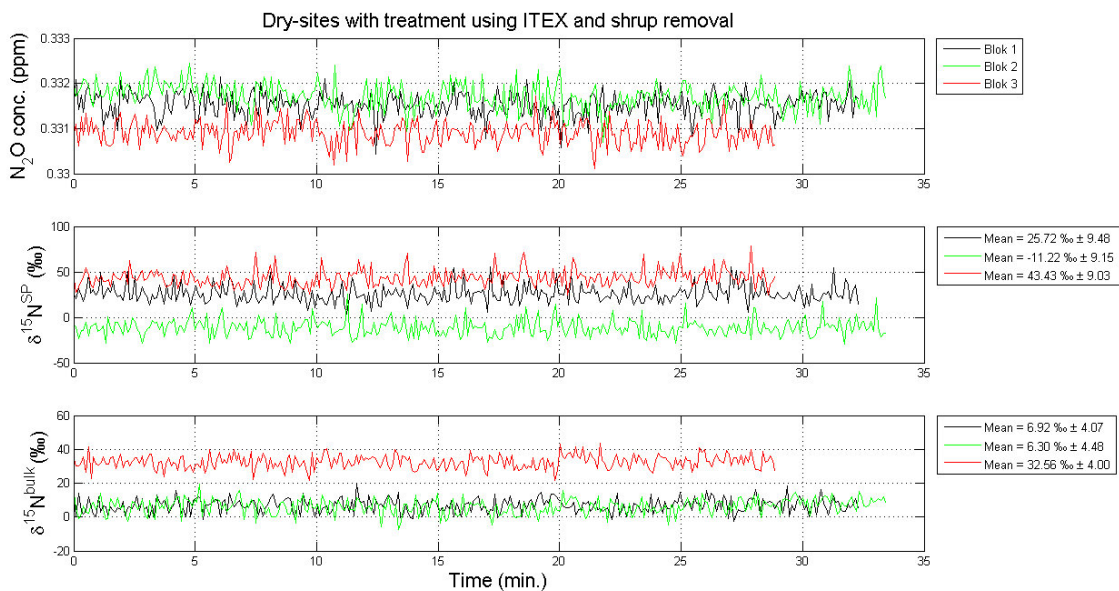


Figure D.4: The  $N_2O$  concentration Site preference and Bulk-value from measurements of the plots with ITEX and Shrub removal treatment.

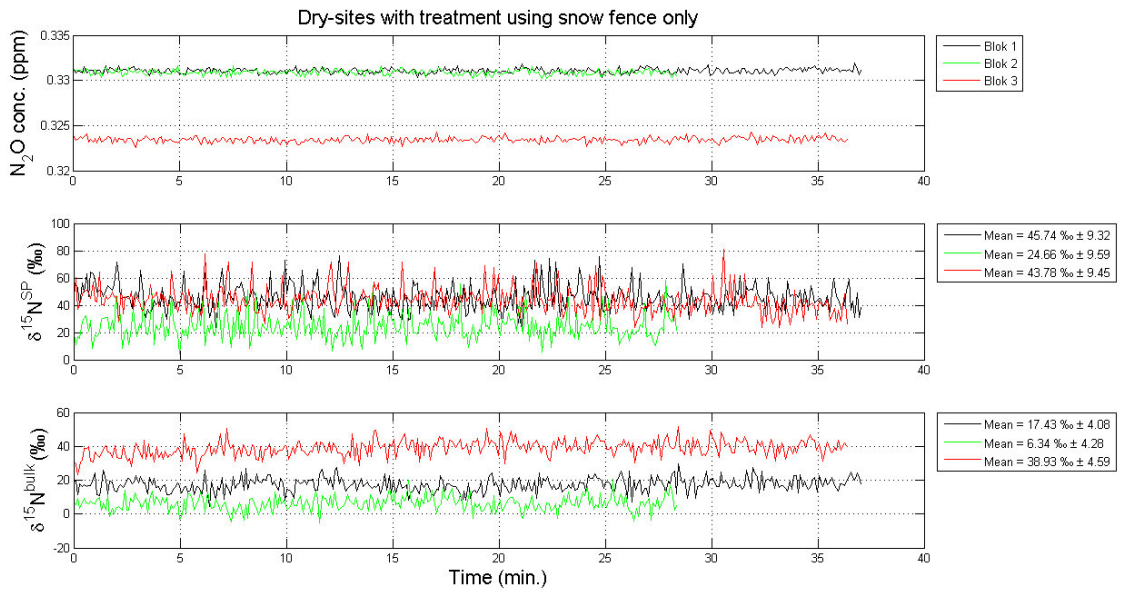


Figure D.5: *The  $N_2O$  concentration Site preference and Bulk-value from measurements of the plots with snow-fence treatment.*

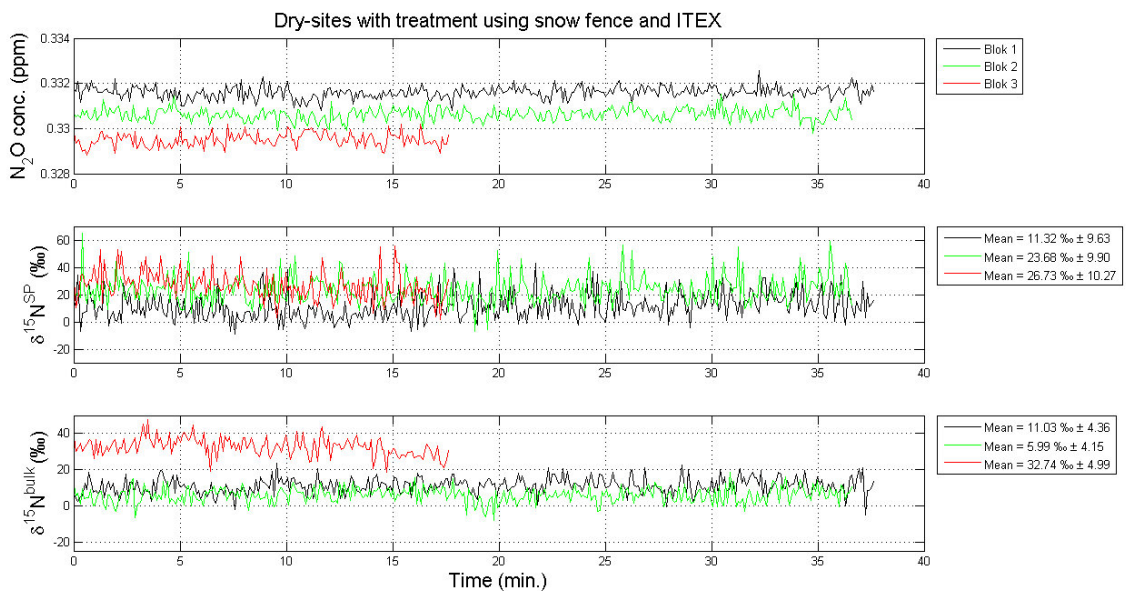


Figure D.6: *The  $N_2O$  concentration Site preference and Bulk-value from measurements of the plots with snow-fence and ITEX treatment.*

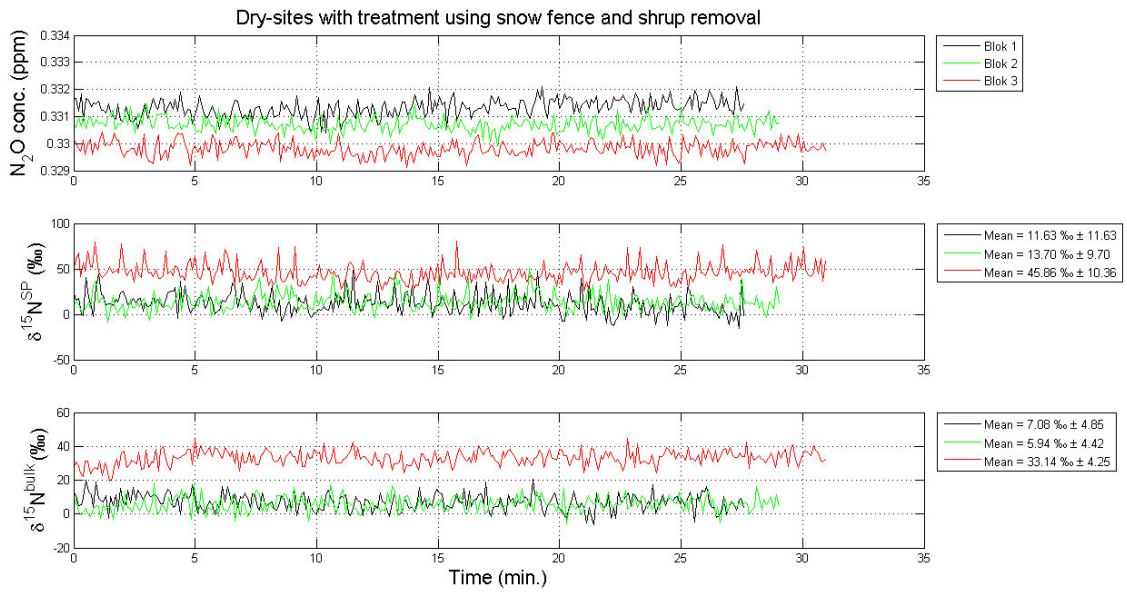


Figure D.7: The  $N_2O$  concentration Site preference and Bulk-value from measurements of the plots with snow-fence and shrub removal treatment.

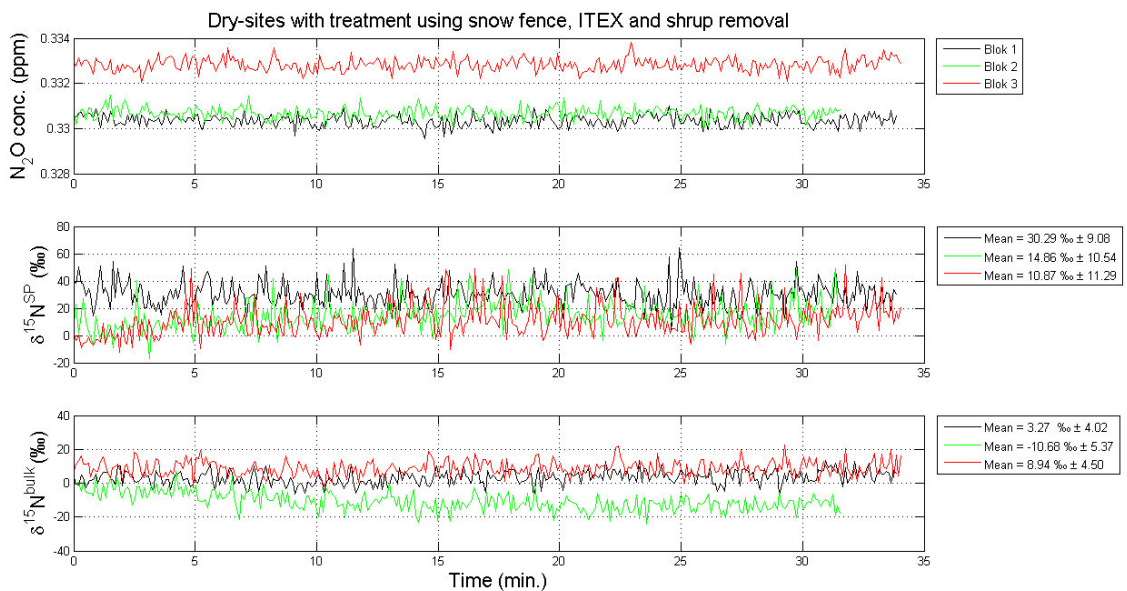


Figure D.8: The  $N_2O$  concentration Site preference and Bulk-value from measurements of the plots with snow-fence, ITEX and shrub removal treatment.



## Active layer experiment plots

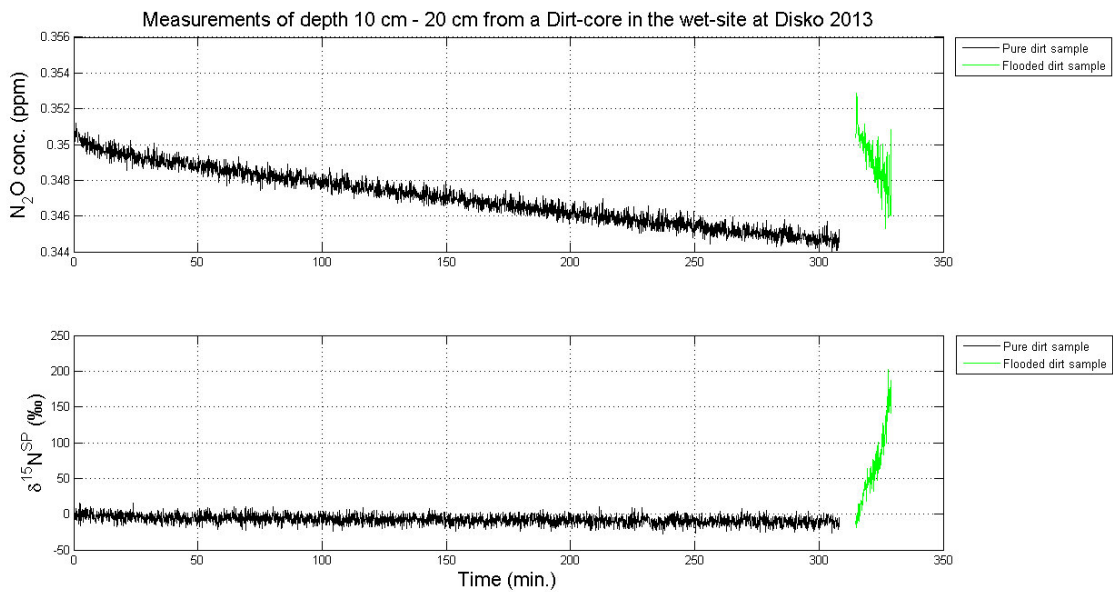


Figure E.1: *The  $N_2O$  concentration Site preference and  $\delta^{15}N$ -value from measurements of*

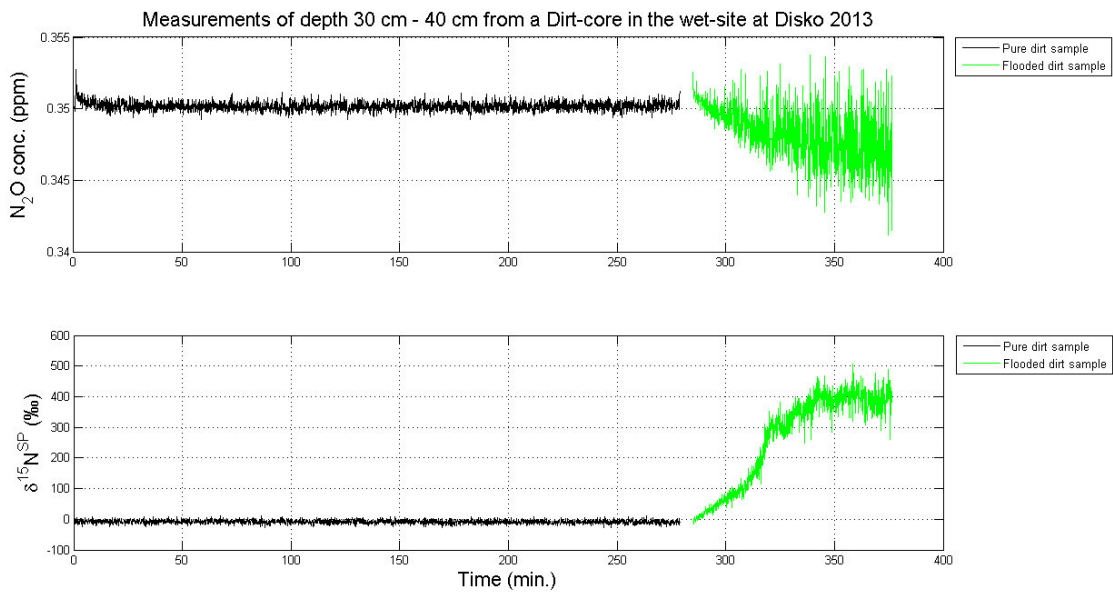


Figure E.2: *The  $N_2O$  concentration Site preference and  $\delta^{15}N$ -value from measurements of the active layer experiment.*